GIMA

Geographical Information Management and Applications

Historical Aerial Imagery for DEM Extraction to Quantify Volumetric Changes between the Years of 1945 and 2017, in the East-Vlieland Coast, the Netherlands

---

José Antonio Cirillo de Assis

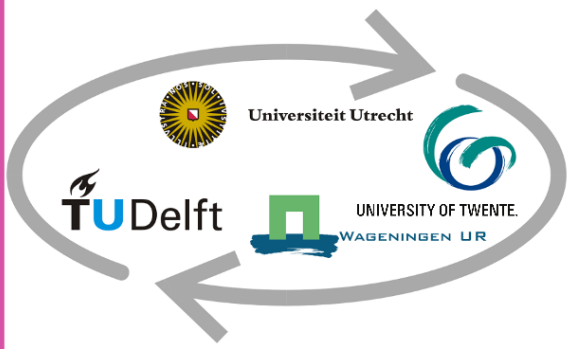

Utrecht University

Historical Aerial Imagery for DEM Extraction to Quantify Volumetric Changes between the Years of 1945 and 2017, in the East-Vlieland Coast, the Netherlands

José Antonio Cirillo de Assis
Solis ID: 6107486
jcirillo.assis@gmail.com
j.a.cirillodeassis@students.uu.nl

Supervisor: Drs. Maarten Zeylmans Van Emmichoven
Faculty of Geosciences
Utrecht University

Professor: Prof. Dr. Steven de Jong
Faculty of Geosciences
Utrecht University

1st of March 2019

Acknowledgments

This master's thesis was written under the fulfillment requirements of the master of Geographical Information Management and Applications (GIMA). It was a long way to finish this research report, with many calculations and time-consuming activities, but I would say that I am happy and satisfied to have learned newer remote sensing techniques, using different software, giving such a different result to aerial photographs as I used to give being a geologist.

Firstly, I would like to thank my supervisor Drs. Maarten Zeylmans Van Emmichoven for guiding me during this research, but also for introducing this subject back there in module 6, during the first year of GIMA. I must say that his enthusiasm in this research field gave me much energy and motivation to perform my own thesis.

Finally, I would like to thank my wife and my family there in Brazil, which without their support, motivation and confidence I would not be achieving my life and professional goals.

José Antonio Cirillo de Assis,

Utrecht - March 2019

Summary

The area of remote sensing has been gaining new markets and applications in recent years. It comprises the representation and collection of data of a given region on the Earth's surface without the need for direct contact, that is, the treatment, storage and analysis of the collected data, intending to better understand the environment of the monitored surface. Aerial photographs were intensely used in the 20th century in remote sensing, and when newer approaches emerged and grew within this field, such as LiDAR, satellite images and drones, the photographs lost their force. However, as the use of laser scanning equipment is way expensive comparing with photogrammetry methods, and with the advent of the digital cameras, the aerial photographs began to be widely used again.

This master thesis is inserted in the remote sensing research field, making use of aerial photographs and photogrammetry methods to recreate or reconstruct the Earth's surface of the study area. The purpose of this research was to calculate volumetric changes at the East-Vlieland island, in the Netherlands, by using a comparison between DEMs constructed from historical aerial photographs and recent LiDAR and AHN datasets, comprising a time period of 72 years, from 1945 to 2017.

The aerial photographs of 1945 and 1981 were first evaluated to check if they had stereopairs or give photogrammetry stereoscopic. After that, the sets of images were georeferenced in the ERDAS Imagine software, by setting up ground control points (GCPs), which are reference points with known coordinates. They add the height or Z values to the photographs, giving the three-dimensional context.

Then, image-based point clouds were made from the aerial photographs, by using two different image matching process, Normalized Cross Correlation (NCC) and Semi-Global Matching (SGM). With these datasets, DEMs of East-Vlieland were made for the years 1945 and 1981. After, this research compared the DEMs with LiDAR and AHN data to verify where the changes took place along the decades. This was done by using the DEM of Difference analysis method, which corresponds to the subtraction between two different surfaces times the area of the rasters pixel, which in this case was 1 meter per 1 meter. The volumetric changes were calculated through the subtracting of old DEM from the newer DEM.

The results showed that for 72 years, the volume of East-Vlieland decreased in cubic meters, reinforcing that deforestation and erosion were usually present. The biggest changes occurred in the dunes' area, for volume increasing, and at the south-southwest part marked by the vegetation area, for volume decreasing. At the extreme east also occurred a lot of decrease in volume, where the ocean eroded a considerable amount of the dunes and beaches.

This study also assessed the quality of the deliverables during the extraction of the DEMs. In order to have a reliable representation of the surface, it is necessary to have a good point cloud data, which may have better accuracy having an accurate and precise georeferenced aerial photographs. The best point cloud performed in this research was made for the year of 1981 using the NCC method, because it delivered the lowest value for standard deviation. The other point cloud data, created with the SGM algorithm, also had positive aspects, such as point count and point density. The point cloud made with SGM for the set of images from 1945 had the worst outcome possible, not being usable for further processing. As the 1981-NCC point cloud was the best dataset created, the DEM made from it was also considered the best among the others, giving a more realistic result for the surface of the area.

The best image matching process was the NCC method which point clouds data contributed for better, more accurate and visual appealing deliverables. Despite what was expected considering the literature, that the SGM would get better results, this research showed the opposite. However, it can be pointed out that SGM resulted in a denser point cloud data.

Content

List of Figures

List of Tables

List of Abbreviations

AHN Actueel Hoogtebestand Nederland

ATE Automatic Terrain Extraction

DEM Digital Elevation Models

DTM Digital Terrain Model

eATE Enhanced Automatic Terrain Extraction

GIS Geo-information Sciences

GCP Ground Control Points

GSD Ground Sample Distance

IDW Inverse Weighted Distance

ISO International Organization for Standardization

LiDAR Light Detection and Ranging

NCC Normalized Cross Correlation

RMSE Root Mean Square Error

SGM Semi-Global Matching

TIN Triangular Irregular Network

1. Research Context

1.1 Introduction

The Digital Elevation Models (DEMs) are models that reproduce a topographic surface of a given location through a set of points with coordinates x and y, in addition to z values, which gives a three-dimensional configuration and continuous variation of the surface. In other words, it is a 3D digital representation of an elevation surface of a determined area. DEMs are an important part in the research of spatial analysis and modelling problems in geosciences, and they are frequently used in study fields such as geology, hydrology, agriculture, geomorphology, ecology, pedology, and others. These digital surface representations are necessary inputs for many specific researches, for instance, mapping of drainage networks, delimitation of river basins, calculating slope and aspect for an area, agricultural applications, morphology and landscape changes, topographic mapping, and modelling and planning urban environments (Pulighe and Fava, 2013).

A successful outcome of DEMs made through historical aerial photographs is the possibility to deliver detailed reconstructions of historical landscapes in three dimensions. Efficient monitoring of coastal areas is fundamental to understand their dynamics, and especially in the Netherlands, as the islands are means of protection against the sea. Historical DEMs may be used for explaining processes and possibly predicting these processes through modelling changes, comparing to current situation. In the present research, modern techniques, as dense image matching algorithms, and specialized software were used to recreate feasible models on East-Vlieland, in the Netherlands.

1.2 Problem definition

Coastlines in natural coastal areas change continuously along time. These changes may occur in different time periods, and are mainly related to atmospheric and hydrodynamic forces, for instance waves and tides. Research of shoreline and dune changes are of great importance for coastal management procedures such as coastal erosion and deposition, regulating the advance and retreat of high and low tides, and rate of coastal land (Leatherman, 2003). Shorelines and dunes can be defined indirectly using remote sensing data, and historical aerial photographs have been a valuable input data for investigating long-term changes in coastal areas.

Around the world, coastal areas of many countries are populated, and especially in low-lying shore zones there are several measures of coastal defense that reduce the risk of flooding. As the Netherlands is under the mean sea level the protection of dunes, dikes and hydraulic structures are permanently protecting the country against flooding. The sand dunes on the coast of the Netherlands are the most important measure taken against the sea.

The wind and the waves from the sea constantly act on some level in the erosion of the dunes. Coastal erosion is a frequent challenge to shorelines around the world, impacting about 70% of coast environments (Bird, 1985). Erosion is the physical removal of soil in a vertical or horizontal direction (Lal, 2001), and the causes of erosion may be of local or global importance such as a decrease in sediment supply and a worldwide change in sea level, respectively (Feagin *et al.*, 2005).

The Dutch government is continuously maintaining the coastline of the Netherlands, and in 1990 the Dutch government decided that the coastline of the Netherlands cannot retreat more than the *'Basiskustlijn'*, which represents a fixed shoreline along the coastal zone of the country (Verhagen, 1990). In order to maintain this *'Basiskustlijn'* the Dutch government annually adds over 7 million cubic meters of sand to the Dutch coasts to prevent degradation of the dunes (Rijkswaterstaat, 2018). According to Hillen *et al.* (2010), the yearly costs for management and maintenance of the several defense methods in the Netherlands are approximately estimated of € 350 million per year. As the country has a total length of 3600 km of flood defenses, the costs are about € 100.000 per km per year.

Historical aerial photographs can be used to generate Digital Elevation Models (DEMs), which may be compared to contemporary 3D elevation models and coastal LiDAR datasets to measure the difference that occurred between different time periods, by means of erosion and deposition.

Volumetric changes quantification may be useful for quantitative assessment of morphological changes of landforms.

1.3 Research Objectives

The objective of this research was to apply the DEM extraction procedure to calculate the volumetric changes of the dunes and the landscape through the coast of East-Vlieland island in the Netherlands. 3D historical data were compared with current situation of coastal LiDAR and AHN (*Actueel Hoogtebestand Nederland*, Current Elevation data for the Netherlands) datasets through DEMs from different time periods, contextualizing the 2D and 3D landscape changes. The study also presented the processes involved to perform a DEM, discussing how quality and accuracy may influence the end results.

Summarizing, this study lead to the following research question and corresponding sub questions:

- How much was the volumetric change in cubic meters of the landscape and the coastal areas of East-Vlieland based on the comparison between the digital elevation models (DEMs) derived from historical aerial photographs and the coastal LiDAR datasets along the years of 1945, 1981, 1997, 2004, 2014 and 2017?"

Sub questions:

- Where did the largest change occur in the coast of East-Vlieland considering the 2D and 3D products along the studied time periods?
- What differences can be pointed out using the methods Normalized Cross Correlation (NCC) and Semi-Global Matching (SGM) for creating point clouds in the study area?
- Which method is most appropriate or accurate for creating point clouds in the study area, NCC or SGM?

1.4 Research Scope

The scope of this research was covered through the objectives stated on the main research question and sub-questions in the last section. Determining the volumetric changes in the coast of East-Vlieland was made by historic aerial photographs and also AHN and LiDAR datasets along the years of 1945 and 2017.

It is important to point out that limitations or uncertainties happened during this research, being mostly related to input datasets, such as aerial photographs and LiDAR datasets. The first subject is represented by lack of photos, as well as not enough stereo pairs for the time periods, and difficulties in DEM extraction of historical photographs. The second subject was about the poor-quality of older LiDAR datasets, with several outliers, influencing the comparison with the extracted DEMs. Besides, the generation of point clouds using NCC through the enhanced Automatic Terrain Extraction button (eATE) and SGM by Tridicon button may be challenging during the stage of data processing, for instance not being useful for non-light contrasting areas or regions with not enough ground control points (GCP). It does not matter what algorithm is being applied, either NCC or SGM, the triangulation step of ground control points will be the same input for both scenarios, so if the project does not have an acceptable number of GCPs or these are not well distributed in the area, a poor triangulation will directly influence the performance of the algorithms, and consequently the extraction of DEMs.

Another limitation in this study was that the calibration report for the 1945 dataset is not available. The camera calibration reports are important because it provides many information regarding the imaging sensor at the moment the photographs were taken. They may be used to identify and correct the distortions that may be present in the image due to the curvature of the lens, focal length, and perspective effects, allowing the calculation of the interior and exterior orientation of the camera. So, as this information must be calculated and estimated, this configures a limitation in

the current research, influencing the process of creating a high-quality DEM, bringing a negative impact on the accuracy and quality of the final products resulted from the year of 1945. Even though that one can calculate the interior and exterior parameters, the practice performed in this study showed that this is very subjective, bringing uncertainty values for the camera settings. It can be especially mentioned that the far western part of the study area for the 1945 dataset could not be used in this research due to a not reliable calculated camera parameters, and consequently it was not possible to perform a triangulation for the GCPs, neither the next steps for the DEM extraction procedure.

Additionally, it must be drowned the attention of what is not part of this research. The investigation and evaluation of coastal dynamics processes such as hydrodynamics, morphology, coastal upwellings, coastal currents, migration of tidal bars, etc., are aspects that are not considered in this study. The main focus was to acquire 2D and 3D DEMs of the area to calculate volumetric changes in each considered time period.

1.5 Scientific Relevance

The present research is of relevance to academia because it uses means of photogrammetry and image processing methods to study historic aerial photographs comparing them to current LiDAR and AHN datasets. Creating 2D and 3D models of different time periods can be useful to verify how is the current status of coastal areas and especially how they were in the past. Calculating the volumetric changes, one can quantify how much these environments have lost or had added sediments, identifying and quantifying the dynamical process such as erosion and deposition that took place along decades. This research may be an input for other research topics that comprises the understanding of coastal systems assisting on their evaluation of current state, past changes, their stability and behaviour, and their prediction of future developments.

1.6 Thesis Outline

This dissertation is divided into 7 chapters. The first chapter showed an introduction of the thesis, including the problem definition, research objectives, motivation and contribution for the theme. Chapter 2 addresses the theoretical context in which the research belongs, providing a literature review for understanding this dissertation. The third chapter introduces the methodology used in this research, illustrating all necessary steps to perform a DEM extraction, as well as how this study approaches the comparison of DEMs from historical aerial photographs and DEMs from LiDAR and AHN datasets, or in other words how the calculations of volumetric changes were done. Chapter 4 presents the results obtained in the current research, highlighting the ground control points used in the study area, the results of point cloud data, and the DEMs extracted from the 1945 and 1981 aerial photographs, as well as their comparison to the LiDAR and AHN datasets. Chapter 5 demonstrates the discussion about the outcomes and deliverables, such as the organization, integration and interpretation of the results. The sixth chapter gives a conclusion for this study, answering the main and sub research questions, moreover presenting suggestions and recommendations for further studies in this research field. Finally, in the last chapter, the seventh, the list of all literature references used in this project are provided.

1.7 Study Area

The Wadden Sea is the sea between the Wadden islands in the north of the Netherlands and the Dutch mainland. The study area of this research is the east part of the Vlieland island. It is the second island from the west in the chain, lying between Texel and Terschelling. It is the second highest inhabited Wadden Island of the Netherlands, with a population of 1,151 inhabitants, and with an area of 37 km² (Dutch Census, 2011). The map below shows the study area (Figure 1).

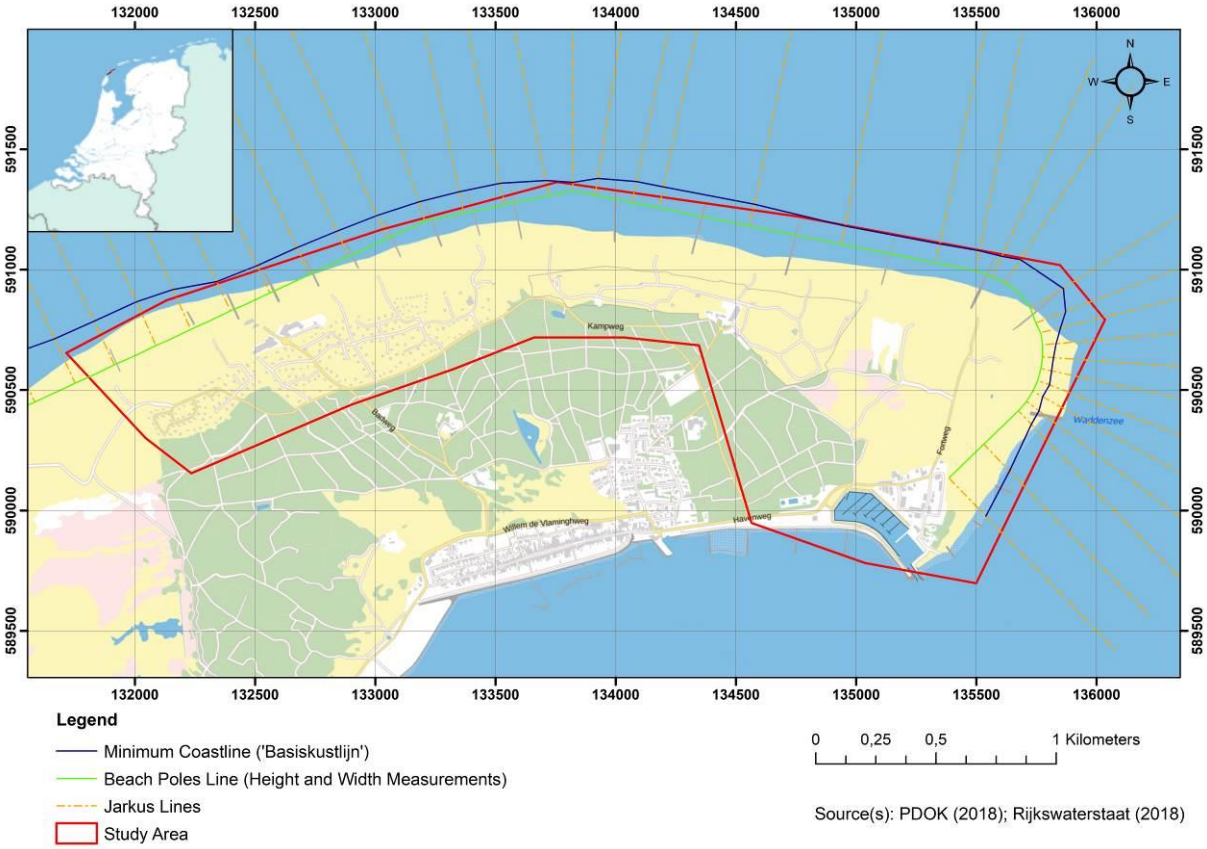

Figure 1: The study area of the current research at East-Vlieland island, the Netherlands.

2. Theoretical Background

2.1 Background History

Photo interpretation is an analytical tool and has an important value to research in the context of urban and landscape studies. The use of this method or technique is well-known and continue its growth. Besides, people with no expertise in the area are able to interpret and analyse air photos because there is no need of specialized knowledge of photographic and photogrammetric processes. Aerial photos provide a basis for defining problems, are useful for knowing study areas, planning field trips or mapping, as well as studying inaccessible areas. These photographs may replace and be used as a map where researchers can save, or record information obtained elsewhere. The photos are also of value as permanent records of continuously landscape changes in specific time and place (Gilliam, 1972).

Aerial photography has been used intensively as a remote sensor in the identification and mapping of natural resources. Due to its potential for use, aerial photographs are used as a working tool in the most different fields, such as: Geography, Geology, Hydrology, Ecology, etc. According to Salichtchev (1973), cartographic representations can be expressed by images, graphic or generalized symbols, retracting the distribution of natural and cultural phenomena with their relations and changes in time and geographical space. The growing need for representation of geographic space and phenomena has enabled the emergence of technological advances such as digital cartography, remote sensing and geoprocessing. This allowed for a constant analysis and systematization of geographical knowledge, improving research in several areas.

Ruff (1954) points out that topographic maps have been commonly used as base map in many areas, but the speed and accuracy of geologic mapping, for example, may be greatly increased by using aerial photographs together with the topographic maps. And in case there are no topographic maps available, the aerial imagery may be an input to construct a topographic map.

Photogrammetry is called as a technology-based science by Linder (2016) with more than a century of development. The advances during this period provided changes from optic-mechanical equipment to a digital workflow world. This science can be defined as the science of measuring with photos, being an important part of Geodesy and Remote Sensing. Again, people with no expertise in the area may benefit of these advances and are able to use these methods.

According to Walstra (2006), the development of photogrammetry initiated in the 19th century, divided by Konecny (1985) into four main phases:

Plane table photogrammetry (1850-1900), which the aerial photographs were used to provide topographic information. The results were utilized in many fields as military, architecture, archaeology and glacial surveys.

Analogue photogrammetry (1900-1960) was the time when the stereoscopy was largely used, and the technological advance allowed that new techniques to have been created and applied, such as aerial survey cameras making vertical photographs with regular overlap.

Analytical photogrammetry (1960-1985) was marked by the creation of the computers when it was possible to process analytical restitution faster.

Digital photogrammetry (1985-present) was the new development into the photogrammetry world, being possible due to the increased or technological advance of the power of computers, which started automated digital processing of the aerial photographs.

2.2 Photogrammetry in the third dimension

The use of vertical aerial photographs among remote sensing products has become increasingly frequent, mainly because it replaces with advantages other cartographic bases. Besides, it also offers great details of the landscape, and for instance also eliminate the difficulty access in certain areas, providing a three-dimensional view, increasing the efficiency and accuracy of mapping activity.

A single aerial photograph represents a two-dimensional plane with two-dimensional coordinates as well. To get a third-dimension context, it is necessary at least two photographs, which their combination will provide enough information to extract the third dimensions coordinates. The stereoscopy viewing is used in photogrammetry to perform the process explained above; using two or more photos of the same area, it is possible to calculate and extract the three-dimensional coordinates of the same points in both photos (Linder, 2016). The calculation of the three-dimensional coordinates (x, y, z) is dependent of the recognition of all geometric parameters when the photos were taken. Identical points in both photos (in overlap part) are calculated by their intersection (Figure 2).

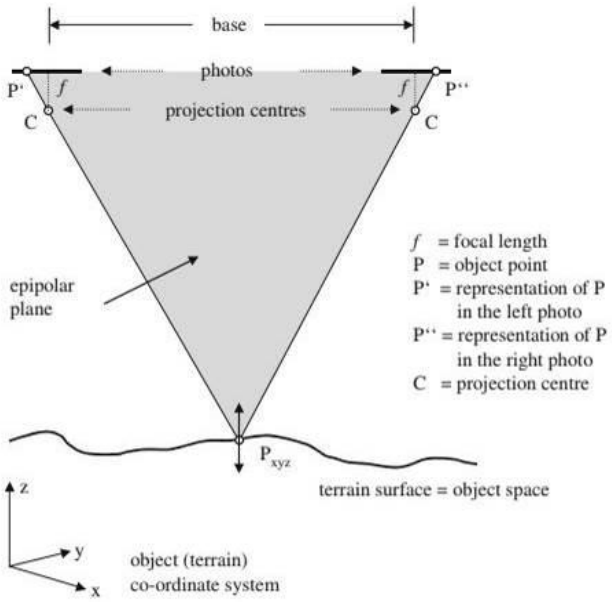

Figure 2: Geometry in an oriented stereo model, an example model of aerial photogrammetry (Linder, 2016).

Generally, the components of an aerial camera are composed by lens, inner cone, focal plane, outer cone, drive mechanism and magazine. The image is then created in the focal plane with fiducial marks, which coordinates are known. These fiducial points can be located at the corner of the images or either in the middle of the four sides (Schenk, 2005).

According to the Natural Resources Canada (2016), the scale of a determined aerial photograph can be calculated by the ratio between the camera's focal length and the plane's altitude above the ground being photographed (Figure 3).

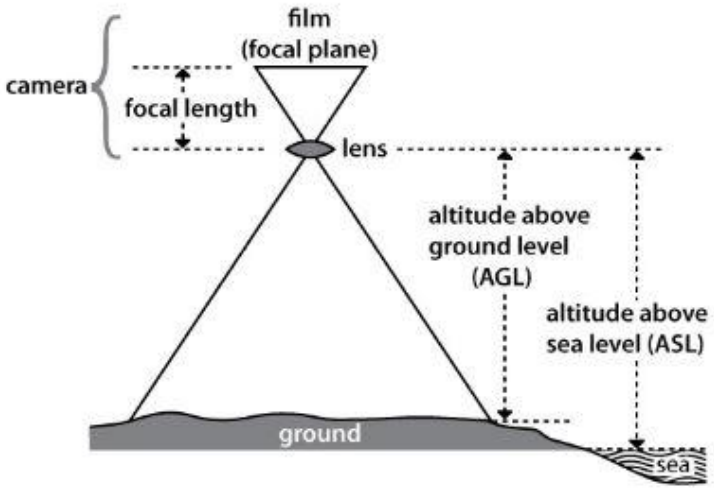

Figure 3: Relation between focal length and altitude above ground level (Natural Resources Canada, 2016).

Aerial photographs are usually taken with a camera coupled to the airplane; when the aircraft moves forward the images are taken, and the stationary objects are recorded at different image locations (Schenk, 2005). The flight strip is made considering 60% of forward overlap and around 30% side overlap between the photos (U.S. Army Corps of Engineer, 1993) (Figure 4).

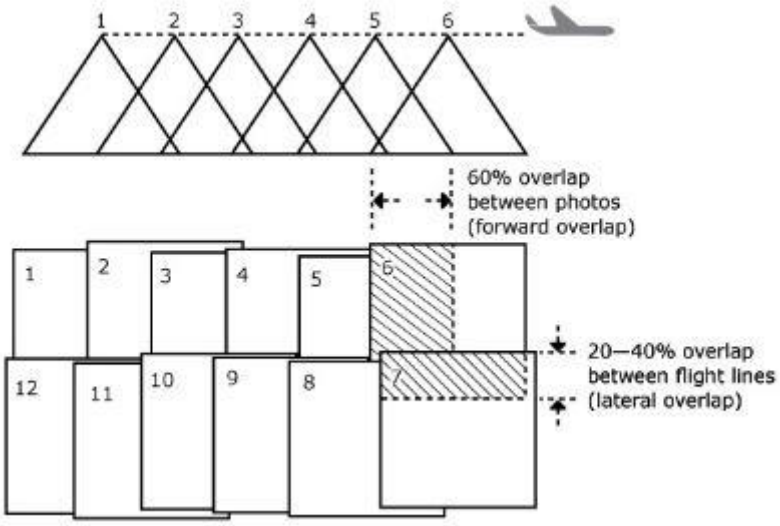

Figure 4: Flight strip of aerial photographs acquisition representing forward and side overlaps (Natural Resources Canada, 2016).

2.3 Stereoscopy

One of the most important outcomes of photogrammetry is the stereoscopy property as already explained before. Using stereo pairs of aerial imageries, one can perform a huge amount of analysis; there is a broad amount of field applications, such as remote sensing, topographic mapping, geology, archaeology, architecture, engineering, etc. The stereopairs can be used as input to create Digital Elevation Models, namely Digital Terrain Models (DTM) and Digital Surface Model (DSM).

2.4 Digital Terrain Model (DTM) and Digital Surface Model (DSM)

The DTM is a digital representation of the terrain given by the three-dimensional coordinates (x, y, z). It is defined as a two-dimensional discrete function of a morphometric variable, being the topographic surface set of values measured or computed at the grid nodes (Florinsky, 2016). It represents the terrain surface without any objects.

One known type of DEM is the Digital Surface Model (DSM). The DSM is the digital representation of the land surface elevation with respect to any reference datum, containing the z values at the top of objects on the terrain (Linder, 2016), being the simplest form of digital representation of topography (Figure 5). DEMs are used to determine terrain attributes for instance elevation, slope and aspect (Balasubramanian, 2017).

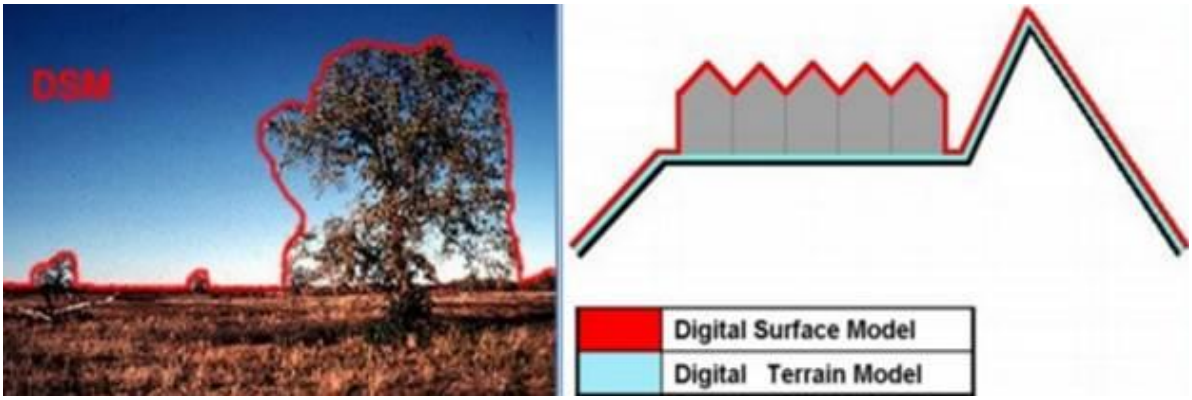

Figure 5: Representation of Digital Elevation Models (DEM), and comparison of Digital Surface Model (DSM) and Digital Terrain Model (Clavijo, 2013).

To perform a DEM, Walstra (2006) explain that rectangular grids or Triangular Irregular Networks (TIN) are necessary. The procedures of creating a DEM are represented by image matching (stereoscopic viewing), surface fitting (or interpolation) and quality control (Schenk, 1996).

The DEM is one of the most employed raster datasets, grid or matrix, in GIS field, having a height value for each square cell of the grid. The elevation values of the cells may be interpreted as two distinct ways, being one with the entire cell area having the same value, and the other with the area between the cell centres presenting intermediate values. The DTM is a continuous, normally smooth surface, that also presents other features, which describe a topographic surface, beyond height values, such as aspect, slope, gradient, and skeletons like pits, saddles, ridges, peaks (Podobnikar, 2009).

Dottori *et al.* (2013) states that considering average cell size, DEM resolution can be divided into three categories, being with low or coarse resolution, a mesh of 20 m or coarser; high or fine in an interval of 5 and 2 m; and very fine resolution less than 2 m. According to Muller (2015), it is common sense in academia that DEMs with a mesh of 2 meters or less are usually classified as high-resolution DEM, but some also consider very fine resolution DEMs with 5 meters mesh.

2.5 Light Detection and Ranging (LiDAR)

Airborne LiDAR data is being performed since the 1980s considering topographic data collection, and it is often used for many purposes, for instance coastal zone monitoring, geomorphological research, infrastructural and environmental projects, and archaeological surveys (Werbrouck, 2011). It is usually accepted as the most prominent technique for delivering highly accurate height data, being an optical remote-sensing method that uses laser light to densely sample the surface of the earth trough highly accurate position (x,y,z) measurements. LiDAR method has direct impact as a cost-effective 3D measurement with high accuracy.

According to Drosos and Farmakis (2006), LiDAR consists of sub-randomly distributed three-dimensional terrain point data, which measures the terrain elevation through a laser pulse originated from the time between emission and reception of reflected pulses, registering the x-, y- and z-coordinates (Figure 6). It is an active remote sensing technique (Mutlu et *al.*, 2008).

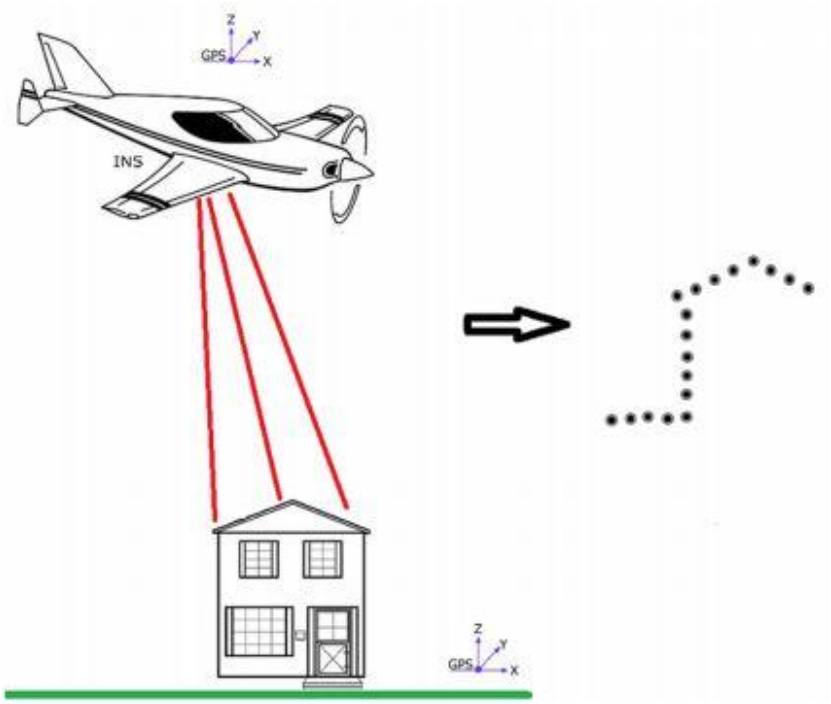

Figure 6: Airborne LiDAR data collection scheme. The laser scanner accoupled to the airplane records the time traveling distance outcoming a point cloud data (Sun, 2013).

LiDAR data are extensively used and brings several important advantages, which five out of total can be namely as, i) high accuracy data, ii) fast data acquisition, iii) large coverage, iv) weather/light independence, it can penetrate canopy and leaves, v) the independence of ground control points (Kim, 2015). High accuracy data and its fast acquisition are challenging and are also requirements for a variety of fields. LiDAR data covers these requirements, filling the increasing demand for 3D data with high density, accuracy and cost-effectiveness.

2.6 Actueel Hoogtebestand Nederland or Current Elevation data for the Netherlands (AHN)

The Current Elevation data for the Netherlands (AHN) is the digital height map for the whole Netherlands (Figure 7), containing detailed and precise height data with an average of eight height measurements per square meter (Water boards, 2019). According to van Meijeren (2017), there are three versions available for the AHN, differing in their resolution.

AHN is largely used by organizations such as the water boards, municipalities and *Rijkswaterstaat* for water and flood defense management. Considering the altitude and the gradient of the ground level, some considerations can be made about water flow, for instance if the water can flow sufficiently from the land, how high the water level in the ditches may be, if the water in rivers, floodplains and ditches can be enough drained and whether the dikes still sufficiently high and strong. The water boards also add that the AHN is often used for many different reasons, the daily management and maintenance of dikes, the making of specifications for major maintenance, 3D mapping, and licensing are among the types (Water boards, 2019).

The measurement of AHN is basically made through laser altimetry or LiDAR, using an aircraft or helicopter with a laser beam scanning the earth's surface. The measurement of the running time of the laser reflection and of the position of the aircraft together give a very accurate result (van Meijeren, 2017). To perform a complete AHN dataset takes several years (Water boards, 2019).

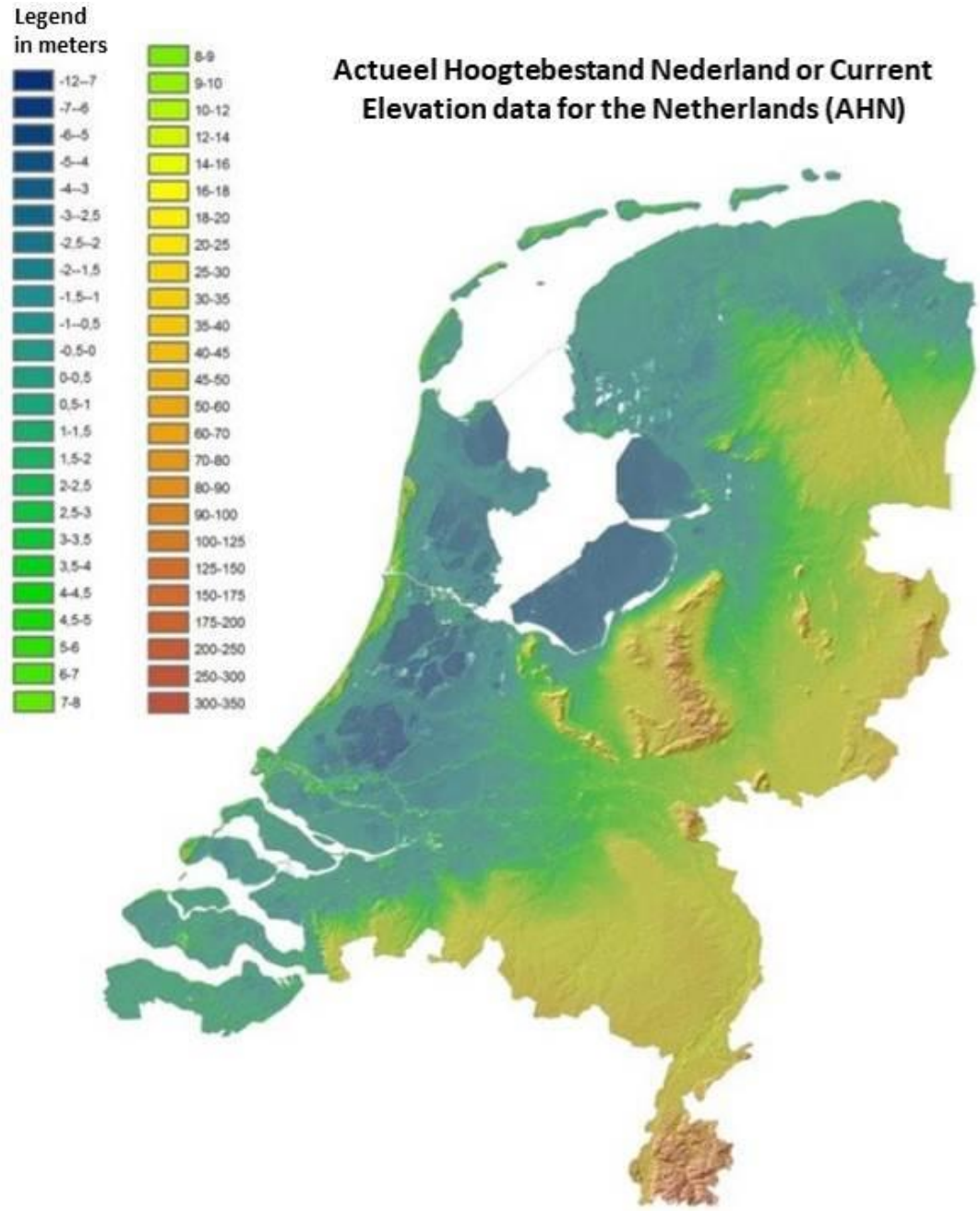

Figure 7: Current Elevation data for the Netherlands (AHN) (Modified from van der Sande *et al.*, 2010).

2.7 Dense Image Matching

Image matching can be defined as the correspondence between two or more images, estimating the correspondence of x, y and z coordinates through collinearity. Digital imaging technology allowed the creation of automated image matching methods. In the early 1990s, the automatic extraction of DSMs from aerial photographs using stereo-image matching was introduced. It started using based matching algorithms, extracting feature points and correlating them with their match in the overlapping images. These innovative image-matching algorithms and new improvements in hardware made photogrammetry be re-emerged in the automated photogrammetry field (Remondino *et al.*, 2013).

Dall'Asta and Roncella (2014) explain that there are two main domains regarding dense matching algorithms, local methods, and global/semi-global methods. The first one evaluates the correspondences between one point at a time, while the other two enforce the results through estimation. Local methods are very efficient and accurate, but also very sensitive for sudden variations along the study area. On the other hand, global and semi-global algorithms tend to be more effective considering such disparities, making assumptions on the regularity of the results, overcoming the local limitation. An example of local method is the normalized cross correlation method (NCC), and the semi-global matching (SGM) is an example of the global method.

2.7.1 Normalized Cross Correlation (NCC)

The NCC method is a local method using the point-wise approach, or evaluating the correspondences of one point at time, through their radiometric intensities within a finite support window. It works with a reference image and a slave image, searching for a similarity between their points where the patch window looks for all possible location in the slave image that corresponds to the reference one (Dall'Asta, 2016) (Figure 8).

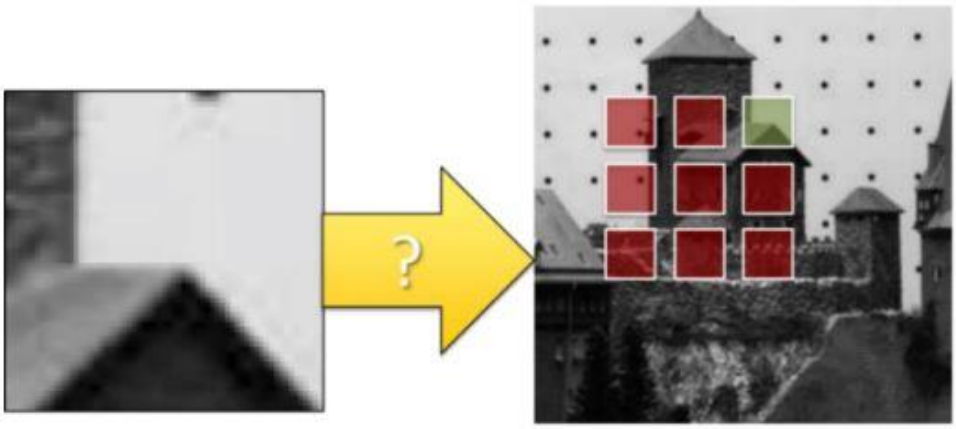

Figure 8: NCC takes a template in the reference image on the left and moves it along the slave image on the right to match its corresponding area (Dall'Asta, 2016).

Suri (2010) adds that this method is very useful for misaligned small shifts on imagery, both on vertical and horizontal directions. Zhao *et al.* (2006) corroborates affirming that NCC has a limitation being sensitive to scale and rotation changes, however it is a simple and suitable method for similarity measurement, being stable or balanced considering linear brightness and contrast changes.

2.7.2 Semi-Global Matching (SGM)

The SGM method is a global method that performs a pixel-wise matching using a minimization of a global smoothness constraint, relating each pixel coordinate in the base image to its corresponding pixel coordinate in the match image (Haala, 2011). This method was originally introduced by Hirschmüller (2005) and most of the dense image matchers use SGM.

The algorithm symmetrically computes the pixel matching cost considering many paths in the image, and using a known disparity value, it relies on the extraction costs for each path, summing afterwards the costs for each pixel and disparity value, resulting in a pixel matching solution with the minimum cost (Dall'Asta and Roncella, 2014) (Figure 9). According to Haala and Rothermel (2012), using high-resolution digital airborne imagery, SGM can perform a successfully matching procedure resulting in a 99% of all pixels. It also can reach matching accuracy of 0.1 to 0.2 pixels in image space or 0.25 ground sample distance (GSD) in object space.

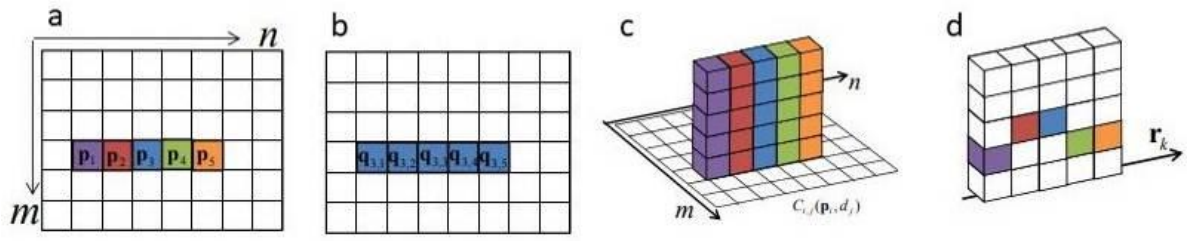

Figure 9: Base image pixels and their potential correspondences in the match image (a and b). Costs related to the 3D cost cube and the minimal cost path along the match image, c and d respectively (Modified from Haala, 2011).

2.8 Data Quality

The International Organization for Standardization (ISO) considers five components of data quality: completeness; logical consistency; positional accuracy, temporal accuracy, and thematic accuracy. The DEM extraction performed in this research was evaluated in terms of accuracy, specifically the positional accuracy of the outcomes, represented by point cloud data and the DEMs, and their comparison using two different methods as NCC and SGM.

Assessment of DEMs are mostly related to the analyses of the input datasets and the methods used to perform the models. The absolute and relative accuracy of the data can be distinguished, as well as the horizontal and vertical position of objects, assigning accuracy and irregularities in the shapes of the DEMs, for instance ridges on the edges and sink holes, one can provide an analysis on their quality (Podobnikar, 2009).

There are also two terms that directly relates to accuracy: precision and error. The first one correlates to resolution and scale, while the second one stands for a lack of quality or even little or no accuracy. In addition, both terms can also be determined through the standard deviation (σ), when considering precision, and the root mean square error (RMSE), when considering a level of error (Podobnikar, 2009).

The standard deviation is a parameter that is used to quantify the variation or dispersion of values in a data. When the values of standard deviation are increasing, they are getting more spread and distant of the mean values, resulting in a worse product, meaning that the point cloud data gets worse. A smaller standard deviation results in a better product, due to the values getting closer to the mean, resulting in a more accurate point cloud dataset (Alexiou and Ebrahimi, 2018).

Root mean squared error (RMSE) is a quadratic scoring rule that measures the average magnitude of the error. It is the square root of the average of squared differences between prediction and actual observation. In the field of geosciences, many authors present the RMSE as a standard metric for model errors e.g. McKeen *et al.*, (2013) and Savage *et al.* (2013); and RMSE has been used as a standard statistical metric to measure model performance such as in meteorology, climate and geospatial research.

As a convention, RMSE is calculated to assess the accuracy of the resultant geometric correction. It is based on the resultant vector from x and y residuals of the GCPs and may be estimated through $RSE = \sqrt{u^2 + v^2}$ where u is the residual of x and v is the residual in the y coordinate. The total RMSE is determined by the equation:

$$Total\_RMSE = \sqrt{\frac{1}{n}\sum_{i=1}^{n}\left(u^2 + v^2\right)}$$

,

where n is the number of GCPs. Some authors stated that when the GCPs that have high value of RMSE are removed, the total RMSE result may improve the quality of the georeferencing model, which means that the RMSE is reduced (Nguyen, 2015).

Martínez-Carricondo *et al.* (2018) states that the accuracy of the DEM and orthophoto is a consequence of the photogrammetric process, dependent of the number and distribution of the GCPs, also adding that as the flight height increases the accuracy gets worse. Despite the determination of the GCPs and the tie points is time-consuming, this measurement is highly recommended since it affects the quality of photogrammetric outcome (Kim *et al.*, 2014).

Besides the statistical evaluation of point clouds, another quality assessment method that can be applied to DEMs is the visualization. Visual methods for assessing data quality do not consider statistical elements, but only visual aspects to identify errors or problems with the extracted DEM. Derivatives from digital elevation models may be used for this visual evaluation and may include, for instance, slope, aspect, terrain roughness, cost surfaces, curvature, and contour lines. A clear example is provided in the Figure 10, where two different DTMs are compared through a cross section of the same area showing distinct roughness (Podobnikar, 2009).

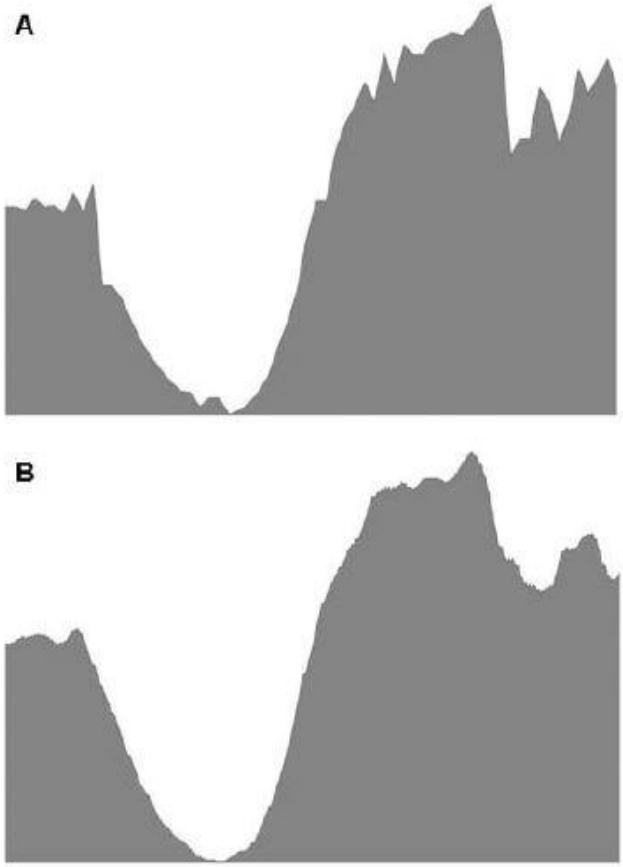

Figure 10: Terrain profiles from the same area from two different DTMs. The first one (A) is much rougher than the second (B) (Podobnikar, 2009).

3. Methodology

The current research quantified the volumetric changes of the coastal areas of East-Vlieland, Province of North Holland, in the Netherlands. The research methods that were applied combined geo-information sciences (GIS) techniques to perform DEMs in the study area, and calculations regarding the volumetric changes in the coast. The study was oriented towards to accuracy, efficiency, appearance and reliability of the DEMs and the final outputs (the mosaic of the orthorectified aerial photographs and the volumetric changes in the coast).

The study made use of digital photogrammetry, by means of historical aerial photographs from the East-Vlieland island, as well as AHN and LiDAR datasets of the study area. The software ERDAS Imagine 2018 was used for digital image processing, creating point clouds and DEMs for each period considered in this study, the years of 1945 and 1981. Methods as NCC (eATE) and SGM (Tridicon) were used and compared during the quality assessment of the DEM extraction.

3.1 Research Workflow

The current research made use of historical data as aerial photographs to perform DEMs of the study area quantifying the volumetric and landscape changes along 72 years, between 1945 and 2017, and comparing the results with AHN and LiDAR datasets. First, a literature review considering the subjects photogrammetry, DEM, LiDAR, AHN, and data quality assessment is necessary to provide an overview and in-depth knowledge about the theme. Then, the second step is the data pre-processing, organizing and preparing all necessary datasets for this research. After that, the data processing took place, which is the most time-consuming step in this project, and it is where the creation and calculation of point clouds and the DEMs of each dataset were made. Fourth phase is represented by the data analysis, when calculations and changes of the volumes and landscape of the study area were performed. Finally, all outputs and results are presented in this thesis dissertation or research report. The workflow is illustrated in the Figure 11.

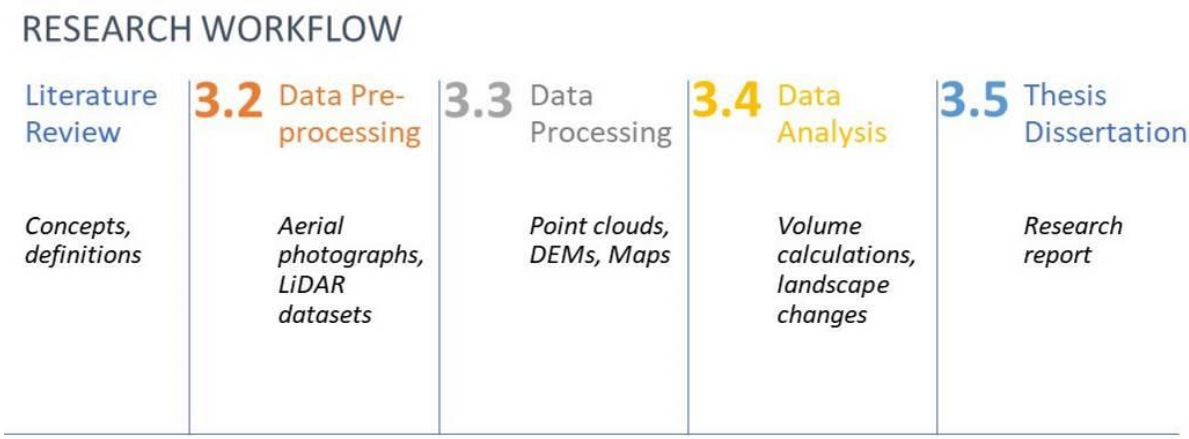

Figure 11: Workflow of the current research.

3.2 Data Pre-processing

This research was carried out with data retrieved from different databases. The set-up consists of historical aerial photographs, coastal LiDAR datasets, and the *'Actueel Hoogtebestand Nederland'* (AHN) in Dutch or Current Elevation data for the Netherlands.

The aerial imagery used belongs to the years of 1945, 1981; and are given by courtesy of Dotka Data BV and Utrecht University, respectively (Table 1). For this set of imagery, the spatial reference system chosen is the UTM (zone 31 North) and the vertical datum the WGS 84. The reason behind this choice is influenced by selecting Google Earth Pro as a reference for the determination of the GCPs in the study area, which also uses UTM and WGS84 coordinate system.

Year	Imagery	Camera	Image scale
1945	Royal Air Force (RAF), Analog, Grayscale, 3 strips	Frame camera; Focal Length: 914.00mm	1:7400
1984	Analog, Grayscale, 3 strips	Leica RC10; Frame camera; Focal Length: 151.56mm	1:5000

Table 1: Aerial imagery information used for the study.

The AHN used covers the year of 2014 and contains detailed and precise height data with eight points per square meter. The AHN available for Vlieland used in the current research was provided by courtesy of PDOK website (https://www.pdok.nl/) via Utrecht University server. In addition, coastal LiDAR datasets, in raster formats were also utilized to perform the comparison with the extracted DEMs. The LiDAR data used correspond to the years of 1997, 2004, 2014 and 2017. These data are also courtesy of Utrecht University.

3.3 Data Processing

The software that was used for the DEM extraction was ERDAS Imagine 2018, a digital image processing software. Moreover, ArcMap 15.1 was used for processing the data when required, for instance clipping datasets, creating DEMs of difference, volumetric calculations, visualization and creation of maps from the study area with the results. ArcScene was also utilized for 3D visualization of the point clouds data and the DEMs. In addition, as mentioned before, Google Earth Pro was used as a reference during the processing steps of the aerial imagery, retrieving the x, y, and z coordinates of the GCPs. All steps that were taken during the DEM extraction are explained below and illustrated in the Figure 12.

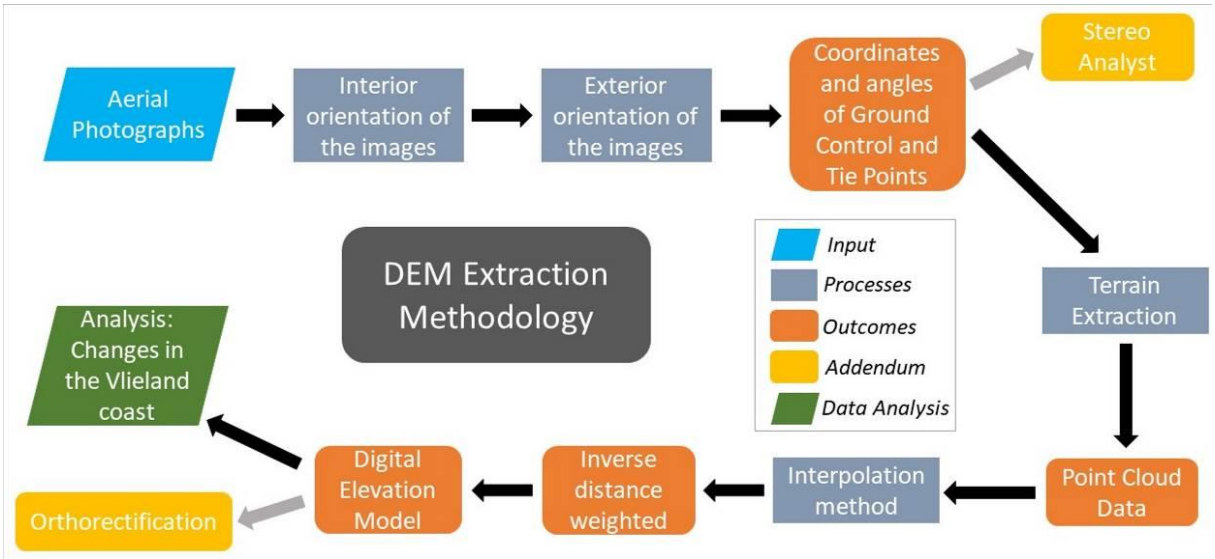

Figure 12: Flowchart of all steps that were performed during the DEM extraction.

3.3.1 Processing aerial photographs

For the construction of precision topographic maps, it is necessary to reconstruct the exact position of each photograph at the time they were taken. This procedure is known as the interior orientation of the stereoscopic model. The relative orientation is the reconstruction of the position of one photograph relative to another, which is obtained by taking the pairs of images of the same object in both consecutive photographs. Absolute orientation is the location of both photographs relative to the terrain (Walstra, 2006).

3.3.2 Interior Orientation

Wolf and Dewitt (2000) point out that the elements of interior orientation define the internal geometry of a camera. Aerial mapping cameras have their calibration certificates usually provided by the camera manufacturer, which informs the location of the principal point, focal length, photo coordinates of the fiducial marks, and measures of lens distortion. The focal length is the distance from the principal point to the perspective center, and this principal point is a line from the rear nodal point of the camera lens, being perpendicular to the focal plane. The principal point recognition is also supported by the fiducial points of the photo, which are on four sides of the images and have a known position relative to the principal point (Walstra, 2006).

3.3.3 Exterior Orientation

According to Sijmons (2018), the exterior orientation is the relationship between the digital image (pixel) coordinate and object space (latitude and longitude) coordinate system. In order to obtain the exterior orientation is necessary to obtain the parameters x, y and z coordinates, and the omega, phi and kappa angles as well (Schenk, 2005; Linder, 2016). Zhang *et al.* (2004), point out that for georeferencing the aerial photograph it is necessary to establish some well-defined GCPs. These points are controlling references in the images and are chosen manually. Afterwards, the recognition of control points, or tie points, is defined by an automated process, which also estimates the exterior parameters, improving robustness and accuracy. The triangulation method is then applied determining the spatial intersection of image rays of a finite point from its position on the overlapped photographs. It is an analytical procedure which generates enough image points in order to reference and overlap them with much accuracy as possible (Falkner and Morgan, 2002). It also provides the Root Mean Square Error (RMSE) report for control and checkpoint measurements (Walstra, 2006; Linder, 2016).

3.3.4 Point Clouds

The point cloud is a LAS file where a classification is applied to the individual points. Each point is assigned to one of the following classes: ground level, buildings, water, etc. In addition, extra attributes are included per point. LAS is the standard binary format for storing and exchanging LiDAR data. Performing point clouds from the aerial photograph is a standard step in the current project.

In the photogrammetry project of ERDAS, four different algorithms are included for point cloud generation: Automatic Terrain Extraction (ATE), the enhanced version (eATE), both using using NCC method, and two Semi-Global Matching (SGM) methods (XPro and Tridicon). In the current project, both NCC (eATE) and SGM (Tridicon) were used to generate point clouds from the aerial imageries.

3.3.5 Normalized Cross Correlation (NCC)

Normalized cross correlation (NCC) is an image processing method, an algorithm that computes in the spatial domain of the input images. It uses the code on two stereo pairs through a square template window, which is simultaneously moving along the overlapping area, performing horizontally cross-correlation or image correlation, especially considering their brightness contrast. As this computation is normalized a comparison between the correlation coefficients and between the images can be made (Bickel *et al.*, 2018).

Enhanced Automatic Terrain Extraction (eATE) is a key component of digital photogrammetric software. It performs image correlation using the NCC method, being widely used, resulting in reliable and accurate outcomes. eATE generates multiple elevations of the same point, performing blunder detection, choosing the most reliable and accurate elevation (Zhang *et al.*, 2006). In East-Vlieland, the NCC (eATE) method was used for creating point clouds from the aerial imagery of the years 1945 and 1981.

3.3.6 Semi-Global Matching (SGM)

The Semi-Global Matching (SGM) stereo method is based on pixel matching cost of Mutual Information (MI), balancing the radiometric differences of input images, also using a smoothness constraint. The process is done by developing a global cost function (Hirschmueller, 2008),

aggregating the matching costs in accordance to the smoothness constraints. The minimum set of costs results in a disparity map for a stereo pair and then to a 3D point clouds dataset (Nebiker *et al.*, 2012).

According to Hirschmueller (2005), using SGM provides a high level of matching pixels creating very detailed 3D models. In ERDAS, the difference between the SGM XPro and Tridicon terrain extraction option is that XPro can be only used for digital camera imagery as input, while Tridicon can be used for digital camera imagery and satellite images, however both can generate high-resolution data. For the current study, in East-Vlieland, the SGM Tridicon was used for creating point clouds from the aerial photographs of 1945 and 1981. Since the SGM may not be used with frame cameras, in the current project it was made a test using the aerial photographs as if they were imagery from a digital camera.

3.3.7 Interpolation operation

Two methods can be used to interpolate the points clouds in order to create a surface; the triangular irregular network (TIN) and the inverse weighted distance (IDW), and both can be performed either in ERDAS Imagine or in ArcMap 15.1. Their products represent the surface of a given area and show the intervals of elevation data. In the present study, the chosen interpolation method was IDW, which is a deterministic mathematical interpolation method that assumes that closer values are more related than further values, spatial autocorrelation assumption (Zhang *et al.*, 2016).

3.3.8 Digital Elevation Model (DEM)

The creation of Digital Terrain Models is performed using two or more aerial photographs pre-processed, with interior and exterior parameters, triangulation procedure and point cloud extraction already made. The processes of performing a DEM are represented by image matching (stereoscopic viewing), surface fitting (or interpolation) and quality control (Schenk, 1996). At this phase, a DEM was made for the years of 1945 and 1981 from East-Vlieland, generated from point clouds of NCC and SGM methods.

3.3.9 Orthorectification

The concept of orthorectification is explained by the U.S. Army Corps of Engineer (1993) as being the process of constructing photographs from vertical aerial images without errors, distortions, displacements, and interferences. This process is highly dependent on the quality of the DEM (Jaud *et al.*, 2014). An outcome or deliverable of the current research are the orthorectified photographs of the study area for the years 1945 and 1981, using DEMs made from the point clouds of both different algorithms, NCC and SGM.

3.4 Data Analysis

The DEMs, the LiDAR data and the AHN were used as input to calculate the changes in the East-Vlieland island. These changes were quantified by means of calculating the volumes of the coast for each studied year. Determining the changes is necessary to quantify the coast behaviour along the decades.

In the current research, two main steps were taken in the analysis. The DEM of Difference was made for a visual representation of the elevation changes, and then the Surface Volume tool of ArcMap was used to calculate the volumes. After, a comparison of volumes can be made for the studied years from East-Vlieland island. The workflow of the data analysis is displayed in the figure 13.

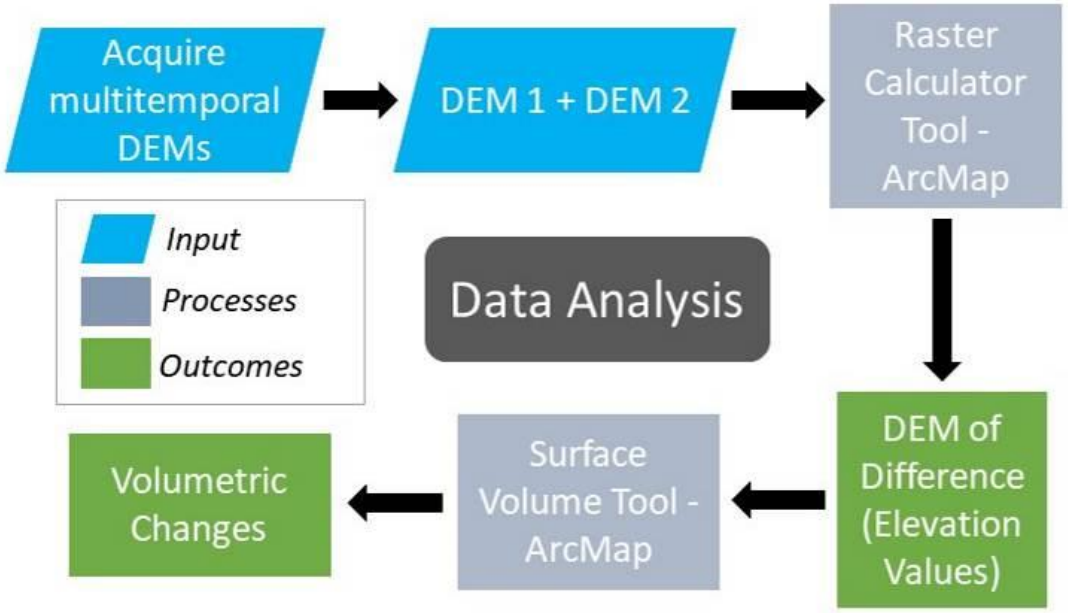

Figure 13: Flowchart of all steps that were performed during the data analysis, when the quantification of volumetric changes took place.

3.4.1 DEM of Difference

The DEM of Difference (DoD) is the result of DEM differencing of an area of interest. It is the quantitative estimation of changes of landforms comparing two DEM products. To apply this technique, it is necessary to subtract elevation values of an older DEM from the elevation values of a newer DEM. The procedure is focused in the subtraction of the pixel values resulting in an output DEM that shows the elevation changes in volume (m^3) (Kaliraj *et al.*, 2017). As pointed out by Williams (2012), a mosaic of morphological change (DoD) will be the output from the following mathematical operation:

$$\delta E = Z_2 - Z_1,$$

where δE is the DoD showing the changes in elevation, Z_2 and Z_1 are the input DEMs from the studied years. The total volumetric change is obtained summing the total change of the produced DoDs (δE). Negative and positive values correspond to erosion and deposition respectively.

The resulting DoDs have elevation values, and to convert this to volumetric change, the elevation changes must be multiplied by the area of the grid cells. The changes in the study area were done using this technique comparing the studied years. On this step, the raster calculator tool in ArcMap was used, but to better automate the process, the ModelBuilder was also applied, where the input DEMs were added, differenced and resulted in the DoDs (Figure 14).

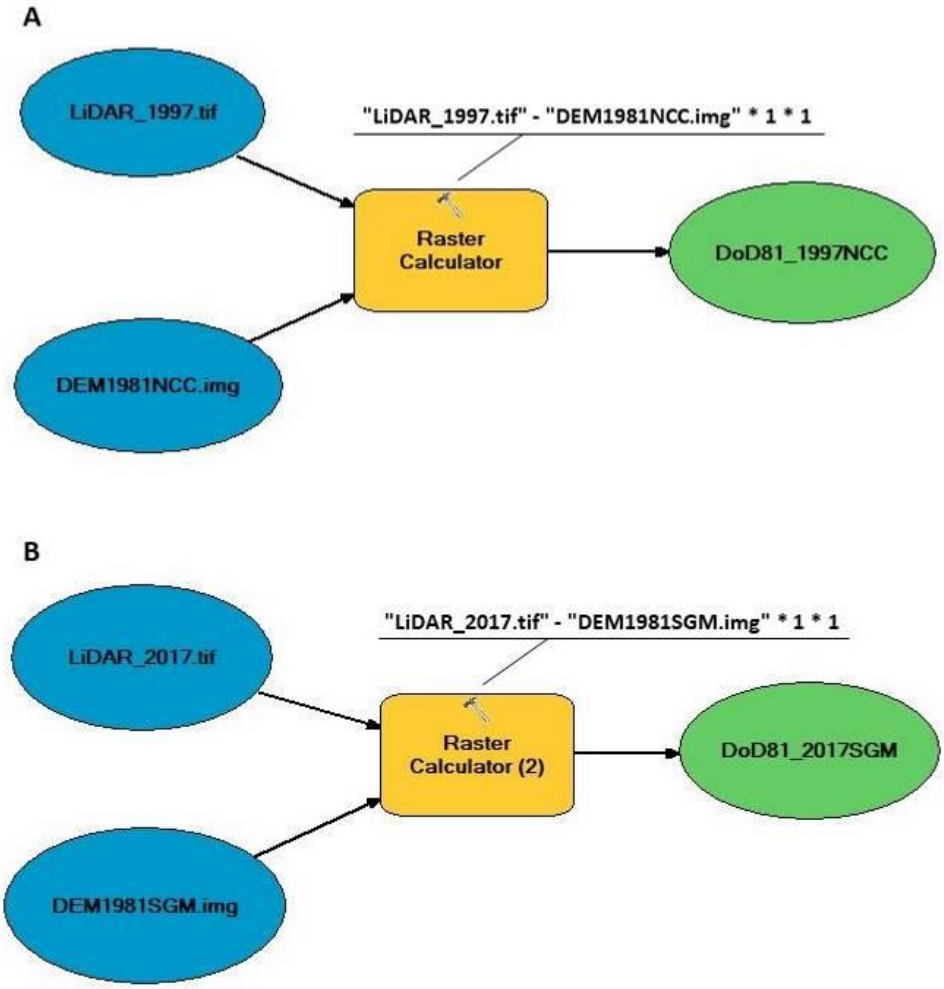

Figure 14: Geoprocessing workflow examples to create the DEMs of Difference using the raster calculator tool, with a highlight for the mathematical functions. A) Comparison between the LiDAR dataset of 1997 with the DEM of 1981 created by the NCC method. B) Subtraction from the DEM LiDAR of 2017 and the DEM of 1981, which was made using the SGM algorithm.

In order to calculate the volumetric changes, it is necessary to make use of the Surface Volume tool from ArcMap. It calculates the area and volume of a raster, TIN, or even a terrain dataset of the region between a reference plane and a surface, which can be above or below considering the reference plane. For this research, the volume calculations were also made in the ModelBuilder processing faster the results (Figure 15).

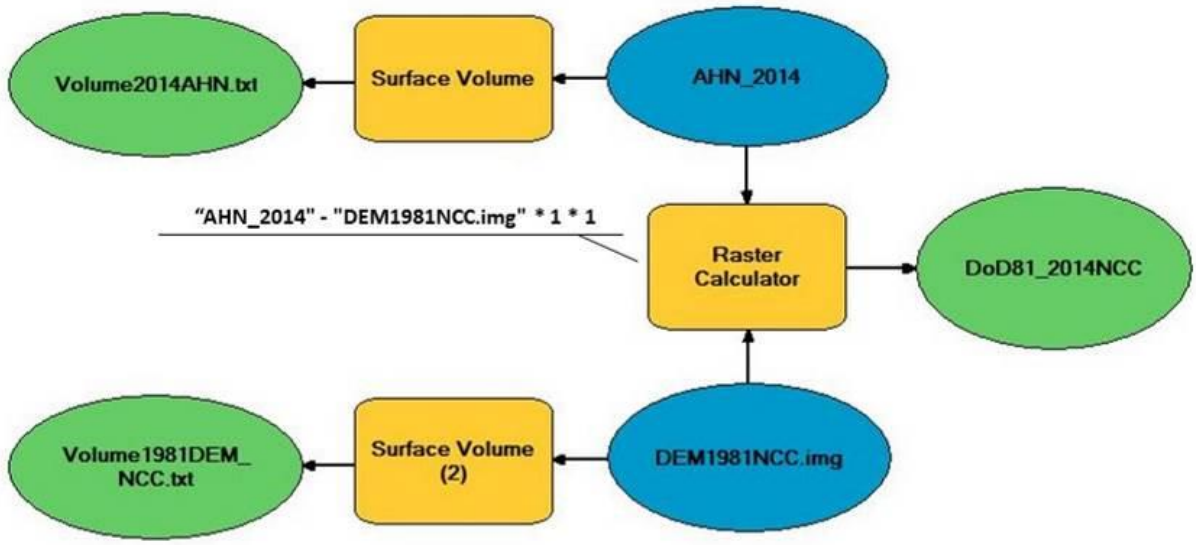

Figure 15: Geoprocessing workflow example to create the DoD using as input the AHN from 2014 and the DEM of 1981 made with the NCC method, and the application of the Surface Volume tool to calculate the volumes of the input rasters.

It is important to point out that to perform the data analysis it is of great importance to harmonize all input datasets. As some DEMs were created in ERDAS, and other came ready for use from different database or servers, such as the LiDAR and AHN products, they had different features. For instance, the grid cells of the rasters had different values, with resolution of 2 meters x 2 meters, 5 meters x 5 meters, and, most of them had the datum RD_New/Amersfoort as coordinate system.

To harmonize all inputs, first, when needed, they had their coordinate system switched to WGS84, due to the 1945 and 1981 DEMs being created based on WGS84 from Goggle Earth Pro. To make this change it was used the Create Mosaic Dataset tool from ArcMap, allowing to make that change without modifying any other element of the data. After that, the resample tool, once again from ArcMap, was used to resample the rasters to a 1 meter x 1 meter grid cell. These modifications made the input data comparable.

According to Milan *et al.* (2011), the results from the DoD should be critically evaluated, especially considering geomorphological changes. There is a need for assessment of the reliability of the DoD, mainly considering the input DEMs, which could have several factors influencing errors in their generation, for instance point quality, sampling strategy, topography and interpolation methods. This research did not evaluate the DoDs, but the created point cloud data as well as the DEMs used as input have been studied through a detailed data quality assessment explained in a later section of this report.

3.5 Research Report

Finally, the results of the previous steps are integrated and documented in this research report. This dissertation is then consisted of literature review, applied methods, obtained results, discussion, and conclusion with recommendations for further research and a critical reflection on the topic. At the end there are answers for the main research question as well as for the research sub questions, all previously mentioned in the research objectives section.

4. Results

The present research was carried out based on the DEM extraction process from aerial photographs, starting with the imagery georeferencing procedure, going to the generation of image-based point clouds for East-Vlieland for the years of 1945 and 1981, and the multivariate interpolation IDW method to perform the DEMs. The point clouds were made by using two different and common algorithms available for image matching processes, NCC and SGM.

4.1 Study Area and its Aerial Photographs

As illustrated before, the study area is located in the eastern part of the Vlieland island, in the Netherlands. It is lying between Texel and Terschelling in the chain of islands on the north of the country. The set of aerial photographs chosen from the year of 1981 were mosaicked and are shown in the figure 16. A total of 17 images were used for this stage of the research.

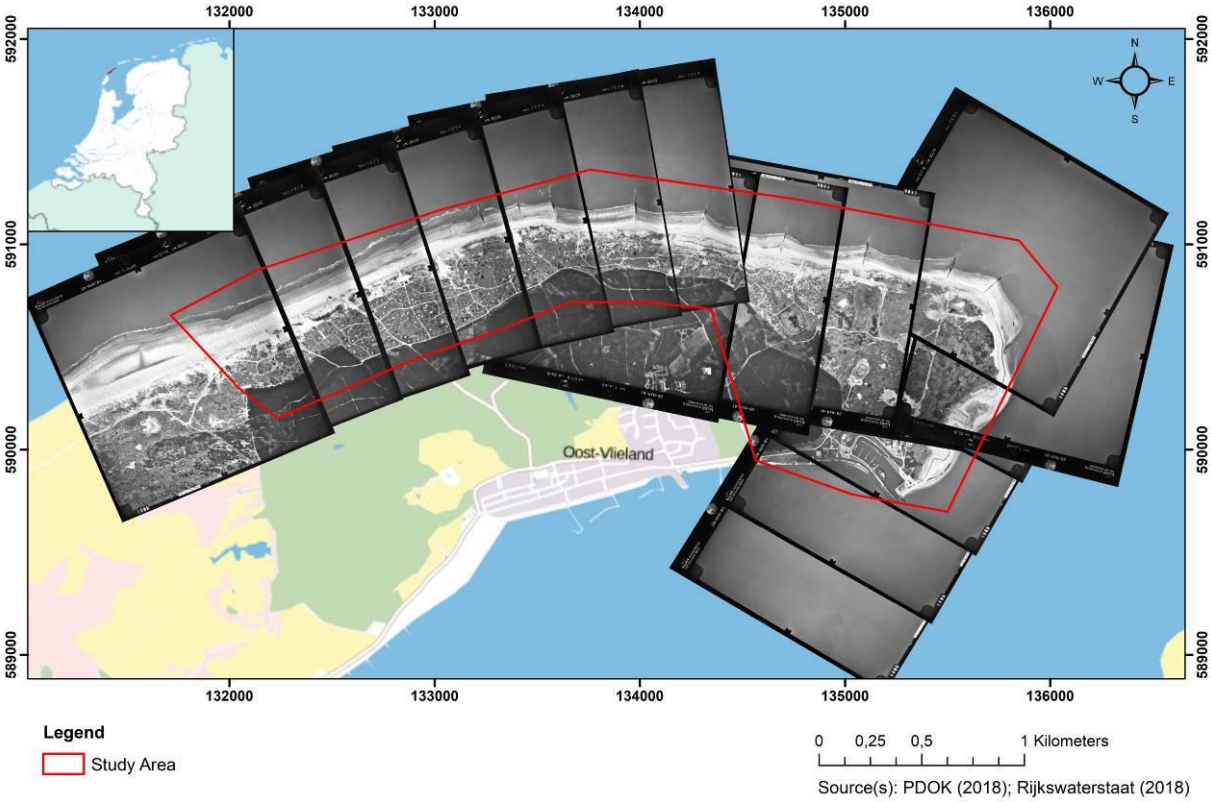

Figure 16: Set of 1981 aerial photography used to extract DEM for the study area.

A total of 13 photos from the 1945 imagery set were also used in this study. They cover the study area with a higher flying height compared to the 1981 set, and the mosaic of the 1945 photographs is shown in the figure 17.

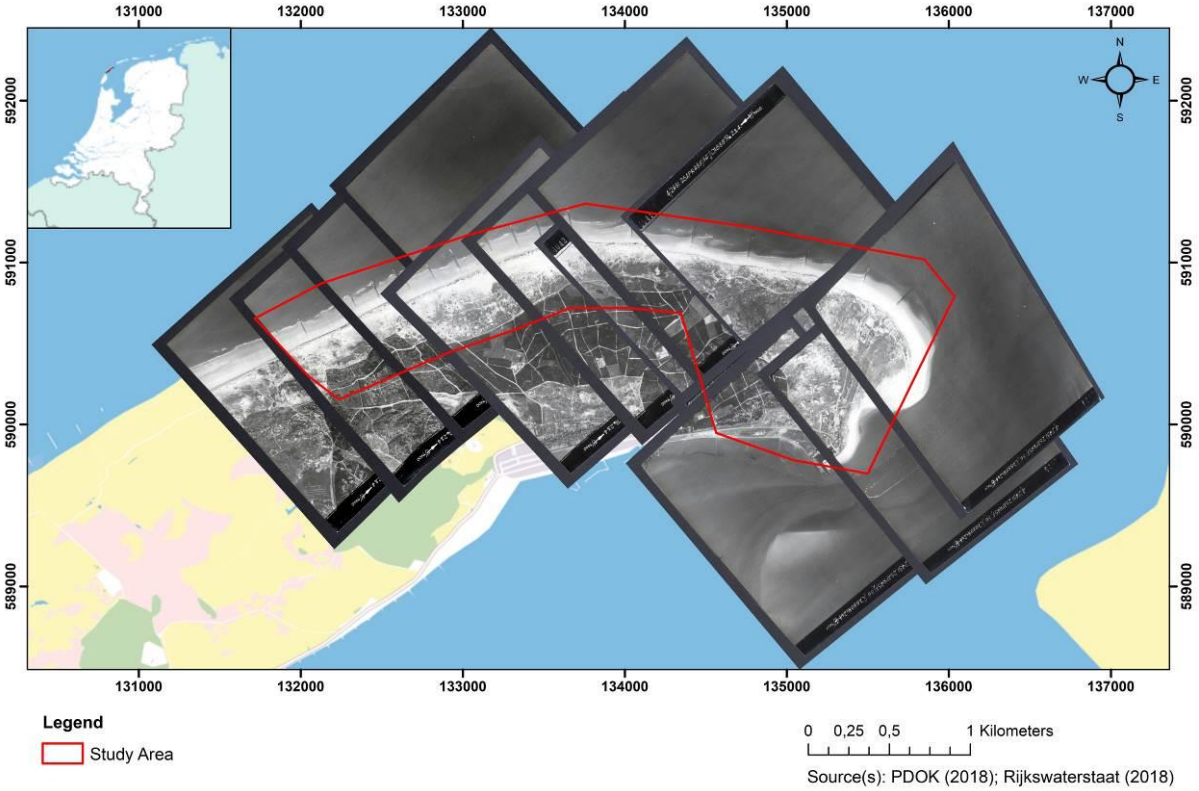

Figure 17: The thirteen aerial photographs from 1945 that were used to extract DEM in East-Vlieland.

4.2 Ground Control Points

Ground control points are precise and easily visible aspects that can be situated precisely both on a map and on the corresponding image. These points can be identified by using a GPS or even using a commonly known computer program as Google Earth Pro, which represents the Earth through satellite imagery. Considering the block of photographs, it is necessary for these points to be visible in at least two photos or more allowing the stereoscopic viewing. Appendix A illustrates an example of the GCPs in a portion of the study area from the ERDAS Imagine viewer, where the points are exactly in the same position in both images, left and right.

According to Liew *et al.* (2012), in order to achieve the accuracy of the geometric correction is necessary to have a precisely positioning and defined reference points in the image as the GCP location has an intrinsic influence in the accuracy of the geometric correction. As a result, you must have a homogeneous arrangement of the control points to reach impartial results in the aerial image rectification.

Portion of aerial photographs that cover coastal areas, the procedure of selecting GCPs and tie points is difficult to do and involves a lot of effort. Moreover, beaches, dunes, and tidal flats present dynamic variability resulting in a lack of identifiable features to use as reference. Another characteristic is that the chosen GCPs certainly will be located on the land side, being not well distributed along the photo which affects the geometric relationships between adjacent photographs, diminishing the quality of aerial photogrammetry (Kim *et al.*, 2014).

In the block of images used for the year of 1945 were identified 114 GCPs along the study area, while for the year of 1981, a total of 92 GCPs were chosen (Figures 18 and 19). For better computation performance, the area was subdivided in three parts considering both years, 1945 and 1981, what improved the quality of the exterior orientation, providing the lowest RMSE value possible for each portion (Table 2). It must be pointed out that this division supported the computation performance also by means of the algorithm calculations for generating point clouds, which tends to push the hardware.

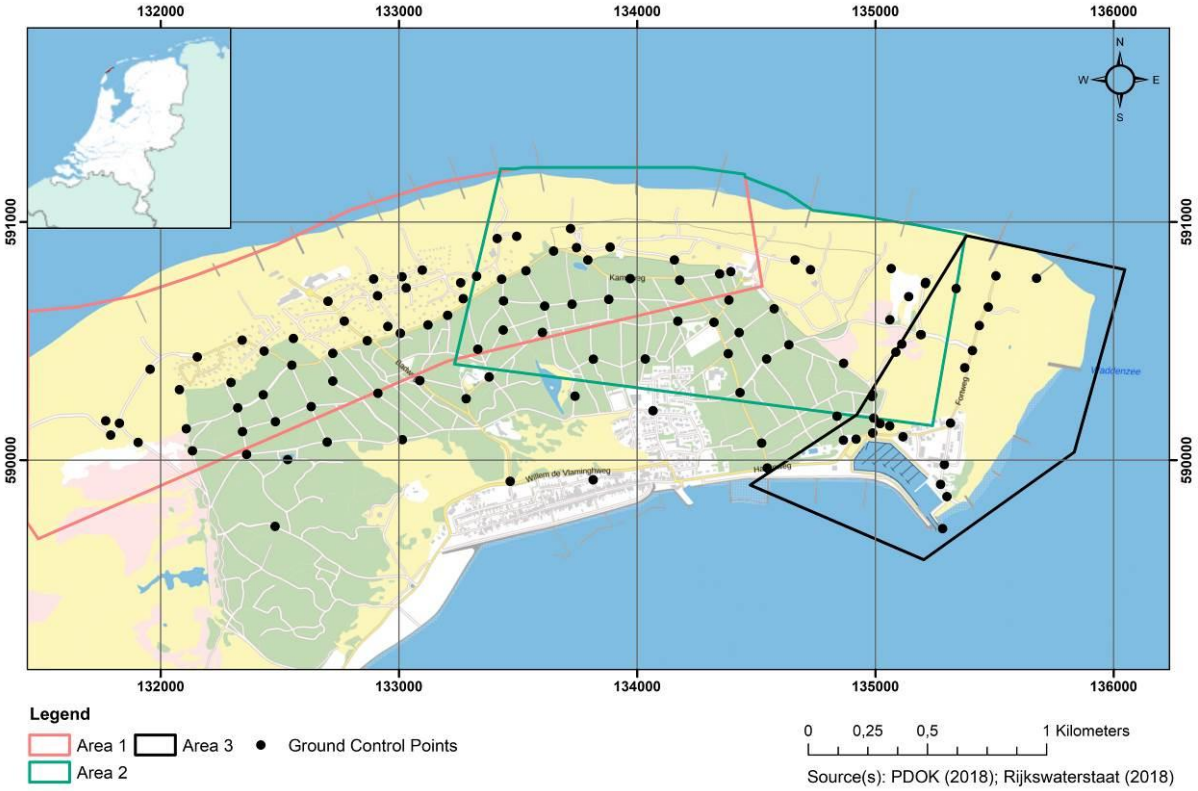

Figure 18: GCPs identified for the year of 1945 in the study area.

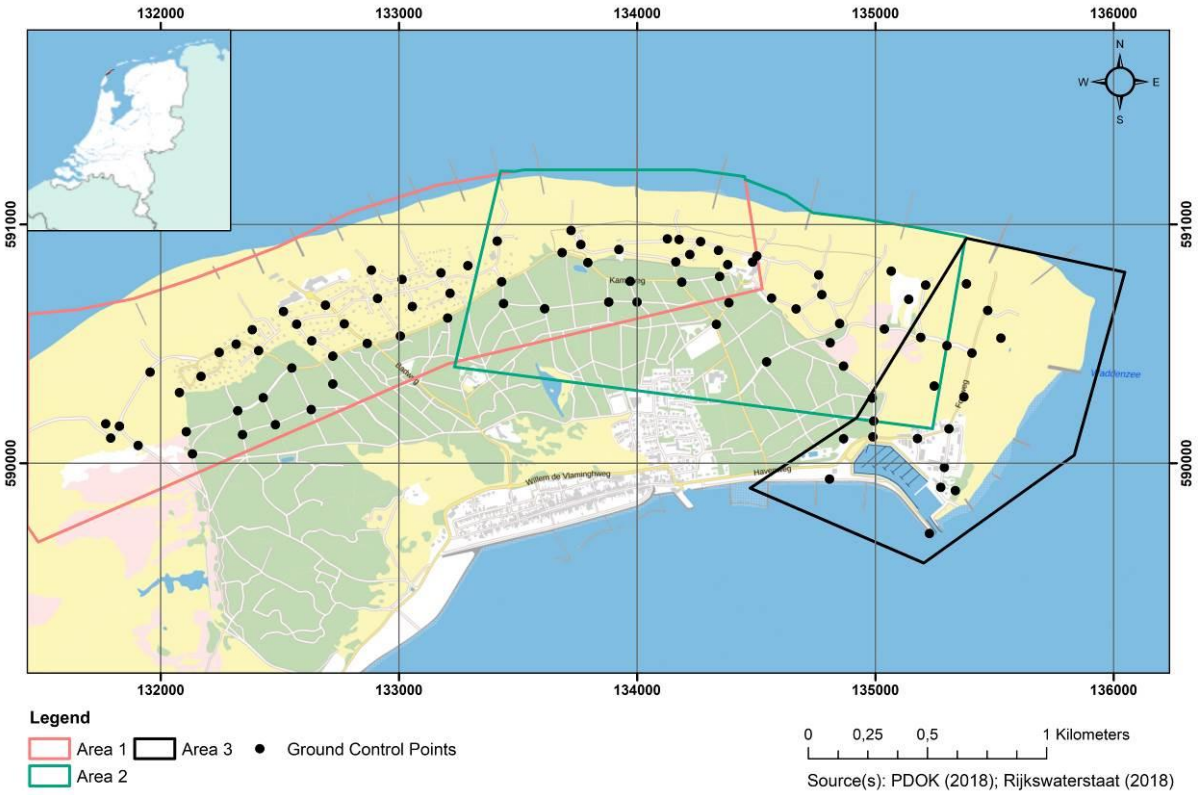

Figure 19: All 92 GCPs selected for the year 1981 in the study area.

Year	Area	RMSEx (Px)	RMSEy (Px)	Total Points (GCP + Tie points)
1945	1	99.742	65.837	273
	2	90.290	73.229	262
	3	153.313	152.226	146
1981	1	46.972	48.941	363
	2	43.990	48.348	209
	3	73.665	69.954	214

Table 2: The mean RMSE for both axis for the total points selected in the 3 domains processed in the study area, for the years of 1945 and 1981.

The mean value of RMSEx, RMSEy found for the combinations of GCPs and tie points shows that a larger number of GCPs provided lower RMSE results and smaller number of GCPs returned higher RMSE values, cases of area 1 and 3 respectively for the both years. The configuration and comparison between the mean RMSE and GCPs/tie points for each area for 1945 and 1981 aerial photographs can be seen in figures 20 and 21, respectively.

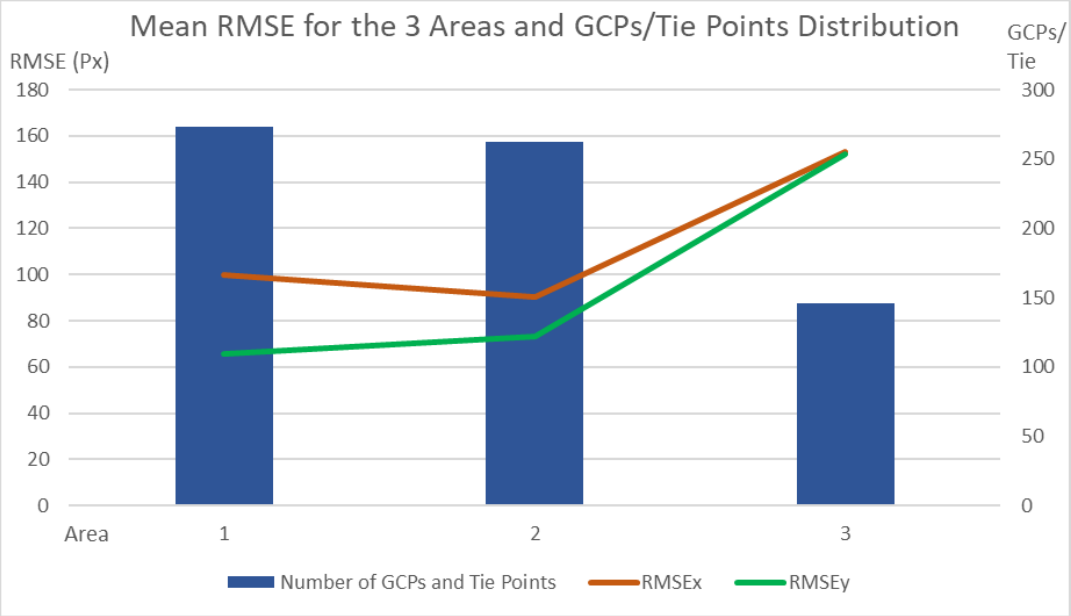

Figure 20: The relation between the quantity of GCPs and tie points with the mean RMSE for the three areas for the year of 1945.

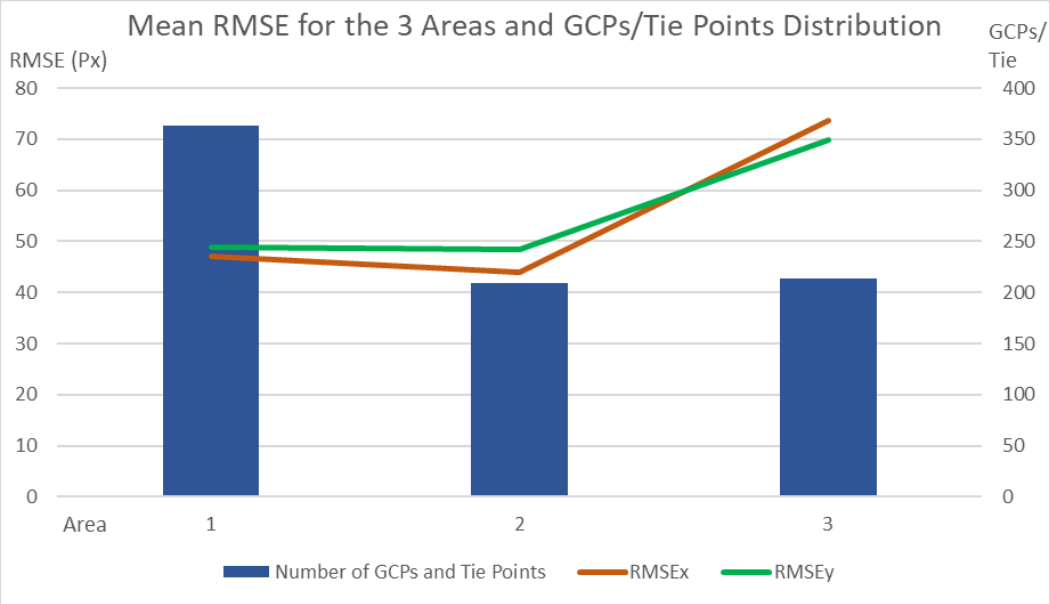

Figure 21: The distribution of GCPs and tie points according the mean RMSE for each area for the year of 1981.

4.3 Point Clouds

The first point cloud product created in the current research was generated from 17 images in 3 different strips from the 1981 imagery. It is essential that quality of this dataset to be sufficient, or in other words, to be in a minimum level of usage, so further processes can be made, like performing a DEM, and the comparison with LiDAR and AHN datasets resulting in a DoD. The main reason that the 1981 point clouds are presented first than the point clouds of 1945 is because the whole process ended better for the 1981 photographs. It is important to have in mind that as the photographs are newer and there is a camera report available, the processing stage flowed smoothly, with less uncertainties. For instance, the 1945 point clouds data made through SGM method could not be used for the further steps due to many errors in the dataset, which will presented later in this report.

The point clouds created in this project, for both years, by using the eATE command in the software ERDAS Imagine, were calculated through the NCC algorithm. So, all point clouds products generated with this method, were made using the default settings in the strategy manager of ERDAS (Table 3).

Correlator	**Window Size**	**Coefficient start**	**Coefficient end**	**Interpolation**	**Point threshold**
NCC	9	0.30	0.80	Spike	5
Search window	**Std deviance tolerance**	**LSQ refinement**	**Edge constraint**	**Smoothing**	
50	3.0	2	3	Low	

Table 3: Settings used to generate the point clouds data during this research, using the NCC method.

These strategy parameters are detailed below, and are based on ERDAS Imagine support (2019) - eATE and Ullah *et al.* (2017):

- Window size: the size of the area (in pixels) used for computing the correlation coefficient between the left and right images. For areas that has minimal topographic variation, grey level or colour intensity, it is recommended to use a window size of 9 or greater. In the other hand, for areas with large topographic variation, grey level changes and even more variation in the colour intensity, the recommendation is to use smaller window size.

- Coefficient start and coefficient end: both coefficients are used for generation of pyramid level. It is explained that higher coefficients range (0.7-0.8) produces higher accuracies for NCC, however fewer points may be matched. Using a lower range (0.3-0.8) should increase the number of correlated points.

- Interpolation method: interpolates any points that have not been correlated, seeding the next-pyramid layer correlation. The interpolation procedure tends to increase the accuracy and point density. There are three options available in ERDAS: Mean, Region and Spike, being this last one the default option.

    ⇒ Mean: It uses a weighted mean algorithm that iteratively searches for known values surrounding missing points, using them to interpolate the missing ones. It considers the weight of the known values contribution.

    ⇒ Region: It is similar to the mean, however it is constrained within the region segmented from the master image. This constraint includes an optional setting to sharpen building boundaries.

    ⇒ Spike: It works as the Region interpolation, but it removes points that are identified as outliers, based on the surrounding elevation values.

- Point Threshold: the number of points that are considered in the interpolation.

- Search window: it has a square shape and it is the maximum search size of the window, given in pixels, working surrounding the point to be interpolated.

- Standard deviance tolerance: it indicates the tolerance, in meters or feet, for determining the standard deviation of the planar fit.

- LSQ refinement: it is an algorithm applied on a specific pyramid level, which uses least squares method to refine the correlation between the pixels in the stereopairs.

- Edge constraint: It is best to use in urban areas, and it is the edge or limit that the interpolation will work, avoiding crossing those boundaries. It is applied by pyramid level.

- Smoothing: Looks for spikes or outliers in elevation, removing the extreme values from the data. There are four options for smoothing, i) none: no smoothing; ii) low: minimal smoothing, for data with few anomalies; iii) moderate: moderate level of smoothing; and iv) high: rigorous smoothing, for data with many anomalies.

Using the SGM algorithm to create point cloud data for the current research was made for both years, being successfully applied for the year of 1981, but not for 1945 block file, which results not reached the minimum level of acceptance to be further used in the project. The image-based point clouds performed were made by using the Tridicon option in the software ERDAS Imagine with the default settings in the semi-global matching tab in ERDAS (Table 4).

Correlator	Image Pair Overlap	Color Band to Match	Last Pyramid Level	Disparity Difference
SGM	50%	Green	0	1

Table 4: Settings of SGM Tridicon method used to generate the point clouds data during this

research.

These SGM settings are also based on ERDAS Imagine support (2019) - Tridicon:

- Image pair: The minimum percentage of overlap between the images of each stereopair are chosen in this part.
- Strategy: In this tab there are three components to be considered, color band to match, last pyramid level and disparity difference.

  ⇒ Color band to match: Chosen band to consider during the calculations. When using RGB images the software always uses the Green band for matching pixels.

  ⇒ Last pyramid level: It is the level of pyramid which the matching process should stop. A value of 0 means full resolution, while greater numbers will result in less resolution. In addition, higher numbers will always decrease the processing time.

  ⇒ Disparity difference: It is used to remove blunders during the reverse matching process by means of a threshold for disparity consistency check.

Another setting to perform the SGM method is the pixel size in x and y directions. For block files in ERDAS Imagine using digital frame cameras is necessary to add this information, which corresponds to the resolution of the sensor in the equipment. The pixel size is given in microns (ERDAS Imagine support, 2019 - Tridicon).

4.3.1 Point clouds of 1981

NCC algorithm

As explained before, for better computation performance, the area was split in three parts, and for this means, firstly the point clouds were created for each portion (Appendix B). After, the three products were merged resulting in a unique LAS file covering the whole study area (Figure 22).

It is possible to verify that the whole coast presents shades of blue colour meaning lower elevation values. Hot colors show higher values for the relief and are most concentrated in the northeast, southeast and southwest of the study area.

There are outliers in the three areas, but the areas one and two can be highlighted because they brought many noises to the main dataset. They have several outliers, especially located in the border continent/sea, being visible on some portions in the north. The water in the north may be the reason for the outliers, because NCC is not able to measure waterbodies correctly, resulting in an inaccurate elevation height. The area number three presents the most realistic results in the study area with a range of -8,5 meters to 44,6 meters.

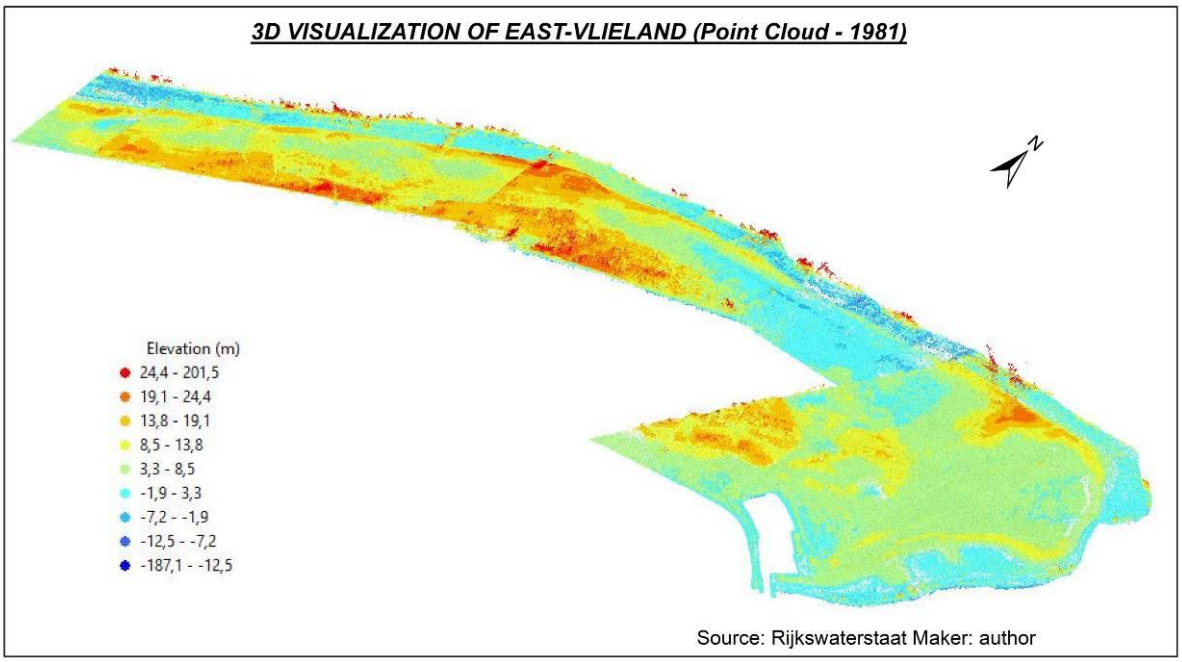

Figure 22: 3D visualization of the merged point cloud dataset, made with the NCC method, from the year of 1981 of the study area at East-Vlieland.

The merged point cloud dataset of 1981 using NCC algorithm retrieved the values for standard deviation and mean as shown in table 5. Further, this information will be compared to the SGM method values obtained.

Min (m)	Max (m)	Mean	Standard Deviation	Point Count	Point Spacing	Point Density (p/m²)
-8,5	90,4	6,8	5,5	128.070.304	0,223	18,4

Table 5: Statistical data from the image-based point cloud of 1981 from NCC method.

SGM algorithm

The producing of point clouds using the SGM method were made following the same steps of the NCC method. The study area was also split in the same three parts, again to increase the computation and time performance. The results from this method showed that outliers are appearing in the border continent/sea, however the most prominent regions with noise are well marked in the borders of the stereopairs. In general, the point cloud data has many more points considering the one made with NCC algorithm.

The Appendix C presents the three areas and the figure 23 shows the merged file. Table 6 also has the statistical information of the merged point cloud data with SGM. The study area is presented similarly using the NCC method, being in shades of blue colour representing lower elevation values located at the coastal zone or beaches. The higher values, despite of the outliers, are located mainly in the northeast, southeast and southwest portion, and are shown in hot colours.

It is noticeable that the area number two does not has the extreme west part in the map, if comparing with the one made with NCC method, this occurred because even having a stereopair covering that location, this stereopair returned with no results in ERDAS Imagine, in other words, the LAS dataset created for this part was empty. Even switching some settings in the Tridicon manager, it repeatedly came without any data.

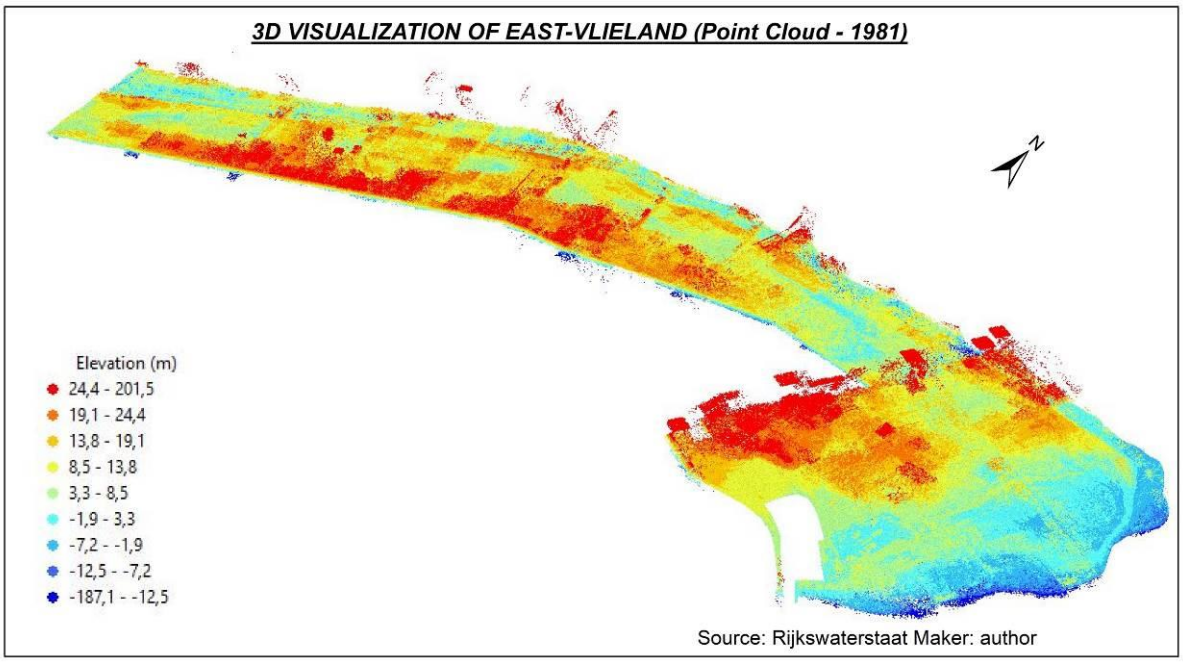

Figure 23: 3D visualization of the merged point cloud dataset made with SGM method from 1981 of East-Vlieland.

Min (m)	Max (m)	Mean	Standard Deviation	Point Count	Point Spacing	Point Density (p/m²)
-187,1	201,5	6,4	10,1	983.175.710	0,080	156,25

Table 6: Statistical data from the image-based point cloud of 1981 made with SGM algorithm.

4.3.2 Point clouds of 1945

NCC algorithm

The point clouds generated for the year of 1945 were also made in three main domains for the NCC method, also allowing a better calculation and time performance, or computation performance. Appendix D shows the image-based point clouds for each area and figure 24 provides a 3D visualization of the study area.

It is clearly visible in all three domains that there are many holes along the study area, being the white background visible. What draw the attention for this point cloud it is the point density of 3,7 p/m², showing that the matching process provided not a very good result. In the other hand, there were not too much outliers with extremely high values in the whole data (< 50 meters), when considering the huge amount obtained for the year of 1981. The merged point cloud presents the elevation values in the range of -8,5 meters to 57,2 meters.

The coast is mostly represented by hot colors, which have higher elevation values, when the expectation was to appear light colors meaning lower values. However, the reason this part concentrates most of the outliers may be because it is located on the border continent/sea, and the NCC method suffers to deal with water bodies.

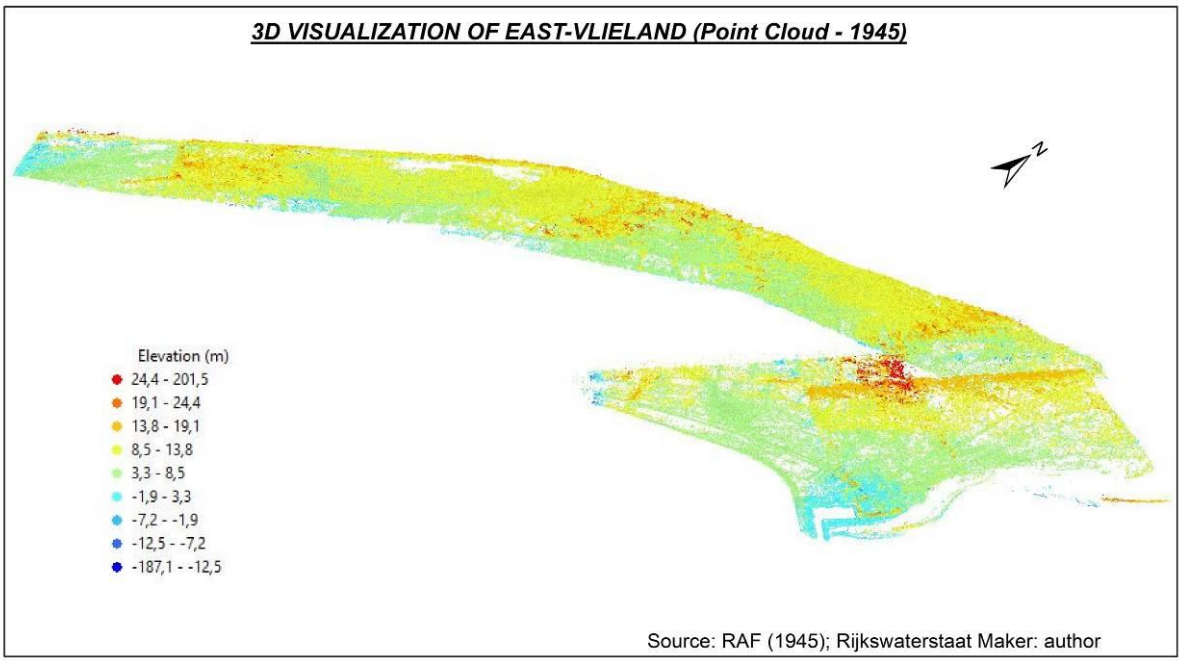

Figure 24: 3D visualization of the merged image-based point cloud from the year 1945 using the NCC method at East-Vlieland.

The point cloud dataset covering the whole study area has the statistical values presented in the table 7, as well as the point count, point spacing and point density. This information will be later compared with the values obtained using the SGM method for 1945.

Min (m)	Max (m)	Mean	Standard Deviation	Point Count	Point Spacing	Point Density (p/m²)
-8,5	57,2	6,8	5,5	21.012.164	0,514	3,7

Table 7: Statistical information of the merged point cloud data generated for the year 1945 using the NCC algorithm.

SGM algorithm

The SGM algorithm applied on the aerial photographs of 1945 did not result in reliable point cloud data. The study area was also subdivided into three main parts, but, differently from the year 1981, the area number three, located at the extreme east, was not possible to process the point clouds data because the triangulation of the GCPs and the tie-points could not be performed well.

As mentioned above, the results of the point clouds data of the areas one and two were not reliable due to several huge outliers for the elevation values. In that sense, one can see that visualizing in 2D the outcome seems correct, being possible to identify the vegetation domains and roads (Appendix E, E1), however in the 3D perspective one may see that the data is not recognizable and not useful for further processing (Appendix E, E2), since the range of elevation values is -6731,4 meters to 3616,5 meters for area 1, for example.

Table 8 displays the statistical data for the image-based point cloud of 1945 using the SGM method for both areas. Even changing settings in Tridicon manager, such as lowering the process resolution through higher value for the pyramid level, changing the pixel size in x and y directions, the data always presented those same results, with no reliable heights.

Area	Min (m)	Max (m)	Mean	Standard Deviation	Point Count	Point Spacing	Point Density (p/m²)
1	-6731,4	3616,5	-17,8	653,6	48.836.524	0,222	20,2
2	-5562,0	4065,5	-42,1	482,5	53.097.498	0,153	42,7

Table 8: Statistical data of 1945 image-based point cloud using the SGM algorithm.

4.4 DEM of 1981

The DEMs from 1981 were derived from the both merged point cloud data of the whole study area made from both methods, NCC and SGM. The two DEMs were done through the IDW interpolation and linear void fill method with the tool LAS dataset to Raster in ArcMap. It can also be pointed out that as this interpolation method is supported by spatial autocorrelation, when creating the DEM, the tool improved the end dataset, filtering out outliers resulting in a more reliable surface. The results of 1981 are also showed first due to the same reason of the point clouds chapter.

NCC algorithm

The DEM created by NCC method also reinforce that low elevation values are concentrated in the coastal part, with dark grey colours, while the higher values are shown in light grey to white colours, and mostly represents either the dunes area or the forest and buildings of the city. The elevation map of East-Vlieland represented by the DEM-NCC is shown in figure 25. The 3D visualization map can be seen in figure 26, and one can perceive in three dimensions the highest portions, such as the forest and the dunes area.

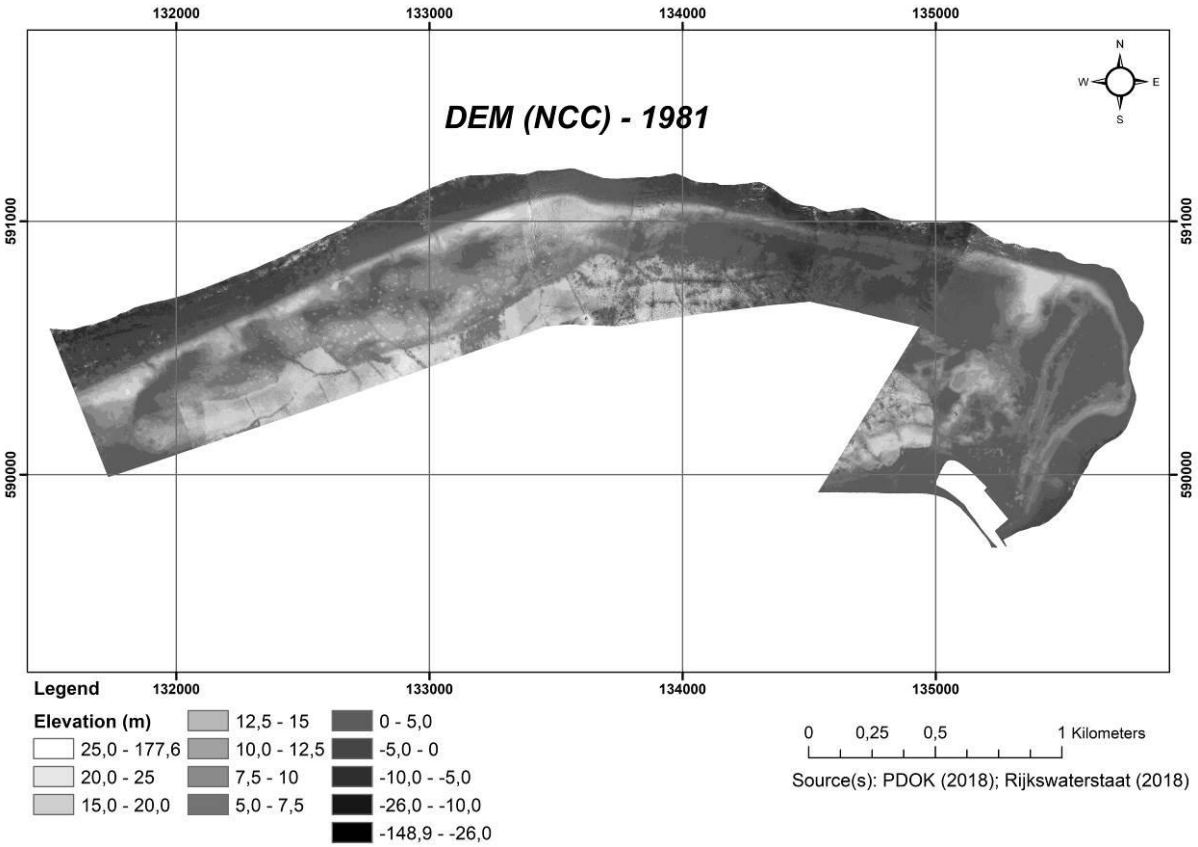

Figure 25: DEM created for the year of 1981 performed using the NCC algorithm.

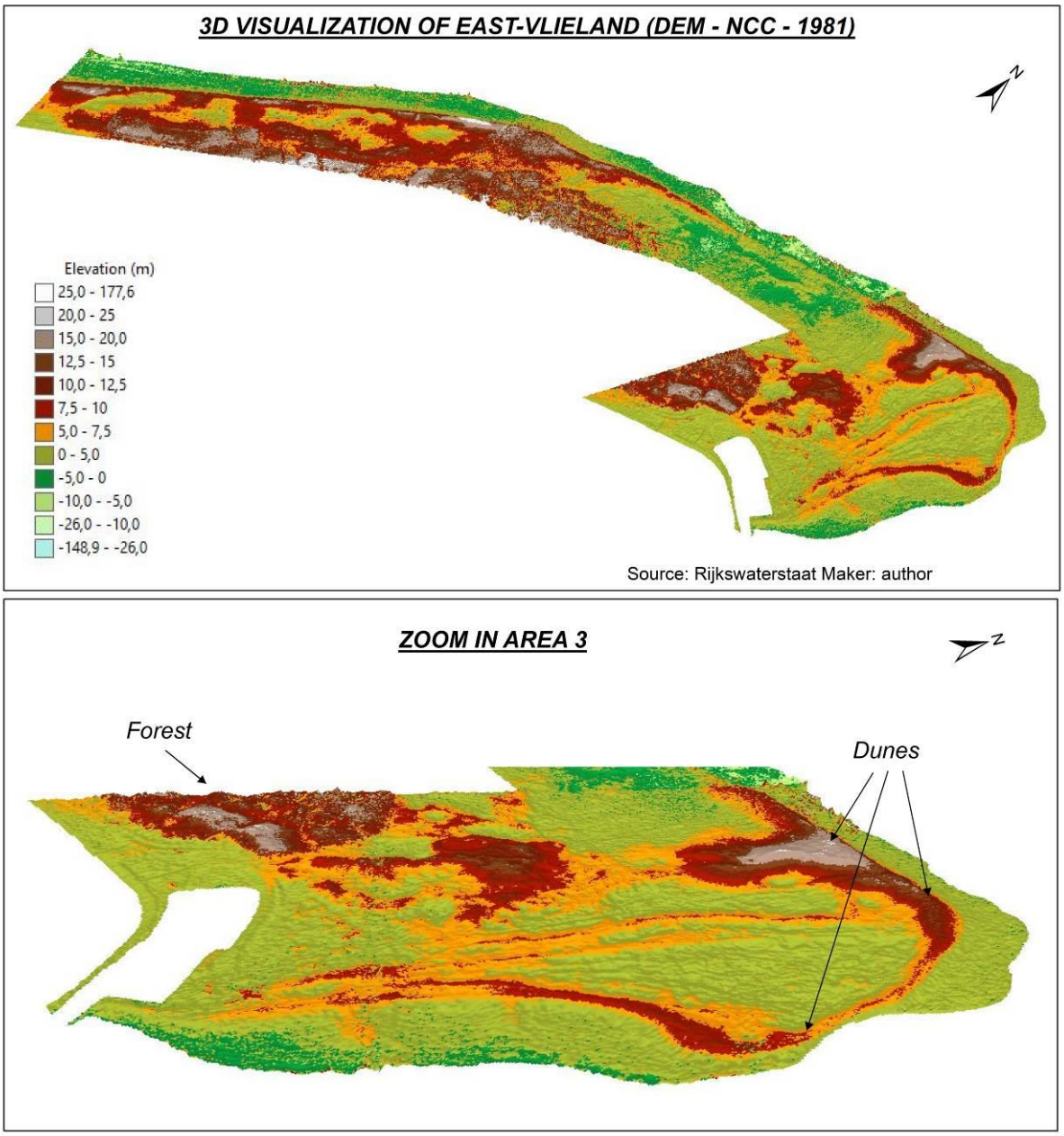

Figure 26: 3D visualization of the DEM of 1981 made with NCC method, colored according to the stretched elevation values. The part of the city and the harbor is highlighted showing the higher locations mostly represented by the dunes and forest.

The statistical information from this DEM shows minimum elevation value of -8,5 meters and maximum value of 66,7 meters. The maximum value does not represent the real surface, however the mean and standard deviation show a more realistic situation, as table 9 presents.

Min (m)	Max (m)	Mean	Standard Deviation	Cell Size (m)
-8,5	66,7	2,7	4,8	1,0 x 1,0

Table 9: Statistical data from the DEM-NCC of 1981.

SGM algorithm

The DEM made with SGM algorithm resulted in a dataset with several outliers with a range of -148,9 to 177,6 meters in elevation. The elevation map DEM-SGM is displayed in figure 27. Even with such a result, the dark greys areas are also representing the beaches and the coast, while the light grey areas are located in the dunes, the forests and buildings. The outliers in this case influenced to much the 3D visualization, which is not possible to be shown smooth as the DEM-NCC surface. Even using a lower elevation from feature setting in ArcScene than the one used to represent the DEM-NCC, the DEM-SGM in general does not look very appealing, especially in the higher areas, like the forest and the dunes (Figure 28).

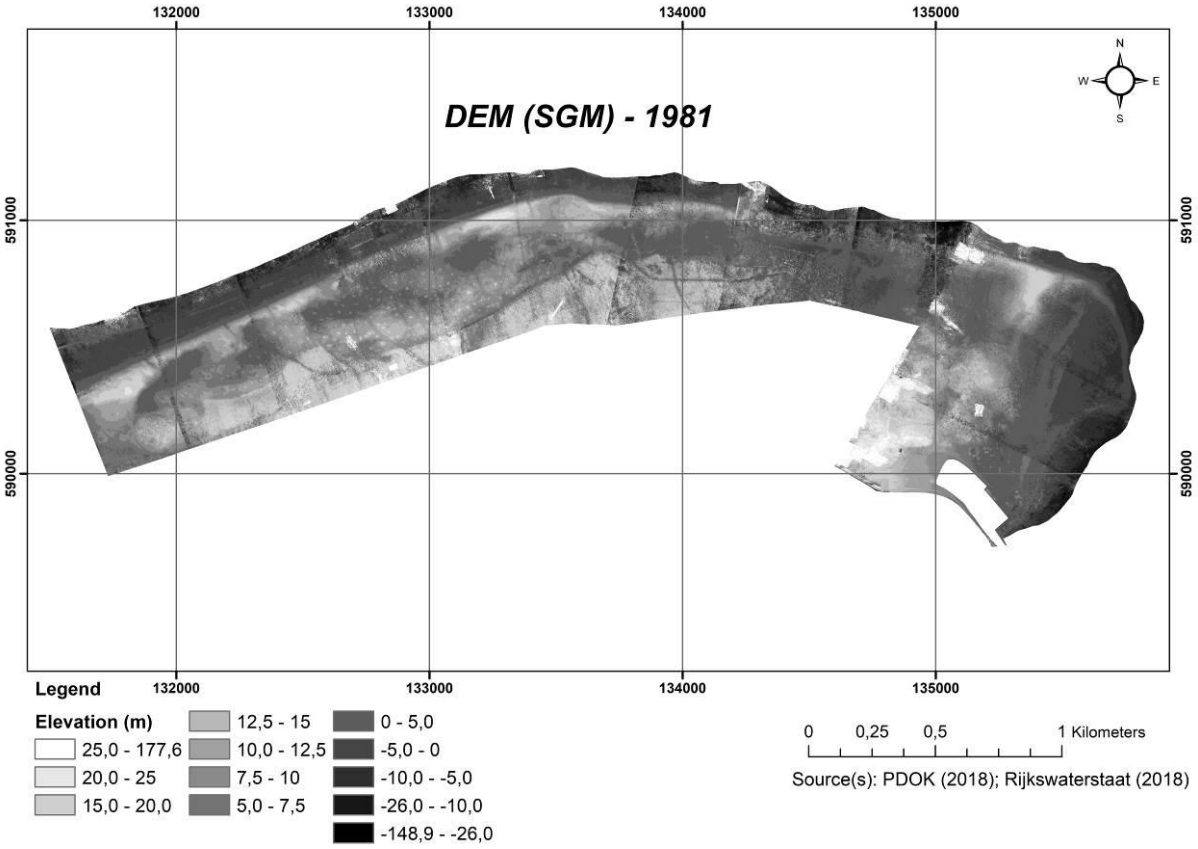

Figure 27: DEM made for the year of 1981 performed using the SGM algorithm.

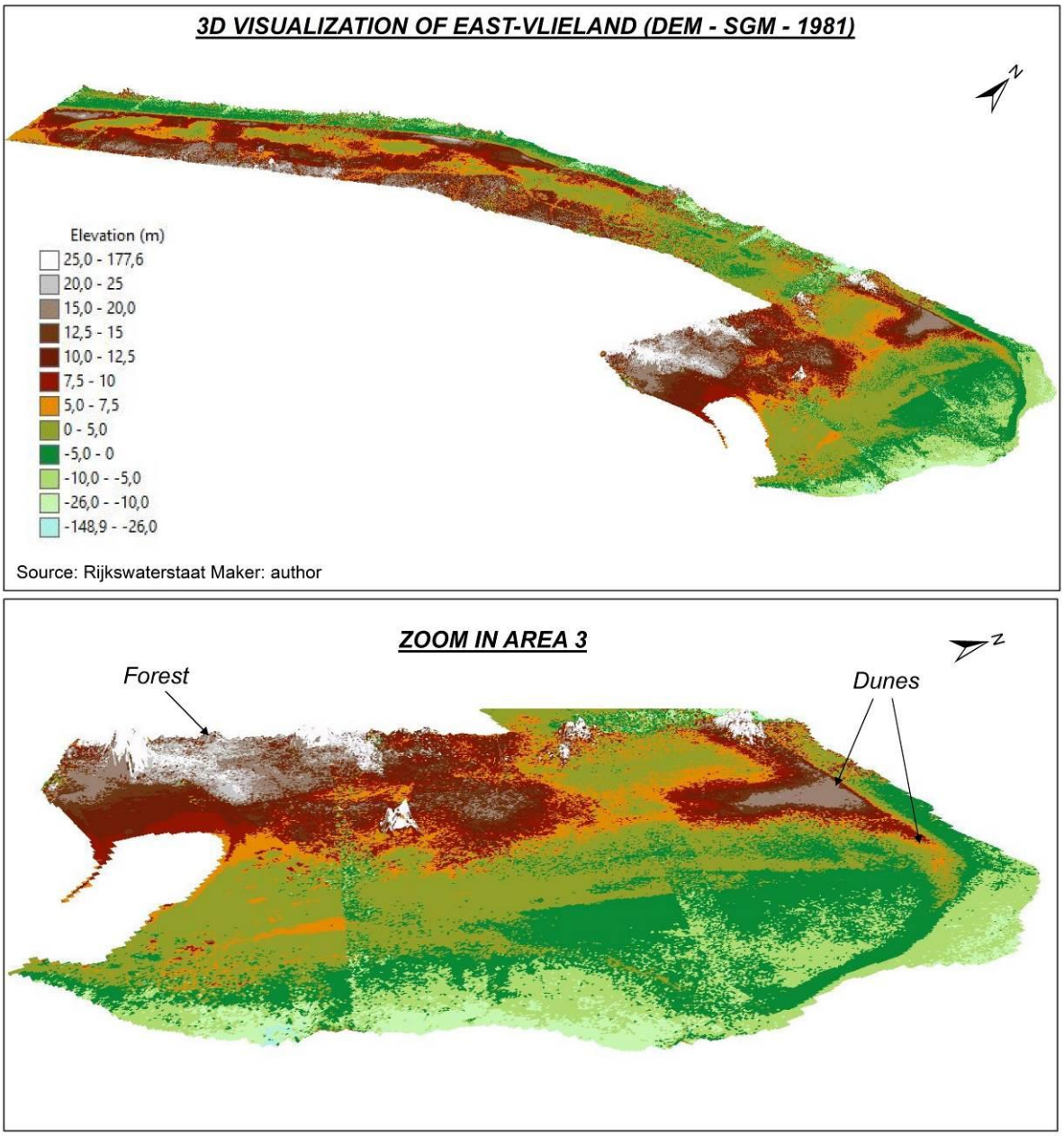

Figure 28: 3D visualization of the DEM of 1981 made with SGM algorithm, colored according to the stretched elevation values. The surface is not smooth and realistic, and it does not represent very well the study area.

The minimum elevation value for this DEM is -148,9 meters and the maximum value is 177,6 meters. Both values are not representing a realistic situation of the height in the study area, while the mean and standard deviation configure better values for the data (Table 10).

Min (m)	Max (m)	Mean	Standard Deviation	Cell Size (m)
-148,9	177,6	5,9	9,3	1,0 x 1,0

Table 10: Statistical information of the 1981 DEM made using the SGM method.

4.5 DEM of 1945

The DEM of 1945 was derived through the NCC method, with the merged point cloud data of the three areas. As the SGM algorithm has not provided usable point clouds results, it was not possible to generate a DEM of the study area considering this method. It can also be pointed out that the 1945 DEM-NCC was performed using the IDW interpolation, and linear void fill method, and it was created through the tool LAS dataset to Raster in ArcMap, same workflow from previous DEMs of 1981.

NCC algorithm

As the point cloud data has many empty spaces or holes, the DEM created by NCC method has these holes filled, interpolated as well, providing coarse areas, where the triangles of the interpolation are easily visible, even being 1 meter x 1 meter the raster resolution. The DEM has minimum and maximum elevation values of -8,5 and 56,6 meters, respectively (Figure 29). Considering the coarse triangulation of the holes, the DEM does not present a smooth appearance, being hard to recognize some features from the photos like the roads, the vegetation area, and the city. The 3D visualization map of figure 30 shows that the surface is not displayed smoothly, and higher areas corresponds mostly to the outliers. The harbour area is easily recognizable in the extreme east part and it is smaller compared to year of 1981 and newer years represented by the LiDAR and AHN datasets.

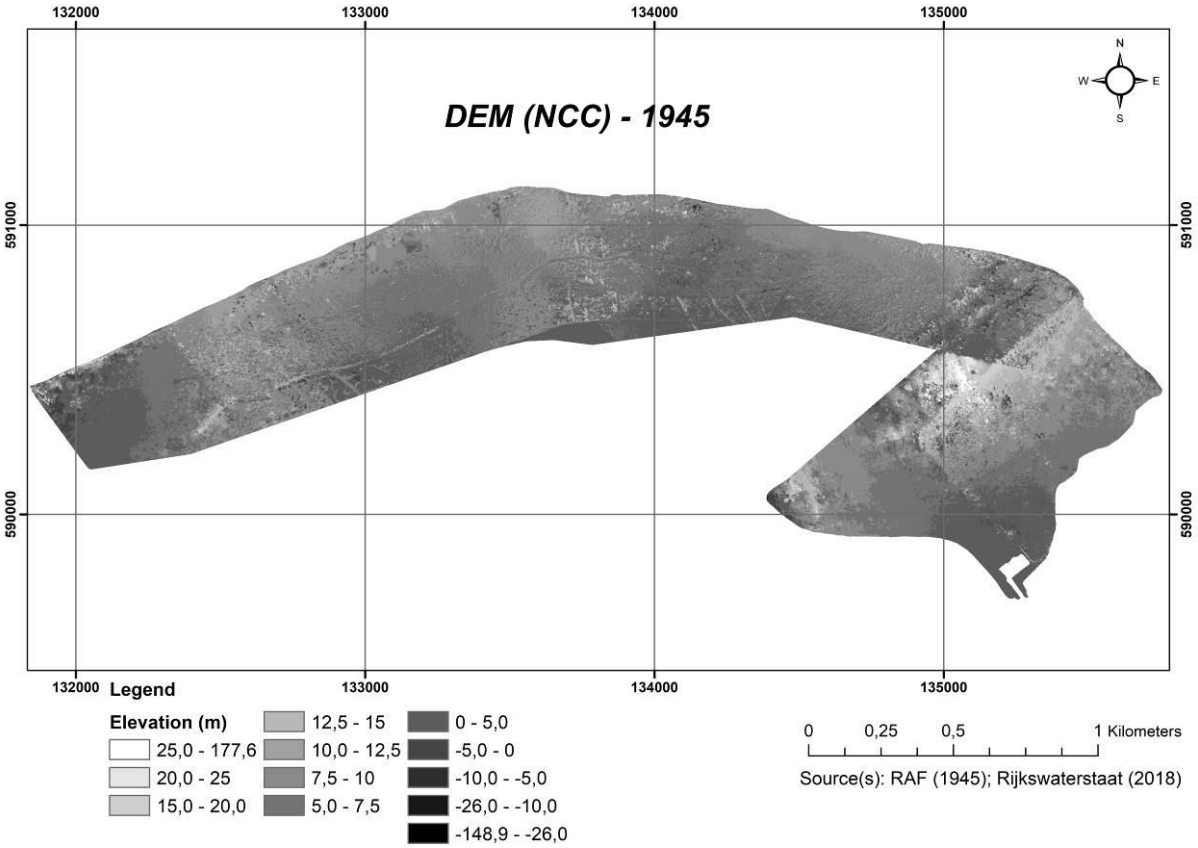

Figure 29: DEM of the year of 1945 made by using the NCC algorithm.

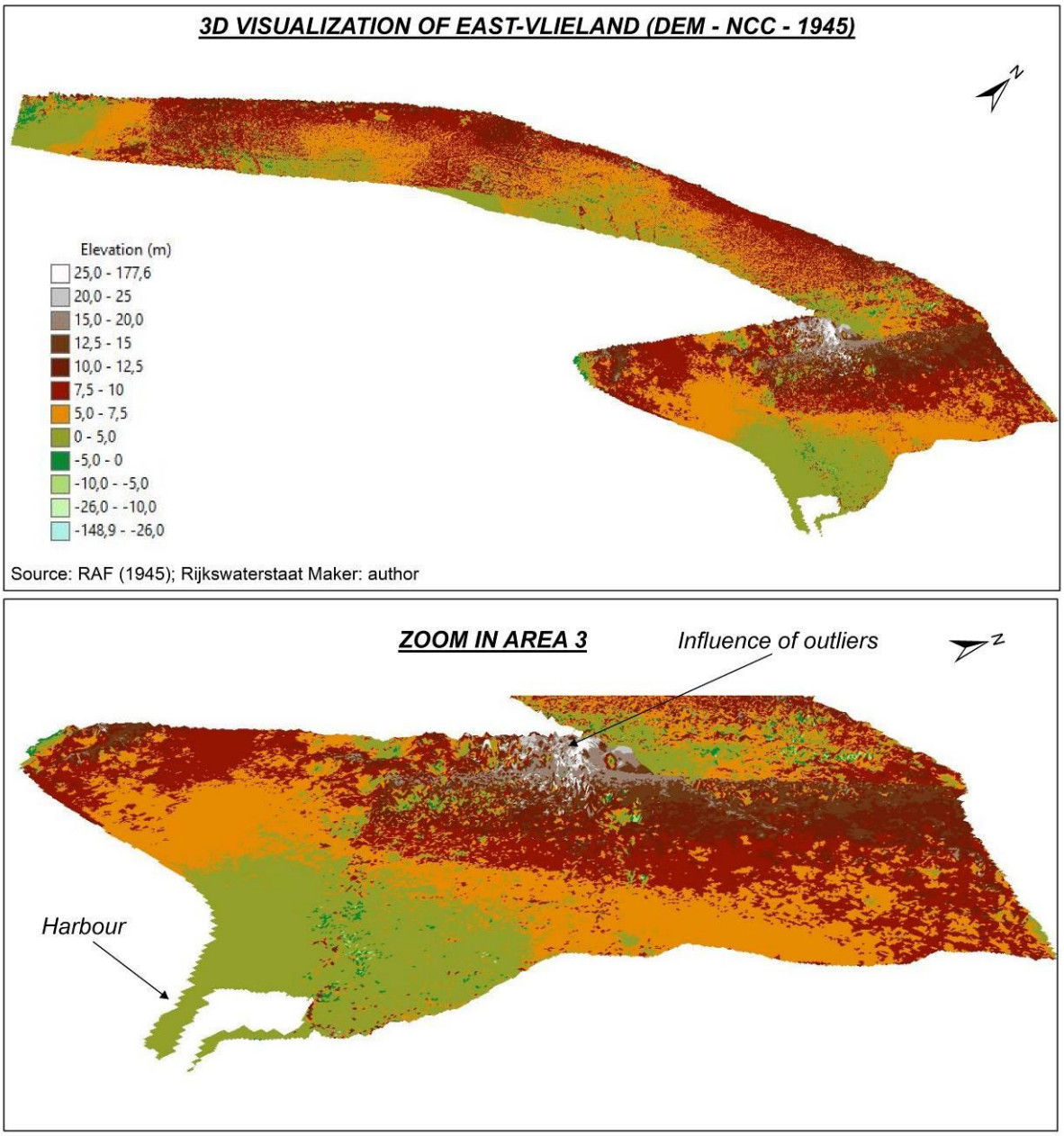

Figure 30: 3D visualization of the DEM of 1945 generated by the NCC algorithm with colors given by the elevation values.

Although the 1945 DEM-NCC results are not visually sufficient, the statistical data seem acceptable, considering both minimum and maximum values, but especially the standard deviation of 3,3 (Table 11).

Min (m)	Max (m)	Mean	Standard Deviation	Cell Size (m)
-8,5	56,6	7,4	3,3	1,0 x 1,0

Table 11: Statistical data of the DEM of 1945, made using the NCC algorithm.

4.6 DoDs

The DoDs are the result of the subtraction of two DEMs multiplied by the area of each cell. They are in raster format and with cell size of 1 meter x 1 meter. In the present research, a total of 10 DoDs was generated, being products of the comparison between the produced DEMs, of 1981 and 1945, with the LiDAR datasets and AHN dataset previously mentioned. The LiDAR data that was used to do the comparison belongs to the years of 1997, 2004, 2014 and 2017, and the AHN dataset is from 2014. For the same reason of the point clouds chapter, the DoDs made using the DEM of the year 1981 are presented first in this report. Then, the DoDs resulted from the comparisons with the DEM of 1945 are shown.

Comparison with 1981

The comparison made in this stage used LiDAR and AHN datasets, which cover the coastal area of the Netherlands, or even the whole country like the AHN, and when necessary they were clipped to the study area. So, for instance, the years of 2017, 2014 and 2004 from the LiDAR data have smaller size compared to the original study area, which can be seen in the point clouds and DEM chapters, in order to be comparable as well for these smaller areas, the DEMs, NCC and SGM, were also clipped when necessary.

DoD: LiDAR 1997 vs DEM-NCC 1981

The DoD created in this step was made with input rasters of LiDAR data from 1997 and the DEM-NCC of 1981 (Figure 31). The green colour represents increase in volume or a gain in volume during this period, while in the beaches at northwest and east occurred loss in volume, considering elevation. As the LiDAR data came with a huge outlier numbers for the minimum and maximum elevation values, the end product DoD in this comparison shows -160,0 and 2508,8 cubic meters, respectively.

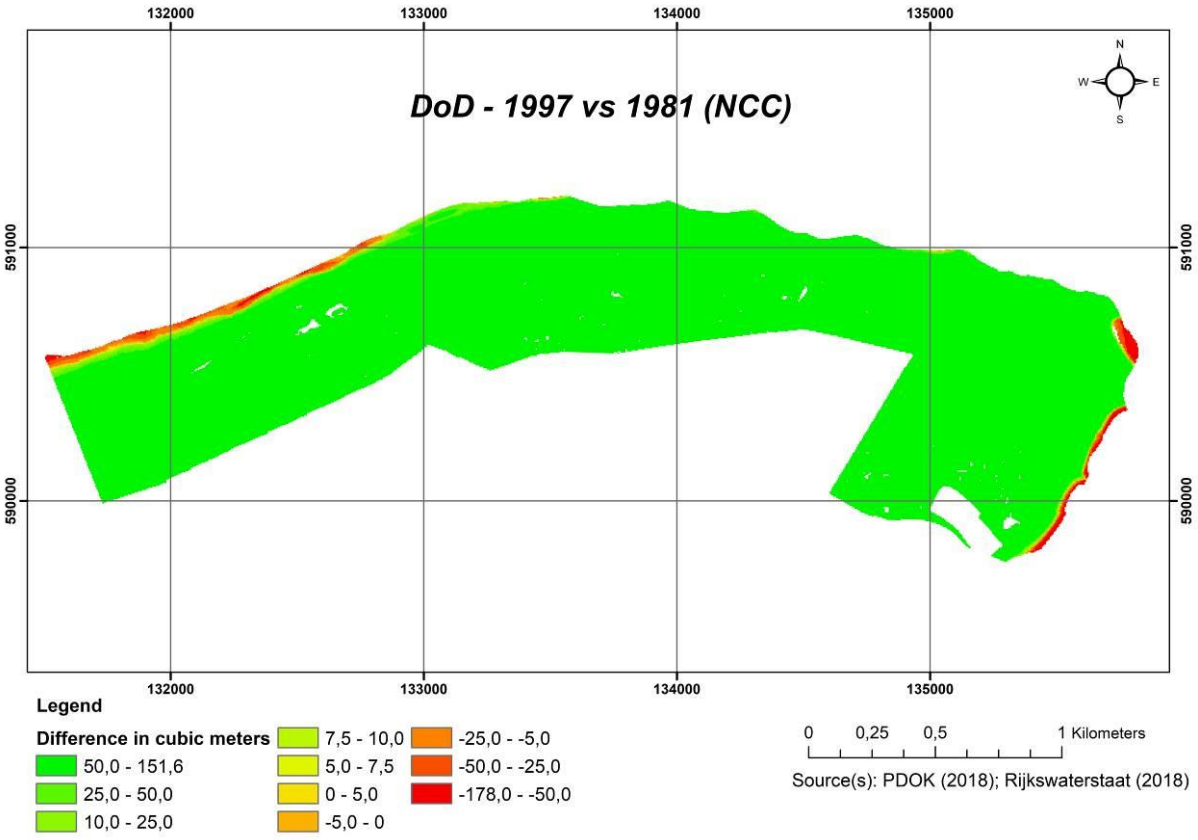

Figure 31: DEM of difference considering 1997 LiDAR and 1981 DEM-NCC.

DoD: LiDAR 2004 vs DEM-NCC 1981

The DoD compared the LiDAR from 2004 and the DEM-NCC from 1981 (Figure 32). As the LiDAR data also came with outlier numbers for the elevation values, the DoD presents minimum value of -172,3 cubic meters and maximum value of 2485,0 cubic meters. Similar to the DoD 1997-1981, it shows a huge increase in volume along the study area, green colour, and decrease at the beaches in northwest and southeast-east (hot colours).

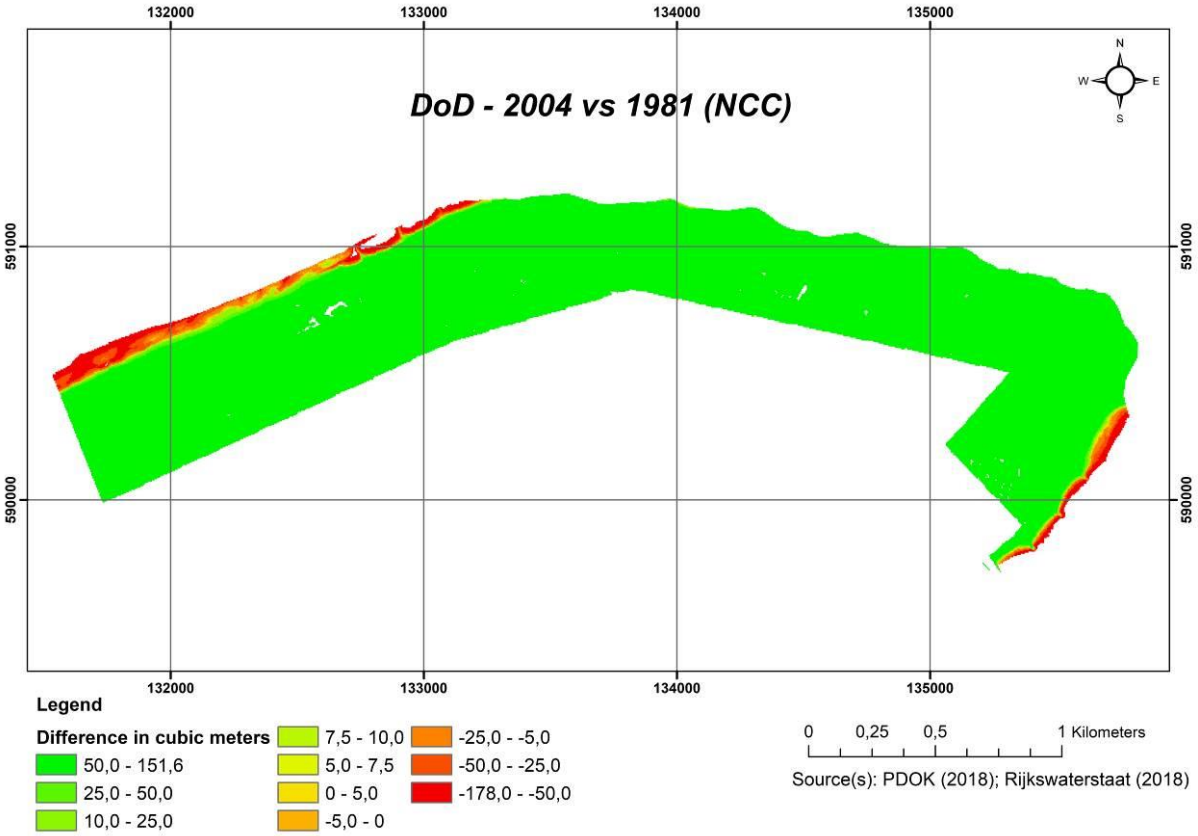

Figure 32: DEM of difference comparing the LiDAR of 2004 and the DEM-NCC of 1981.

DoD: LiDAR 2014 vs DEM-NCC 1981

The LiDAR dataset from 2014 has more realistic maximum and minimum values, without outliers. For this reason, the comparison made with the DEM-NCC of 1981 resulted in a better DoD. As can be seen in figure 33, the dune's area is also showing gaining in sediment, however, is more noticeable that the coast had minimal changes and the losses are more concentrated in the southwest part and especially in the coast located in the extreme east. The DoD presents a minimum value of -65,2 cubic meters and a maximum value of 23,5 cubic meters.

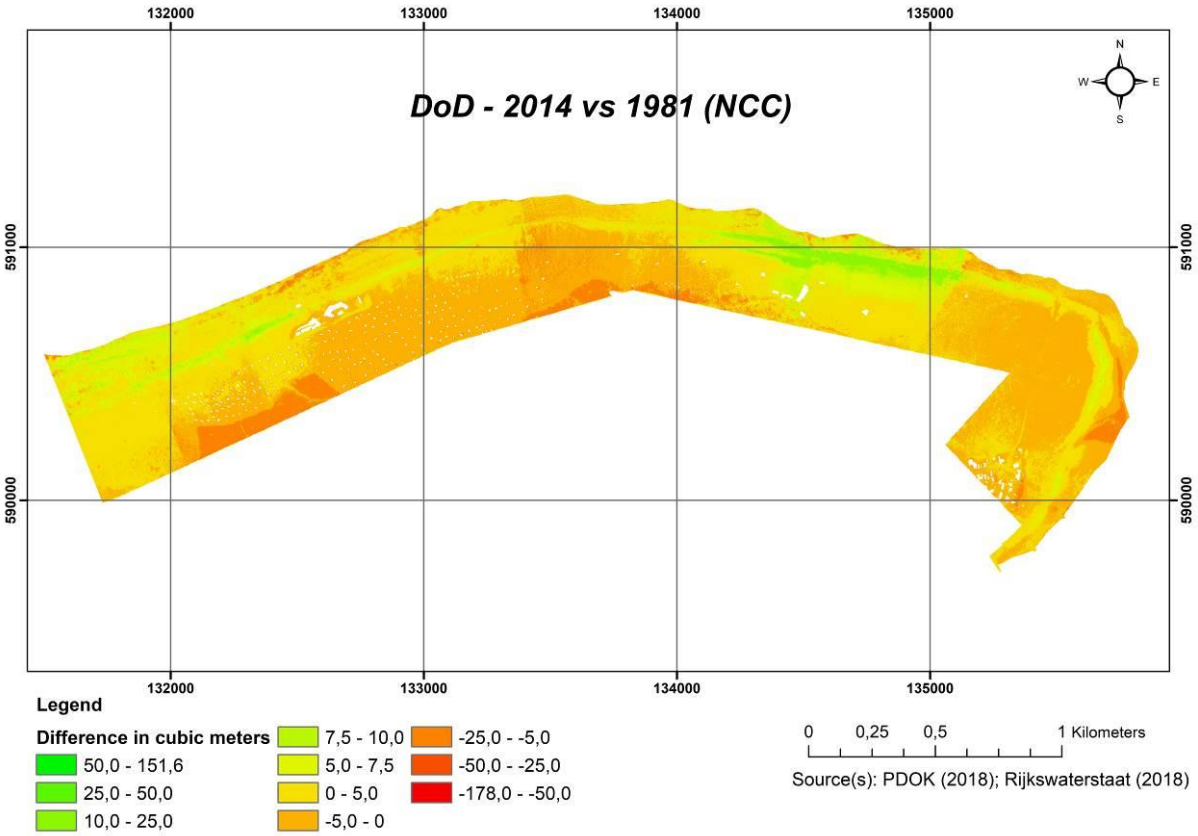

Figure 33: DEM of difference made subtracting the 1981 DEM-NCC from the LiDAR of 2014.

DoD: LiDAR 2017 vs DEM-NCC 1981

The comparison between the LiDAR dataset from 2017 to the DEM-NNC from 1981 had pretty similar results considering the DoD 2014 vs DEM-NCC 1981. The areas that gained in volume are lying on the dune's portion, and the southwest part together with the extreme east represents the area that lost in volume during this time-period. The DoD has -65,1 and 23,6 cubic meters for minimum and maximum values, respectively (Figure 34).

DoD: AHN 2014 vs DEM-NCC 1981

The area of the AHN 2014 dataset that was used for this comparison was clipped to be in the same and original shape of the DEM-NCC 1981, since the original dataset covers the whole Netherlands. The DoD presents minimum value of -65,3 cubic meters and maximum value of 27,9 cubic meters (Figure 35). The result is also similar compared to the DoDs of 2014 and 2017 with LiDAR, though the areas that had a decrease in volume, represented by hot colours, are more spread in the southwest-south part, and are clearly corresponding to the vegetation areas that were supressed during the decades. In addition, the green areas are marked by the dune's region for the beach zone at the extreme northwest portion.

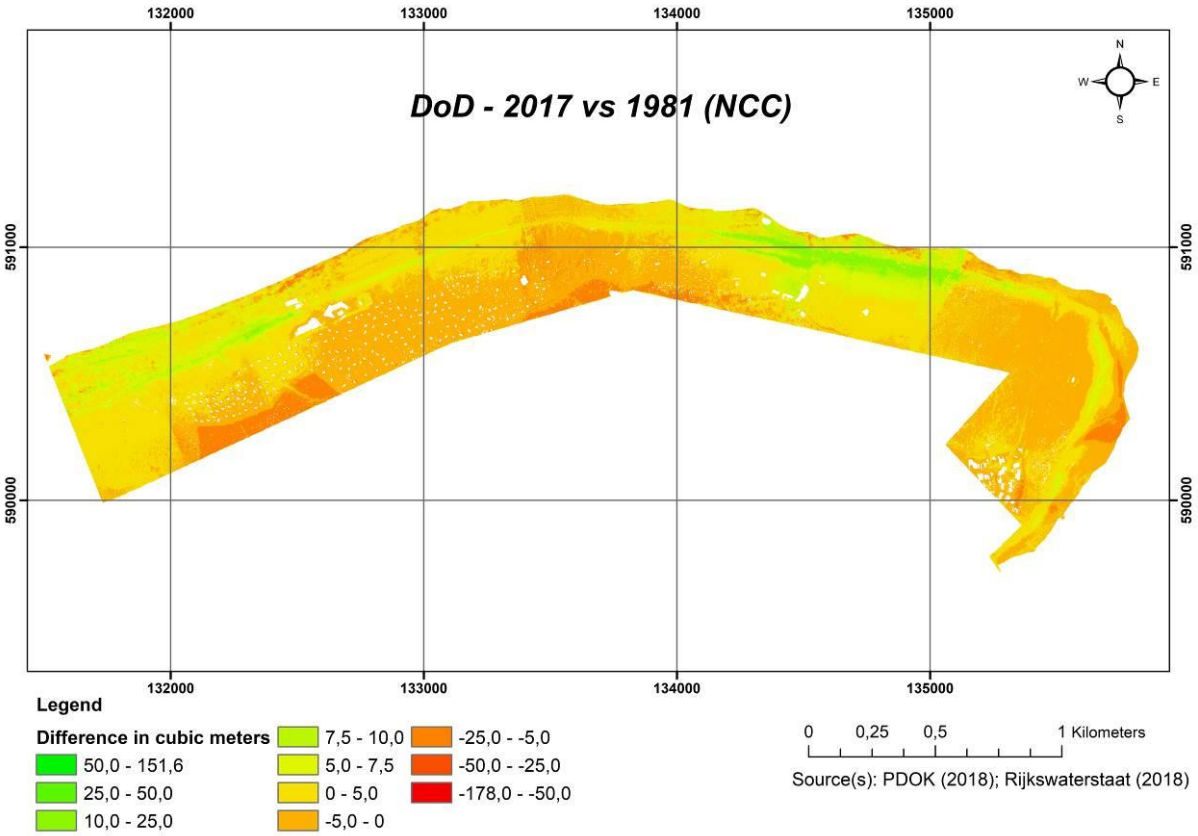

Figure 34: DEM of difference comparing 2017 LiDAR with the DEM-NCC of 1981.

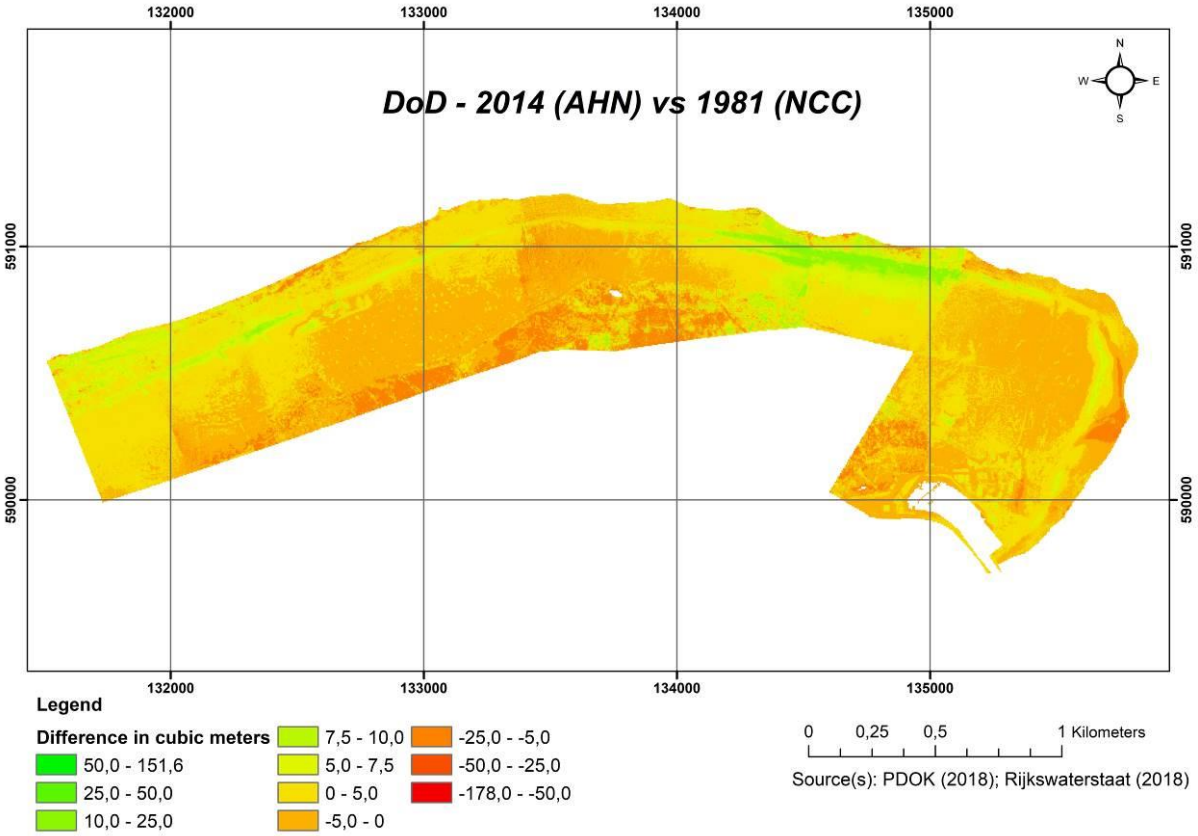

Figure 35: DEM of difference made considering 2014 AHN and 1981 DEM-NCC.

DoD: LiDAR 1997 vs DEM-SGM 1981

The DoD made in this step used as input the LiDAR data from 1997 and the DEM-SGM from 1981. The results show the green colour representing the increased volume, while the red areas, mostly located in the coast at northwest and east, represents the portions that decreased in volume. The values are also not representative due to the many outliers in the LiDAR dataset. The minimum value is -195,6 cubic meters and the maximum value is 2508,7 cubic meters (Figure 36).

DoD: LiDAR 2004 vs DEM-SGM 1981

The subtraction of the DEM-SGM 1981 from the LiDAR of 2004 resulted in a DoD with -249,6 cubic meters as minimum value and 2484,8 cubic meters as maximum value. The increasing in volume is once again visible through the green colour, and the hot colours are spread in the coast showing the decrease in volume (Figure 37).

DoD: LiDAR 2014 vs DEM-SGM 1981

The results from this DoD are -178,1 cubic meters as minimum value and 151,8 cubic meters for the maximum value. The delineation of the dune's area is better noticeable, and it is in green colour. Some parts in the coast appears with red colour, with a decrease in the volume (Figure 38).

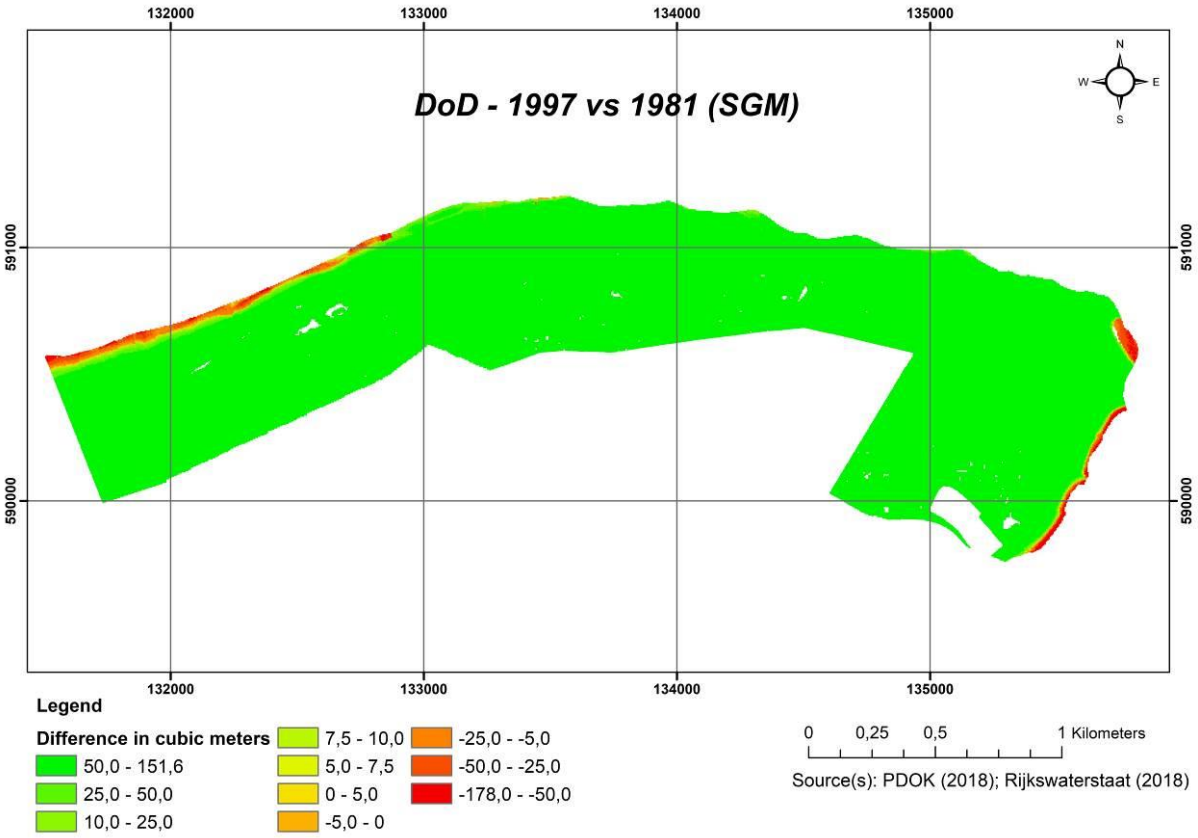

Figure 36: DEM of difference made by using the LiDAR dataset from 1997 and the DEM-SGM of 1981.

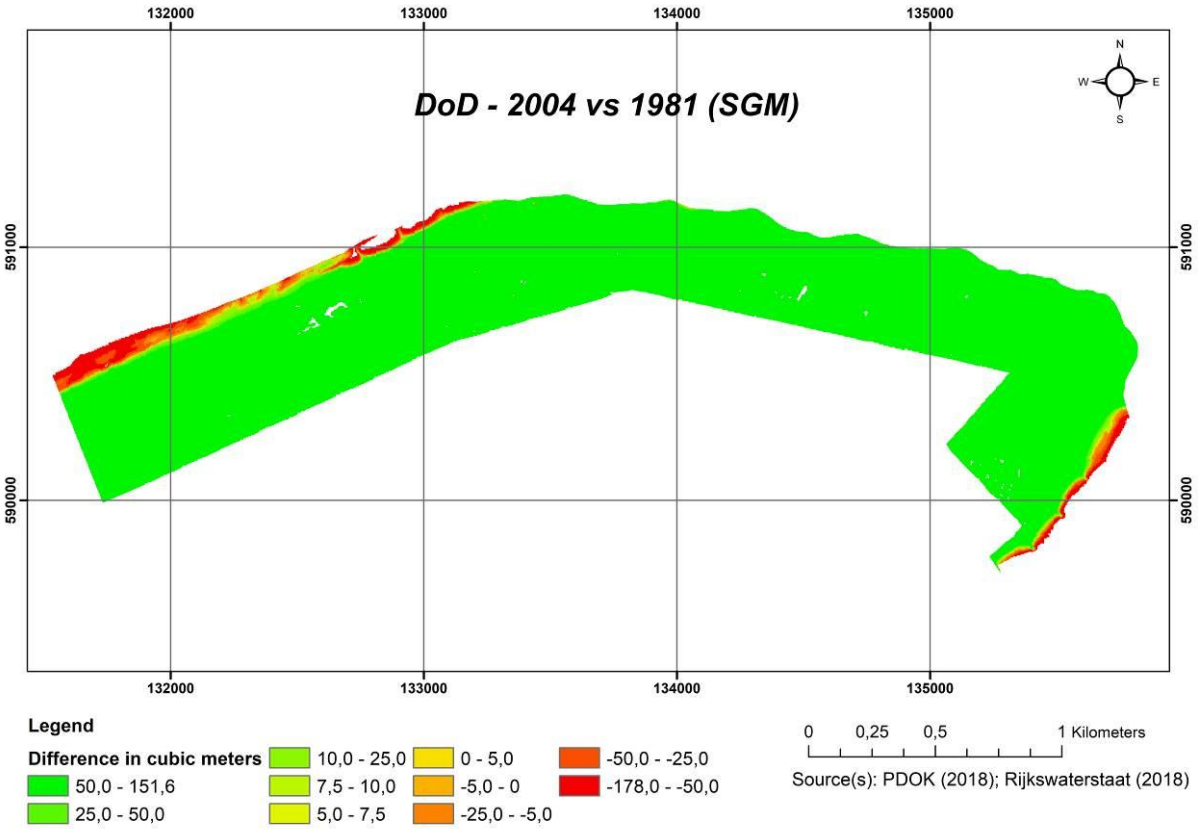

Figure 37: DEM of difference created with 2004 LiDAR and 1981 DEM-SGM.

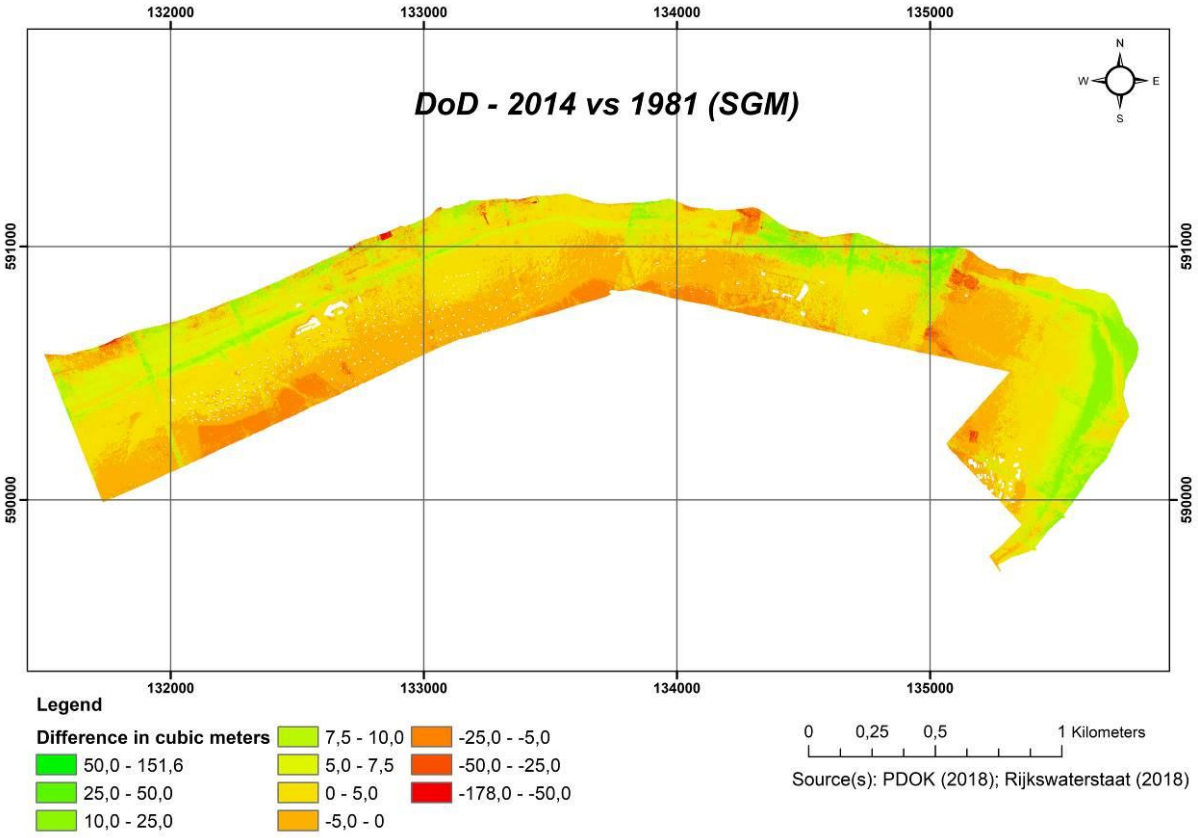

Figure 38: DEM of difference made by using the LiDAR dataset from 1997 and the DEM-SGM of 1981.

DoD: LiDAR 2017 vs DEM-SGM 1981

The LiDAR of 2017 was also compared with the DEM-SGM from 1981 and are similar to the DoD of the same period using the NCC algorithm, however, as the DEM-SGM has many outliers, the outcome was influenced and provides no realistic numbers for the maximum difference values. The minimum value is -177,0 cubic meters and the maximum value is 152,1 cubic meters (Figure 39).

DoD: AHN 2014 vs DEM-SGM 1981

Even the AHN 2014 having a well detailed and reliable elevation values, as the DEM-SGM of 1981 had several outliers, the end DoD is close to the previous two DoDs, 2014 and 2017. The values are given by -178,0 cubic meters for the minimum and 151,6 cubic meters for maximum (Figure 40). In this case, the southwest portion does not show too many changes since the yellow color is predominant is this area.

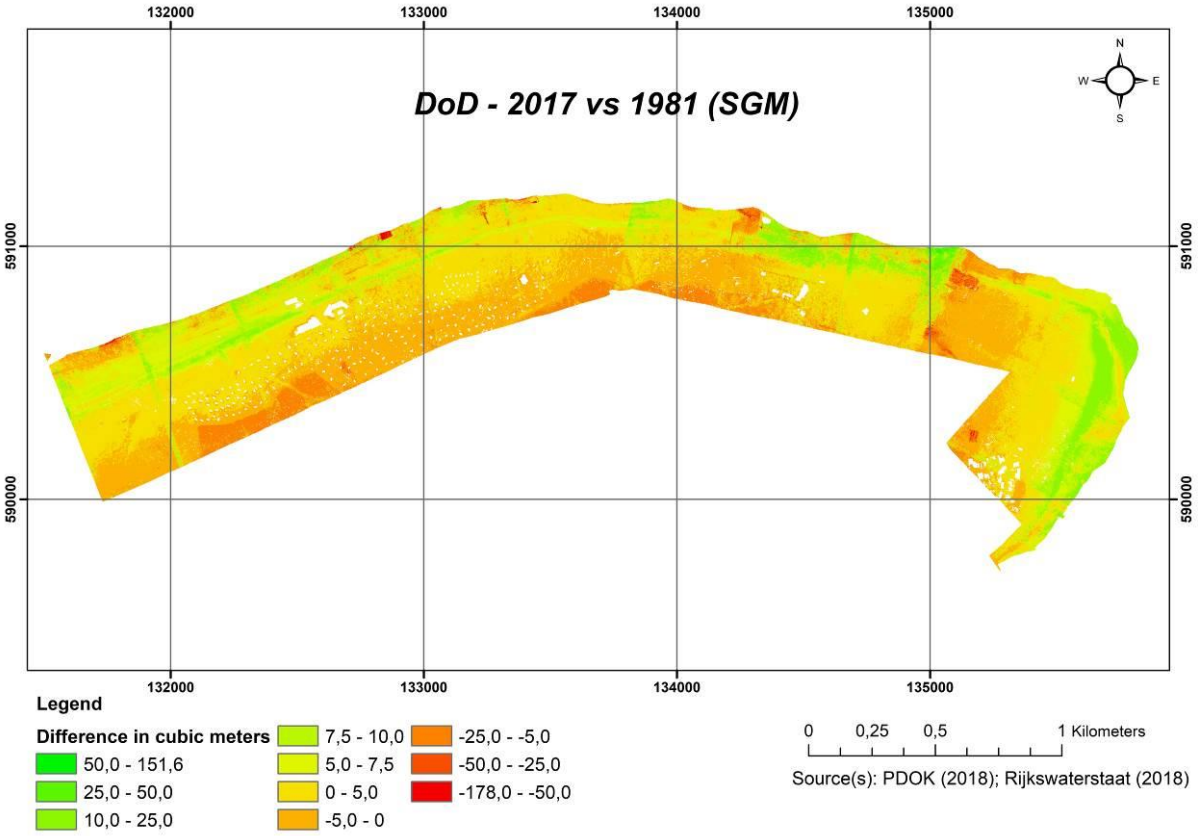

Figure 39: DEM of difference performed with the subtraction of 1981 DEM-SGM from the 2017 LiDAR data.

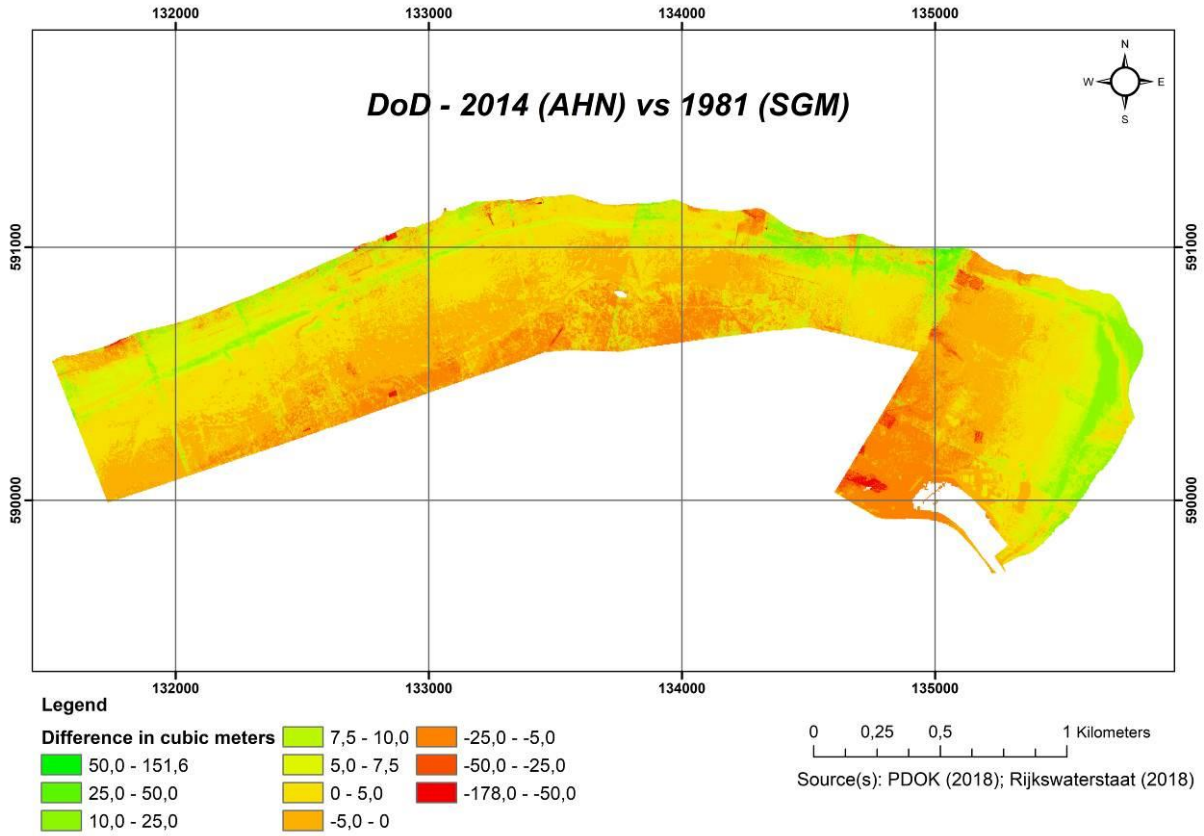

Figure 40: DEM of difference considering the AHN of 2014 and the 1981 DEM - SGM.

Comparison with 1945

The DoDs were again used to show the comparison between the DEM, made through the NCC method for the aerial photographs of 1945, with LiDAR and AHN datasets. The years used to make this correlation were the same as those applied for the 1981 DEMs, being 2017, 2014 and 2004 of LiDAR data and the AHN of 2014. When necessary the datasets were clipped to be comparable between each other. As the DEM could not be generated due to the poor quality of the input point clouds made with the SGM method, for this section of the report, the DoDs were done only utilizing the 1945 DEM-NCC.

DoD: LiDAR 1997 vs DEM-NCC 1945

This comparison was made through the LiDAR data from 1997 and the DEM-NCC 1945 resulting in the DoD of figure 41. The green colour exhibits the gain in volume. This DoD provided non-reliable values due to the input LiDAR dataset bringing several outlier numbers to the correlation. The minimum value is 58,0 cubic meters and the maximum value corresponds to 2522,6 cubic meters.

DoD: LiDAR 2004 vs DEM-NCC 1945

The DoD created in this step was made with the LiDAR data of 2004 and the DEM-NCC of 1945 (Figure 42). The comparison provided values of difference in volume from -17,5 cubic meters to 2499,3 cubic meters. The lower values represent the decrease in volume during this time-period and are shown in hot colours concentrated in the southeast, while the green colour marks the increase of volume in the study area. Similar to the DoD from 1997 vs 1945, this data is non-reliable due to the many outliers in the LiDAR input dataset.

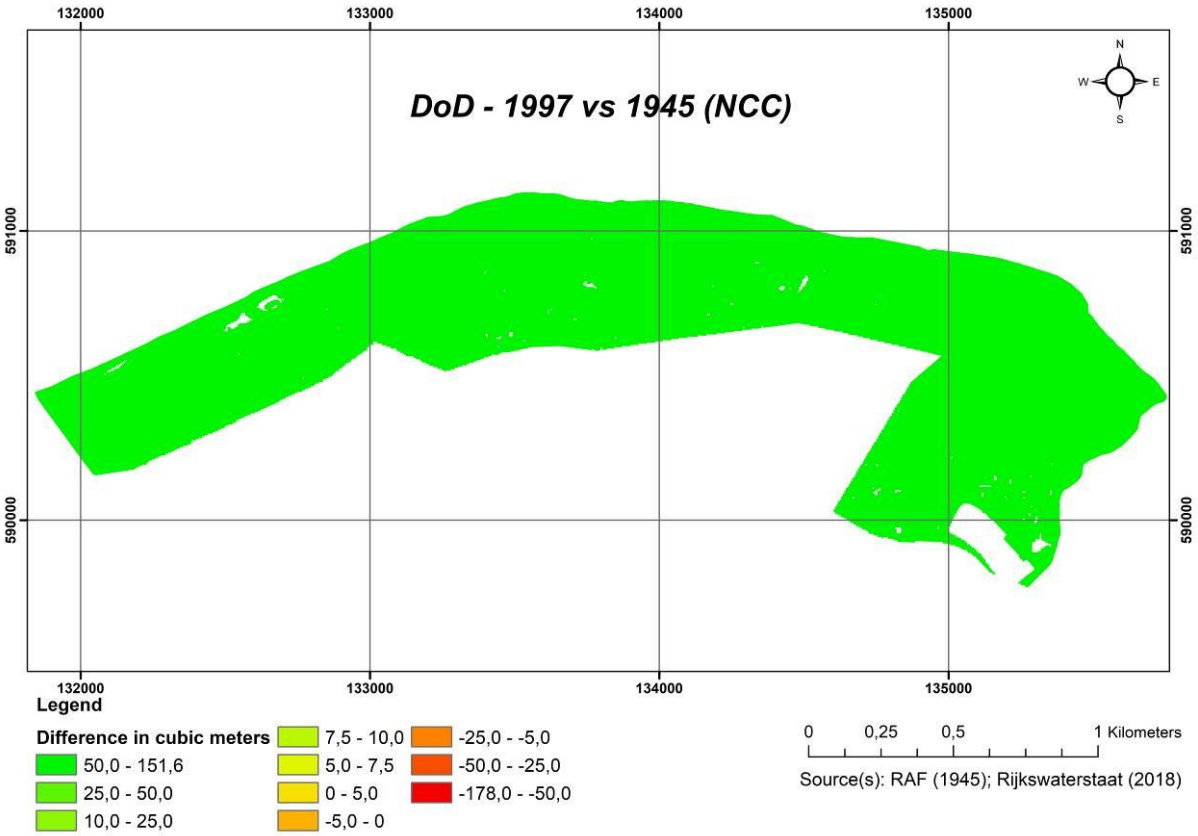

Figure 41: DEM of difference of 1997 LiDAR and 1945 DEM-NCC.

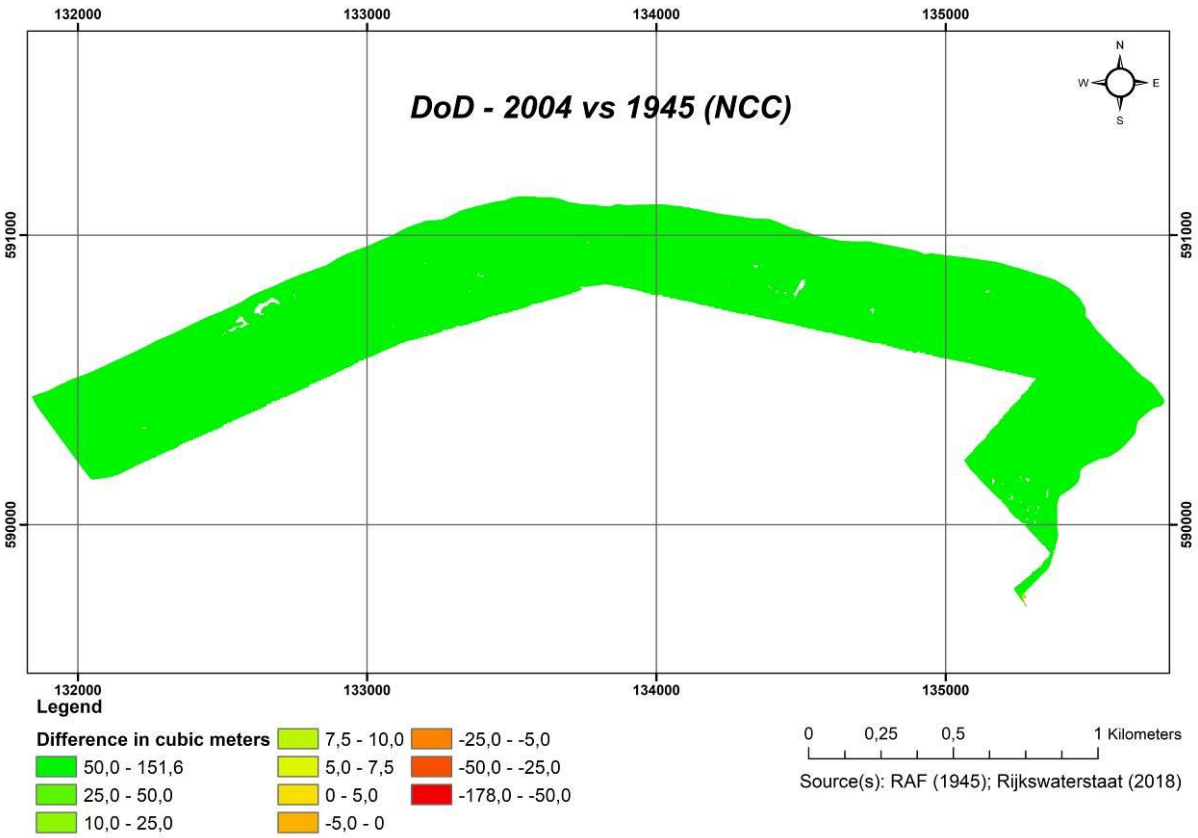

Figure 42: DEM of difference considering 2004 LiDAR data and the DEM-NCC of 1945.

DoD: LiDAR 2014 vs DEM-NCC 1945

As the input data of 2014 LiDAR came with reliable elevation values, this comparison resulted in a DoD more realistic considering the changes in volume of this period (Figure 43). The difference is given in the range from -29,0 to 25,8 cubic meters, and mostly represented by hot colours and green colour, respectively. The dune's area is the most prominent part in terms of volume increasing (green areas).

DoD: LiDAR 2017 vs DEM-NCC 1945

The DoD made with the comparison between the LiDAR of 2017 and the DEM-NCC of 1945 is similar to the DoD using the 2014 LiDAR. The volume changes appear in green and hot colours, being the first one the increase and the second the decrease, both in cubic meters. The thin part where the beaches are located there was a loss of sediment, while in the dune's region, the gain in sediment, or deposition, was more common (Figure 44).

DoD: AHN 2014 vs DEM-NCC 1945

The DoD of AHN 2014 and DEM-NCC 1945 is shown in the figure 45. It has the difference of volumes of -50,1 cubic meters as minimum value and 26,4 cubic meters as maximum value. The gaining in volume is displayed in green colour, and the volume loss is presented by the hot colours along the study area.

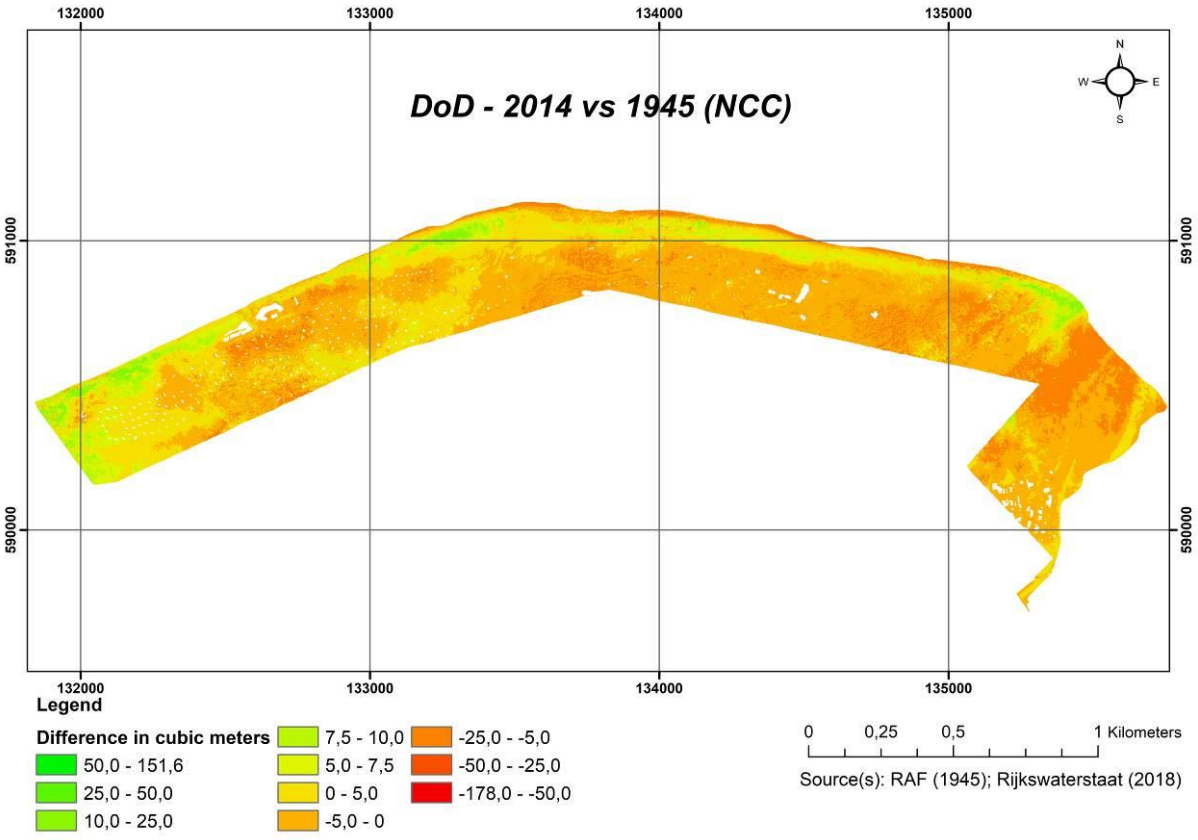

Figure 43: DEM of difference made using the LiDAR dataset of 2014 and the DEM-NCC of 1945.

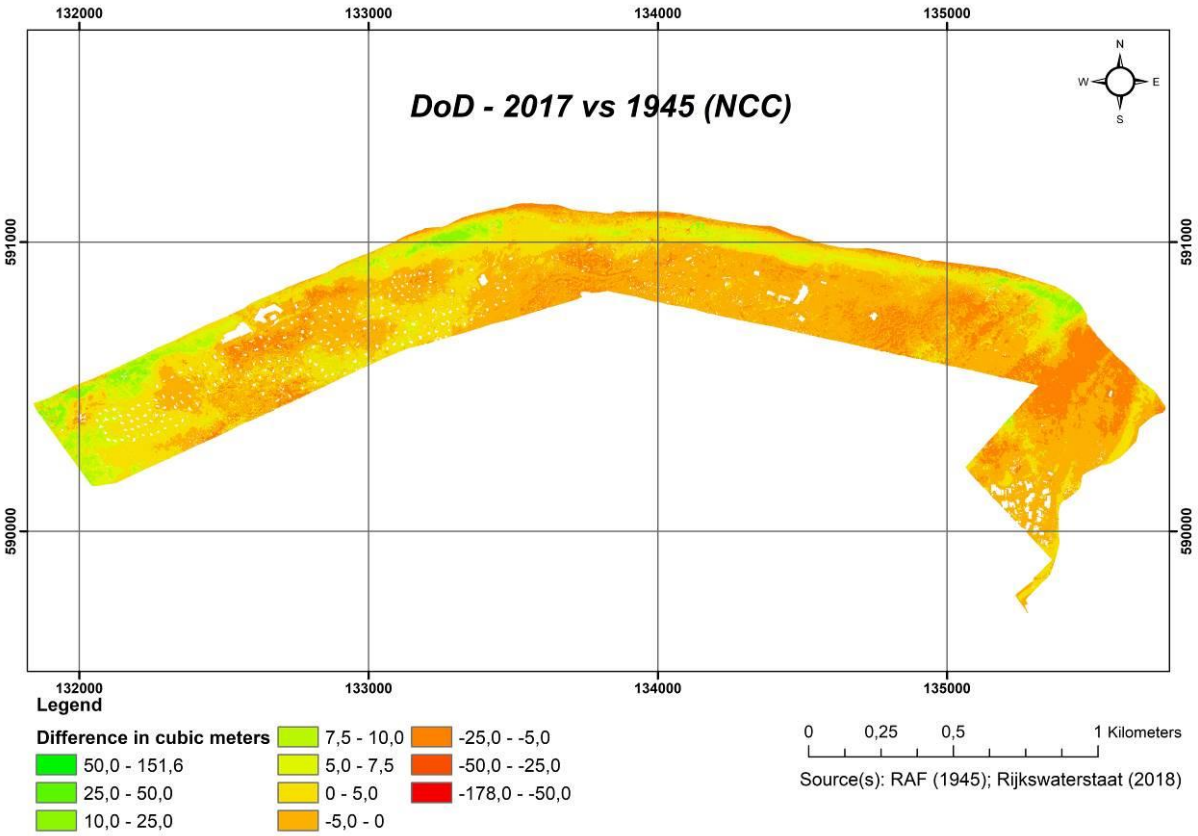

Figure 44: DEM of difference generated through the comparison between the 2017 LiDAR and 1945 DEM-NCC.

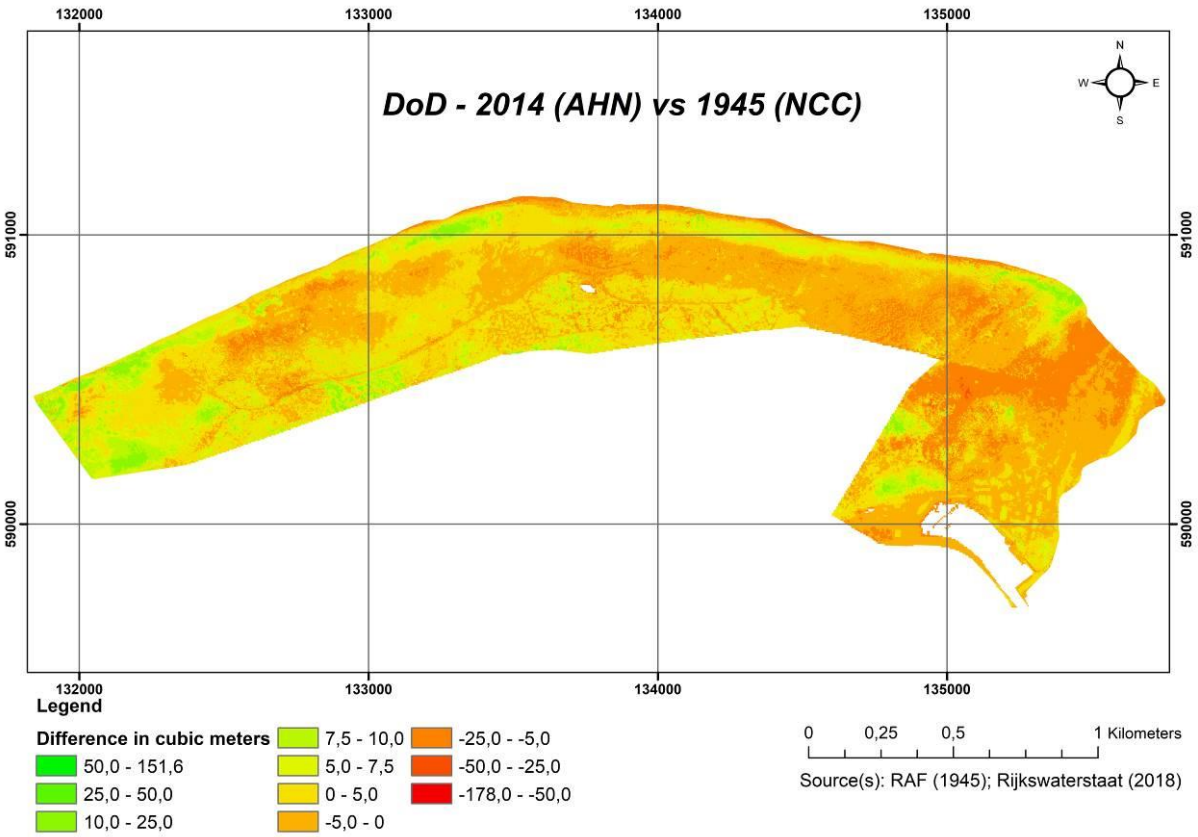

Figure 45: DEM of difference considering 2014 AHN and 1945 DEM-NCC.

Classified maps of the DoDs

The changes in volume can also be showed through classified maps of the study area. Three classes were distinguished for all DoDs, ranging as the following: negative cubic meters values < to -1; -1 to 1; 1 < positive cubic meters values. These classes respectively depict decrease, minimal changes, and increase of volume. The classified maps of the comparison between the studied years are shown in figure 46, 47 and 48, considering the 1981 DEM-NCC, 1981 DEM-SGM and 1945 DEM-NCC.

The classified maps of the DoDs point out that in general, the study area had more losses than gains in the volumetric context. The green colours in the maps shows the increase of volume, while the red colour means loss. The beige or sand colour represents minimal changes along the area. These outcomes arouse and indicate where the main changes are located in East-Vlieland.

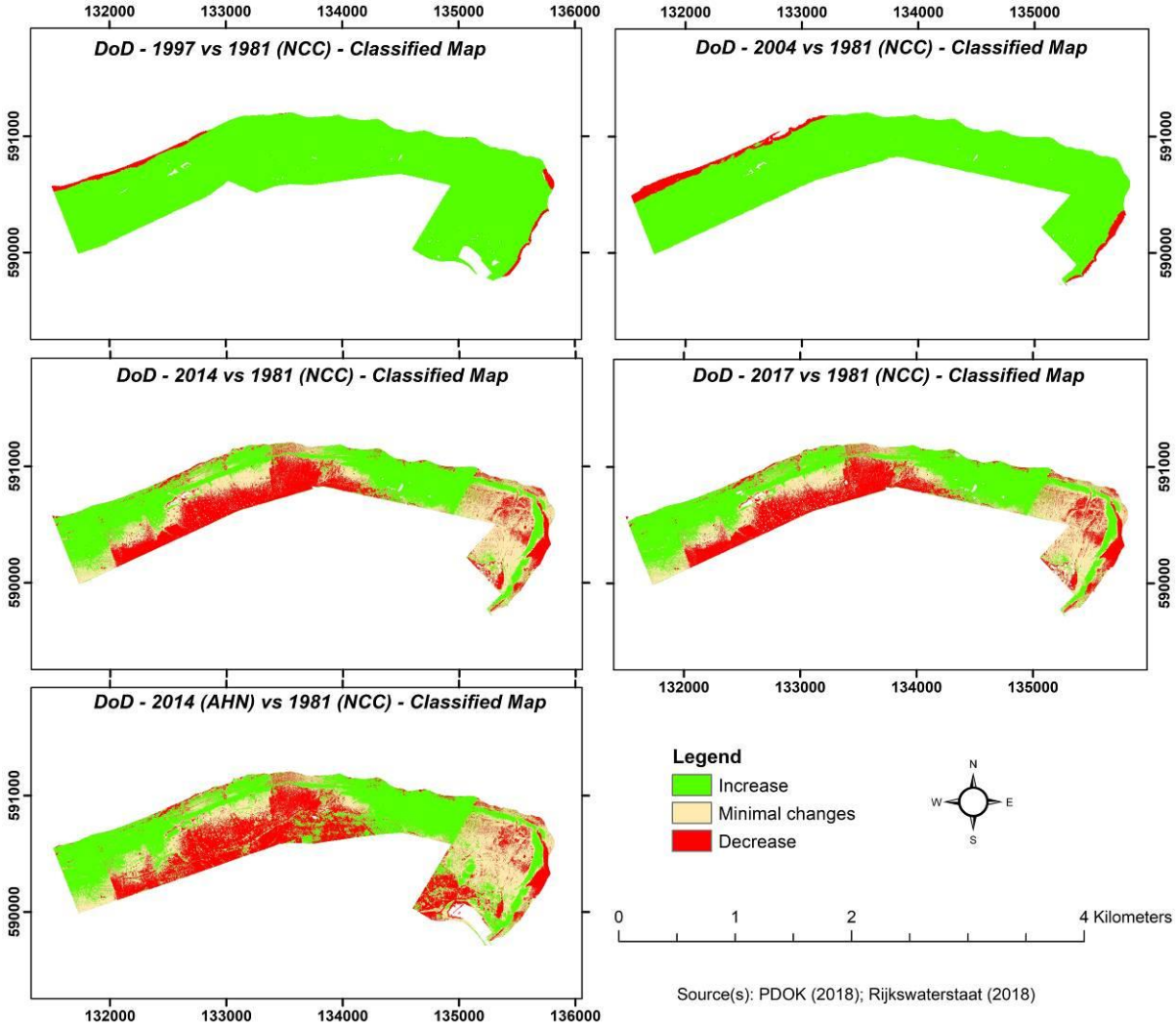

Figure 46: Classified maps of the DoDs considering the LiDAR and AHN datasets, compared to the DEM-NCC of 1981.

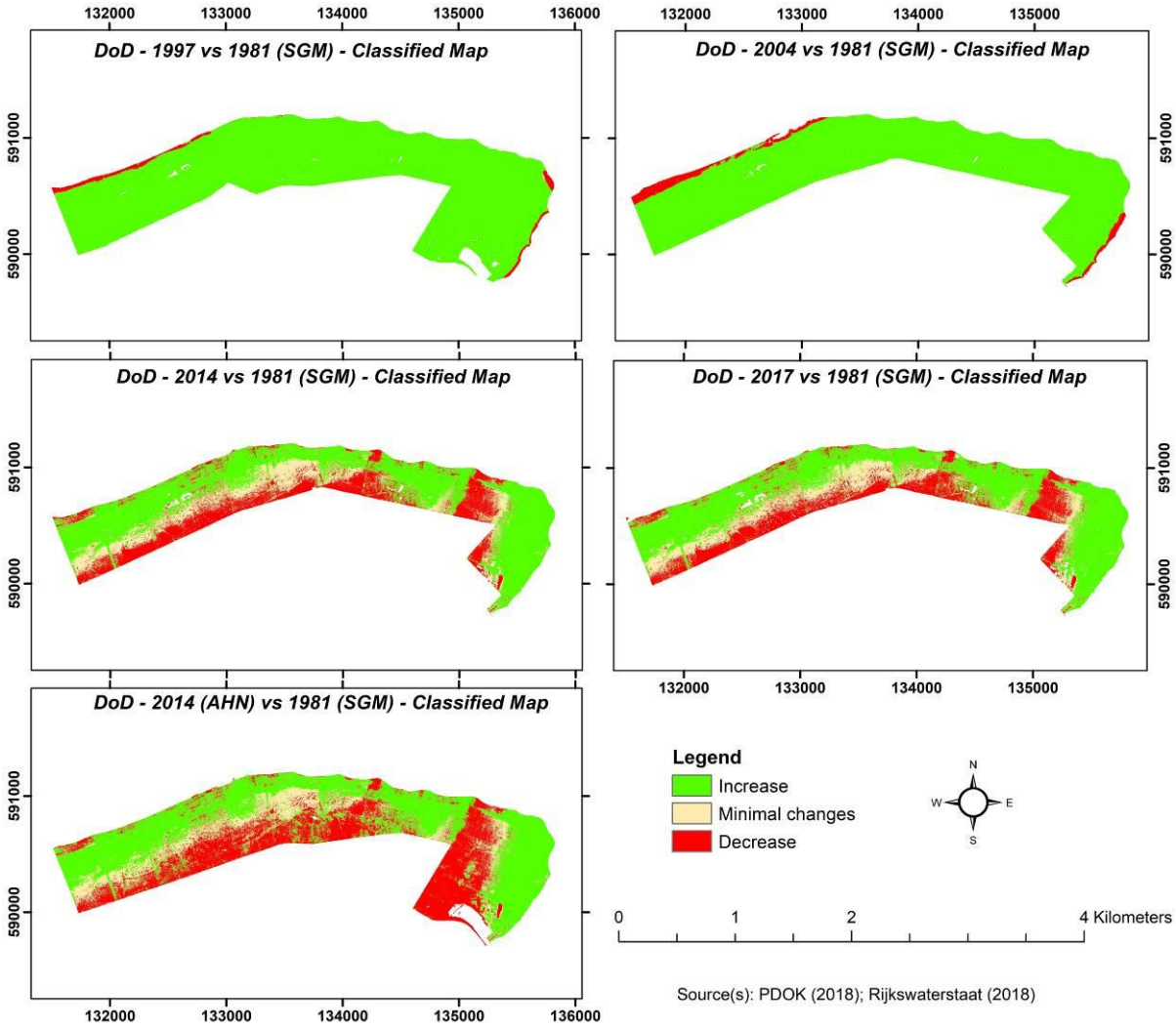

Figure 47: Classified maps of the DoDs made with the comparison between the LiDAR and AHN datasets with the DEM-SGM of 1981.

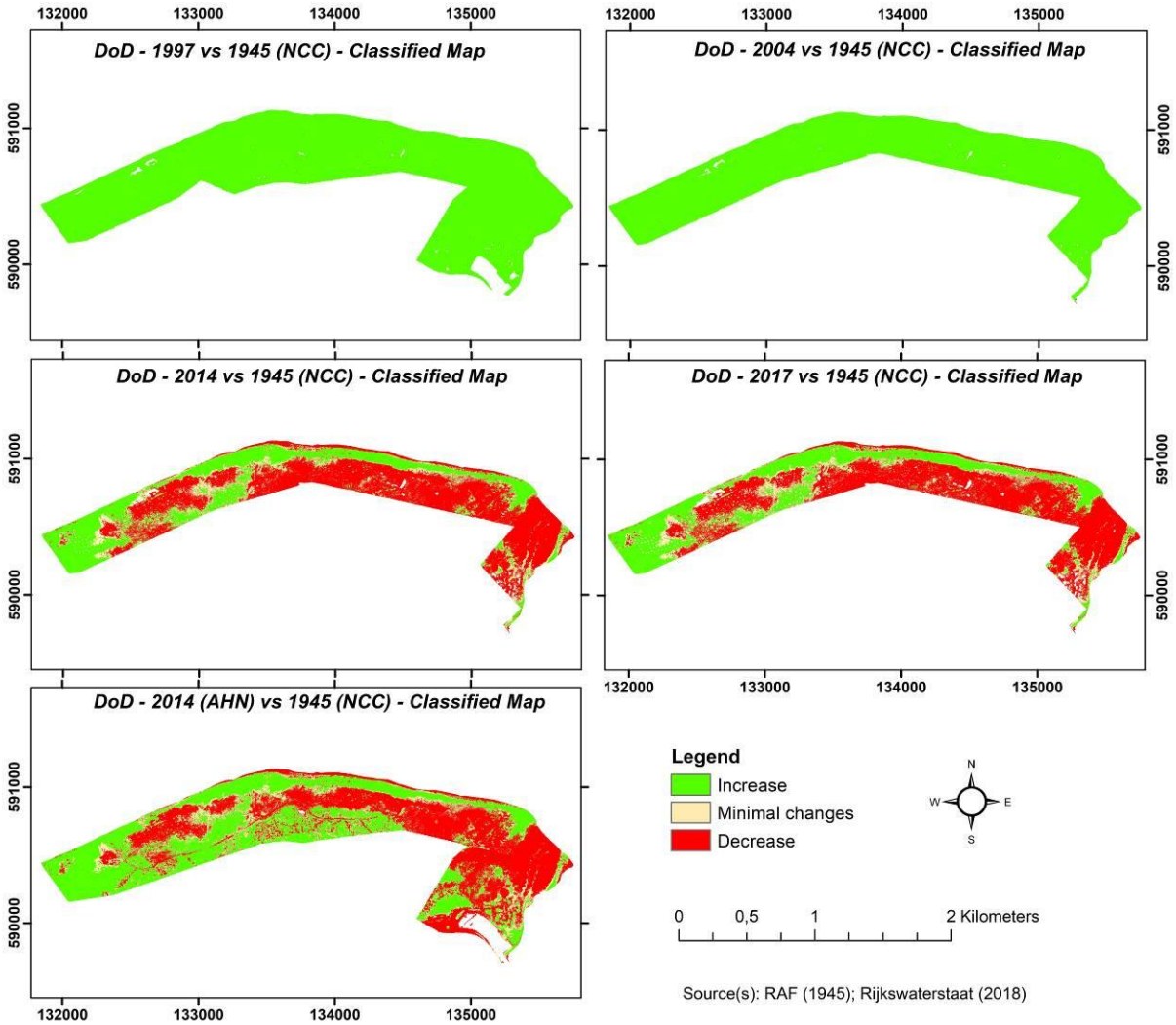

Figure 48: Classified maps of the DoDs made with LiDAR and AHN datasets, and the DEM-NCC of 1945.

4.7 Volumetric changes

The analysis carried out in this phase considered the volumetric changes occurred during the studied time-periods. The surface volume tool of ArcMap was applied to calculate the volumes for each raster used in this research, and the results can be seen in table 12. The results of the DEMs created during this project are given with a margin of error, which was calculated through the input errors of the input geoprocessing step, the RMSE from the GCPs and tie-points.

Year of Comparison	Dataset	Total Volume (m^3)
1981	LiDAR 1997	1.914.962.294
	LiDAR 2004	1.570.137.652
	LiDAR 2014	16.166.255
	LiDAR 2017	15.623.480

	AHN 2014	21.771.983
	DEM-NCC 1981	71.344.725 ± 3
	DEM-NCC 1981 clipped	65.576.072 ± 3
	DEM-SGM 1981	441.720.709 ± 3
	DEM-SGM 1981 clipped	346.022.526 ± 3
1945	LiDAR 1997	1.105.687.763
	LiDAR 2004	1.032.358.528
	LiDAR 2014	10.701.022
	LiDAR 2017	10.723.173
	AHN 2014	17.251.528
	DEM-NCC 1945	35.121.639 ± 3
	DEM-NCC 1945 clipped	24.136.740 ± 3

Table 12: Surface volumes of the rasters used in this study. The LiDAR and AHN datasets are given for both years, 1981 and 1945, because, in order to be comparable, they were clipped according to the DEMs, which have distinct size areas.

The volumetric changes were calculated subtracting the values of the older dataset from the newer, for instance [LiDAR 1997 minus DEM-NCC of 1981] resulting in 1.843.617.569 cubic meters. The results are expressed in cubic meters and can be seen in table 13.

	DEM-NCC		**DEM-SGM**
Datasets	**1981**	**1945**	**1981**
LiDAR 1997	1.843.617.569 ± 3	1.070.566.124 ± 3	1.473.241.585 ± 3
LiDAR 2004	1.504.561.580 ± 3	1.008.221.788 ± 3	1.224.115.125 ± 3
LiDAR 2014	-49.409.817 ± 3	-13.435.719 ± 3	-329.856.271 ± 3
LiDAR 2017	-49.952.592 ± 3	-13.413.568 ± 3	-330.399.046 ± 3
AHN 2014	-49.572.741 ± 3	-17.870.111 ± 3	-419.948.726 ± 3

Table 13: Volumetric changes for the study area along the time-periods contemplated in this research.

As the input data from LiDAR 1997 and 2004 had several outliers, the comparison was also influenced badly, as already showed in the DoD chapter. Analysing the volumetric changes for these two years compared to the DEMs of 1981 and 1945, the results are far from reality, because the calculations for all deliverables are then conditioned to the elevation values and having such a high number like 2485 meters from the 2004 LiDAR, the differencing in volumes are in the scale of billion.

4.8 Orthophotos

The orthophotos show the true location of the pixels, meaning that there is no displacement, errors, distortions and interferences of objects on the photographs. The buildings are exactly from the top view and have the correct location in the real world. Appendix F-F1 show the orthophoto of 1981 with the NCC method, while Appendix F-F2 exhibits the orthophoto made using the 1981 DEM-SGM. The orthophoto of 1945 correlated with the DEM-NCC could not be performed. This means that the errors in the GCPs and the orientation as a whole were not sufficient to deliver an orthophoto.

4.9 Quality Assessment of Point Clouds and DEMs

The quality of the point clouds datasets can be evaluated, improving the understanding of how good the results are, and how they influence next processing steps. The point clouds are normally assessed through their statistical information, composed by the values of mean, standard deviation, and related histograms. The generated DEMs may also be evaluated by the RMSE values found for the GCPs, in the exterior orientation processing step. In addition, DEMs may also be assessed using visual checks, which qualitative analysis help to have a complete understanding of the data quality. These validations can be done by creating extra products from the DEM, such as a map of contours.

4.9.1 Point clouds assessment

The quality of the point clouds have a significant impact on the results of constructing a DEM. The point cloud generation of the imageries was made in ERDAS Imagine using the NCC and SGM image matching algorithms. As already mentioned before, in order to perform this type of data, there are several settings to be chosen in the software, for instance search window, window size, interpolation method in NCC, and last pyramid level and disparity difference in SGM. In the current research, for all calculations there were used the default settings.

There are three point clouds data evaluated in this section, being the 1981-NCC, 1981-SGM and 1945-NCC datasets. As depicted previously in the point clouds 1981 section, the point cloud 1945-SGM was not a usable product for further processing, being not necessary to comment on this data in the current report section.

The sets of point clouds for 1981-NCC, 1981-SGM and 1945-NCC were visually inspected and compared on their statistics data. A visual inspection was also made during this research, meaning that differences were manually checked, especially by using a 3D viewer. This is done to see, if there are obvious differences between sets and if some results do not make sense.

The point clouds datasets were compared on their standard deviation value, which was previously stated and explained that these are measurements to see how the values are spread along the data. A smaller standard deviation means that the elevation values are closer to the mean being more accurate. There are not very steep ridges in the study area, as a coastal zone in the Netherlands, which can cause high differences between the average elevation and the collected elevation values. So, if the standard deviation has a small value, the difference between the mean and the height values obtained are more accurate for the set of point clouds delivered in this study. The comparison and correlation between the statistical data of the point clouds made is shown in table 14.

Min (m)	Max (m)	Mean	Standard Deviation	Point Count	Point Spacing	Point Density (p/m²)
-8,5	90,4	6,8	5,5	128.070.304	0,223	18,4
-187,1	201,5	6,4	10,1	983.175.710	0,080	156,25

-8,5	57,2	6,8	5,5	21.012.164	0,514	3,7

Table 14: Statistical data from the three products of image-based point clouds made in this thesis. The values belong to the point cloud-NCC of 1981, point cloud-SGM of 1981, and point cloud-NCC of 1945 datasets.

The best standard deviation values are from the 1981-NCC and 1945-NCC point clouds, meaning that their elevation values obtained during the calculations are closest to the real situation of the study area. Then, based on visual checks, point count, point spacing and point density, the 1945-NCC point clouds is worse than the 1981-NCC. This because as there are many more points in the data for 1981-NCC, the resolution of this point cloud is more reliable and accurate. Besides, as the IDW interpolation is used afterwards, the results of this point cloud can provide a more accurate DEM. This can be easily observed and be understandable looking into the figure 22/appendix B and figure 24/appendix D, where the point density is visually higher for the 1981-NCC than the 1945-NNC, which has many empty spaces.

The point cloud made with the SGM method resulted in a standard deviation of 10,1. It is the worst standard deviation among the other point clouds, but the mean value was similar to the ones from the 1981-NNC and 1945-NNC point cloud. This means that the standard deviation of 1981-SGM was highly affected by the outliers.

Visual checks on the data shown that the 1981-SGM, made with the Tridicon-SGM in ERDAS, resulted in many clearly visible squares of points. They can also be seen in a cross-section view of the data and are obviously not related with the real landscape of the study area (Figures 49 and 50). In addition, the 1981-SGM point cloud has better point count and point density compared to the others, meaning that the image matching process worked better for this algorithm.

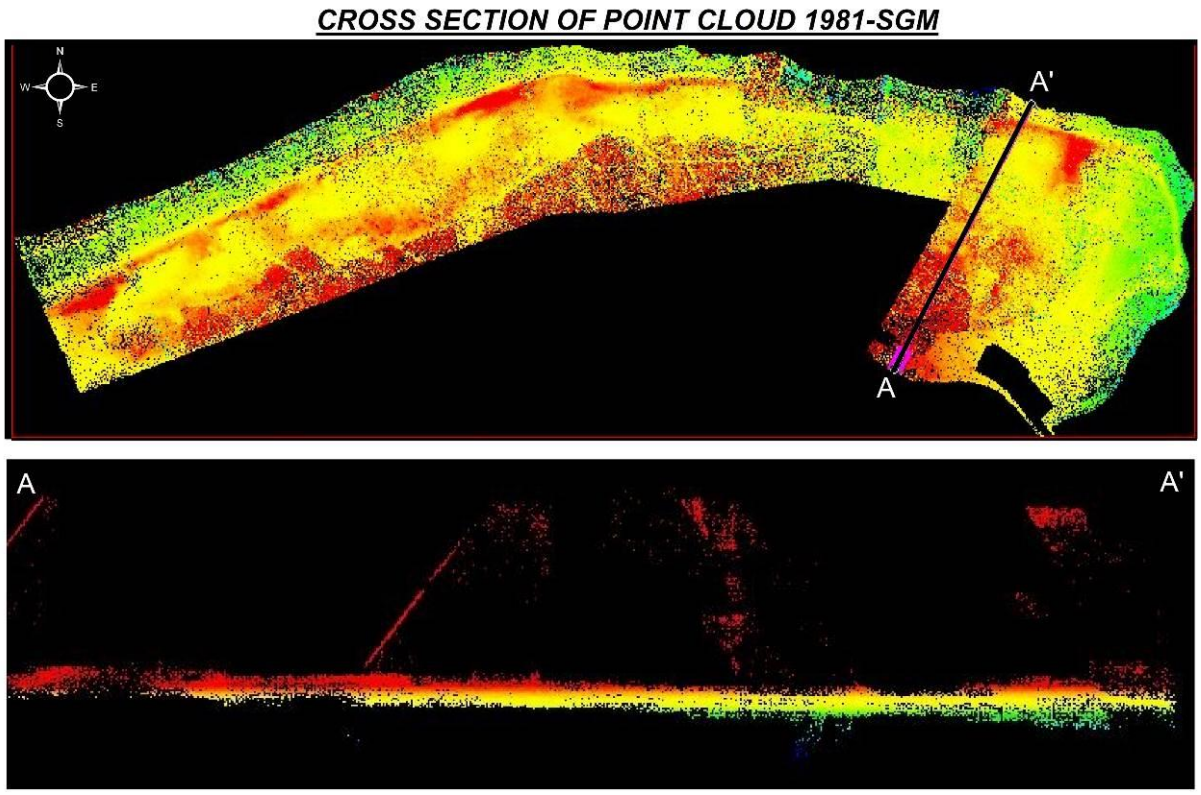

Figure 49: Cross section of the point cloud 1981-SGM dataset showing several outliers. View in ERDAS Imagine.

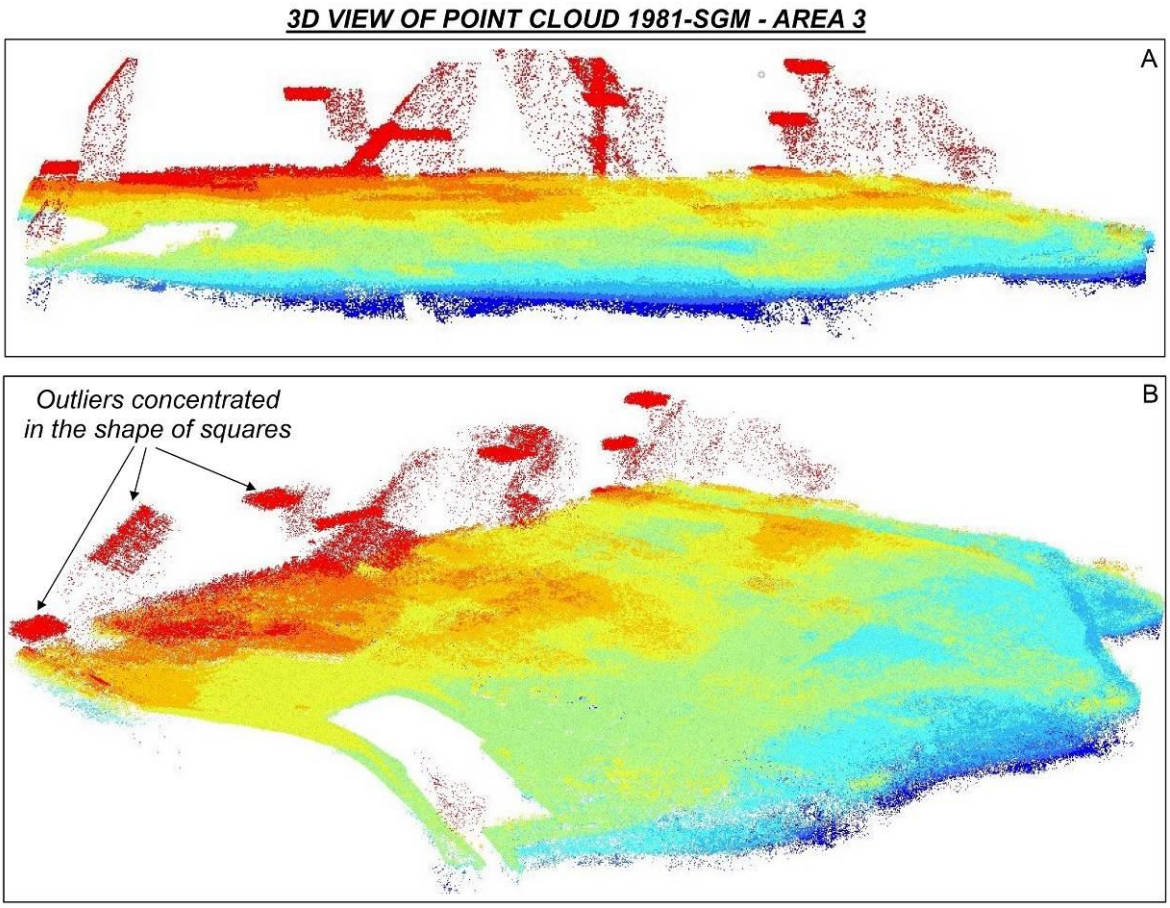

Figure 50: View in ArcScene of the point cloud dataset 1981-SGM of the area three. The outliers in squares shape are easily recognizable. A) View to W. B) View to NW.

The three point clouds data have their histograms shown in figure 51. They point out the descriptive statistics of the datasets. The histogram of 1981-NCC (histogram A) presents that the correlations are mostly clustered in the left side of the graph, meaning that there are more low values than high values, there is also a long peak. The histogram B of the point cloud 1981-SGM shows a long central peak and small range of elevation, meaning that the heights are mostly constant along the study area, despite of the outliers. The histogram C of the point cloud 1945-NCC has a similar pattern to the histogram A, clustered to the left, but it does not present the same variation for the elevation values, and it has two main long peaks.

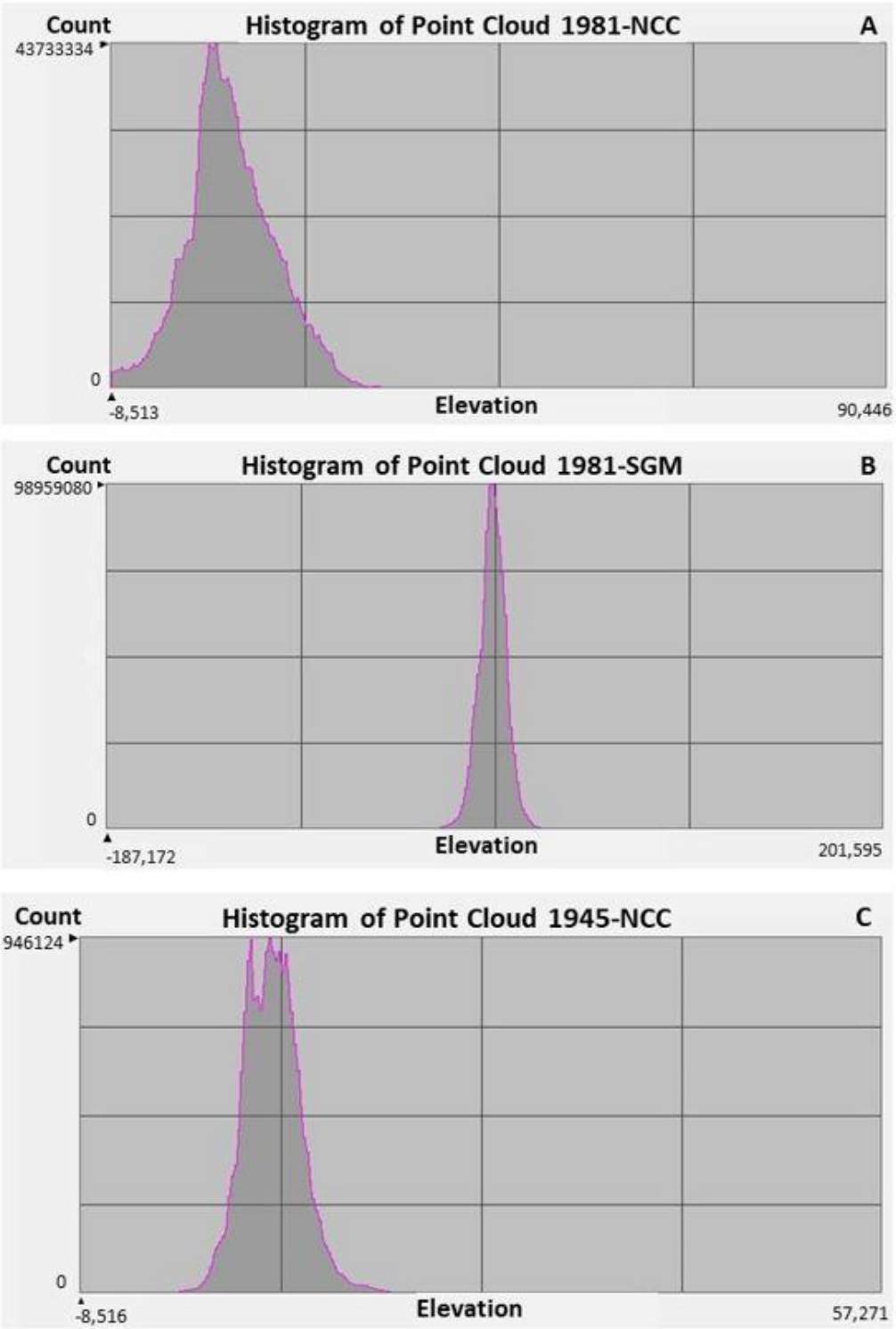

Figure 51: Histograms of the point clouds datasets created in this research.

4.9.2 DEMs

The RMSE results for the GCPs for the three extracted DEMs, 1981 DEM-NCC, 1981 DEM-SGM and 1945 DEM-NCC were shown previously in table 2 and figures 20 and 21. The errors obtained in the exterior orientation process are in the range of 0,01 to 0,04 meters, as can be seen in table 15.

As the orthophoto is an image that is free from distortion due to geometry, and free from displacement due to the relief, knowing the inclination, position and distortion of the aerial camera at

the time of taking an aerial photograph, it is possible to define the projection centre and calculate the coordinates of any point of the image. To achieve this accuracy is necessary to have a precisely positioning and defined reference points in the image. As the creation of orthophotos were done successfully in this research for the 1981 DEMs, the error of the GCPs are in the acceptable range. The orthophoto of 1945 DEM-NCC could not be performed, most probably because the DEM is the less detailed among the others.

A contour map was made from each DEM, using a contour interval of 1 meter. The same portion of the study area is presented for each input DEM in the figure 52. It is possible to notice that the contour maps, in general, have good results, because there are no isolines intersecting each other. It was applied alternation colours scheme to easily identify when intersected isolines appears. The example used in this section shows that the contours generated from the 1981 DEM-SGM has better resolution with more contour lines representing the surface.

Besides, there were created three cross sections for the DEMs generated in this research (Figure 53). They were made from the same A-A' profile from figure 49. It is possible to verify that the terrain profiles are similar in terms of roughness. The dunes zones are well marked by the peaks in the right part of the graphs of 1981, however in the 1945 profile they are subtler. The peak around the 200 meters distance in the 1981 DEM-SGM profile is highest part of the DEM. In the cross section of 1945 DEM-NCC there is a peak of 34 meters in elevation around the 600 meters distance, corresponding to outliers in the dataset, because it is unlikely that there is such a high elevation in East-Vlieland.

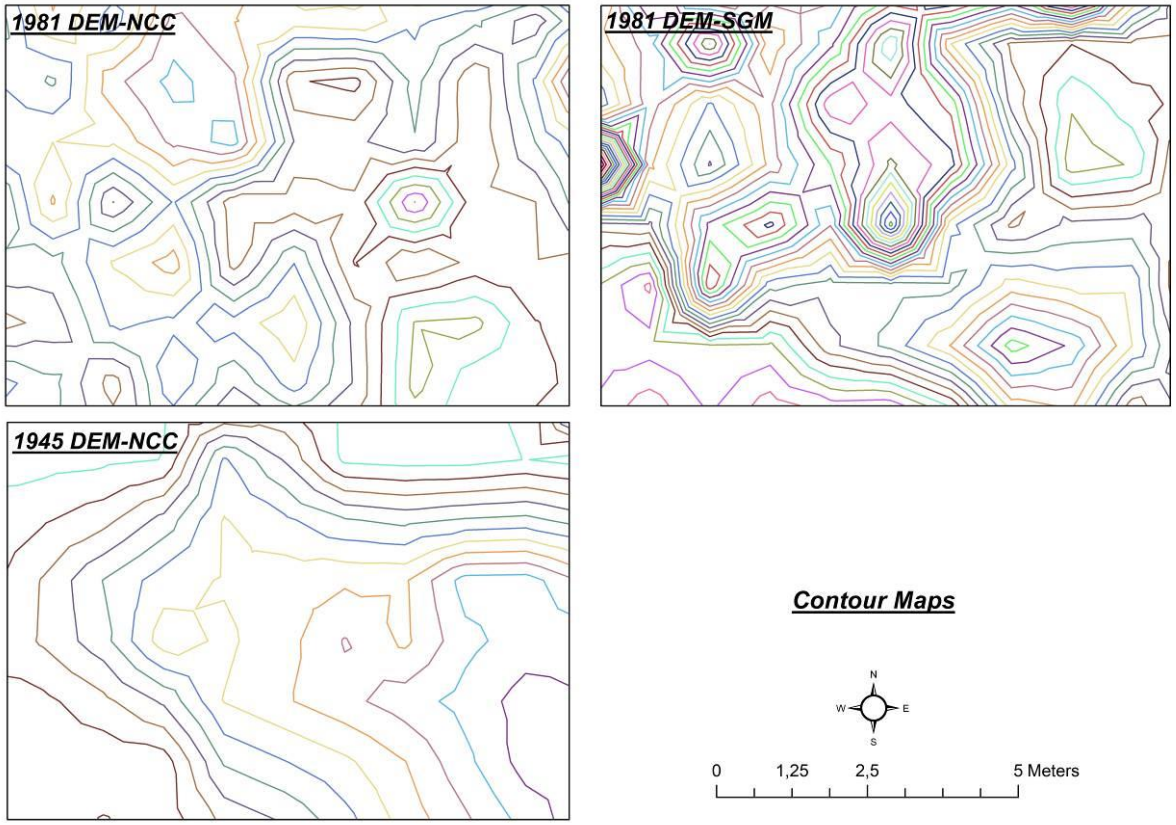

Figure 52: Contour maps generated from the DEMs of 1981 and 1945. The same location of East-Vlieland is shown in the three maps.

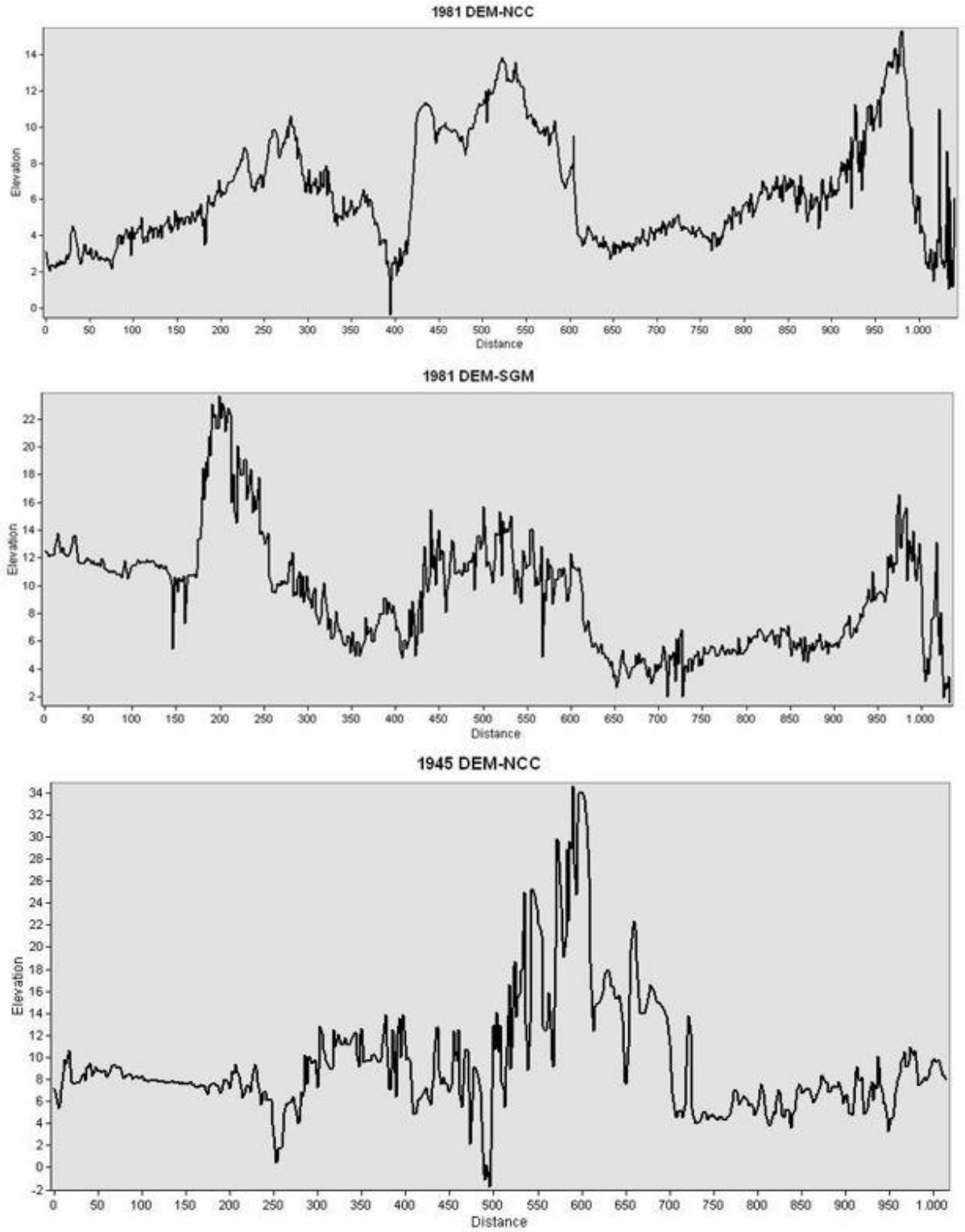

Figure 53: Terrain profiles for each DEM extracted from historical aerial photographs during this study.

5. Discussion

The purpose of this research was to make use of historical aerial photographs to perform reliable DEMs of the East-Vlieland island in the Netherlands, for the years 1981 and 1945, being then compared to DEMs of recent LiDAR data and AHN data. The main objective was to provide the volumetric changes that occurred in the studied time-periods. Secondary achievements were discussing where the largest change happened in the study area, as well as which image matching method had a better response in creating DEMs, NCC or SGM, and what differences between the algorithms can be pointed out. It was also an addition to the topic a quality assessment for creating point clouds and DEMs from historical aerial photographs, also addressing the discussion to which method of image matching provided the best results.

The objectives were achieved, giving deliverables as DEMs of 1981, made using the two algorithms NCC and SGM, DEM of 1945 using the NCC method, and the volumetric changes along 72 years. The extraction procedure of DEMs ended successfully for the set of images from 1981, for both image matching methods, however, for the year of 1945, only the DEM made with the NNC algorithm had a result.

It is important to point out that the volumetric changes calculated during this research are very prone to errors due to poor input datasets, outliers, noise or even interferences such as vegetation. This is very sensitive especially because the volumes are measured through DEMs, and those features mentioned above may not represent the real world, marking improperly elevated areas and then influencing the volume calculations.

Quickly relating the DEMs extracted from aerial photographs and LiDAR data and AHN, these are collected and measure despite of vegetation, because LiDAR is able to measure through leaves, while the imagery does not have this option. In the coast of the Netherlands, normally the Water bodies and Rijkswaterstaat captures aerial photos in early spring when there are fewer leaves, and the surface is more visible.

5.1 GCPs

The selection of GCPs for georeferencing aerial photographs is a very important and sensitive part during the processing step. It is sensitive by means of that the errors may directly influence the results. During this research, the collection of GCPs was conditioned to Google Earth Pro, which was the topographic reference for the points. According to Linder (2016), at least three GCPs are needed to set the orientation of a photograph, however it is added that quality of the orientation is highly susceptible to the quantity and the distribution of GCPs, in other words, as much as possible points, better results may be achieved. In total, there were selected 92 GCPs for the imagery set from the year 1981, while a total of 114 GCPs were chosen for the 1945 photographs.

The distribution of the GCPs in both set of images were difficult to be guaranteed during this study. Area one in both years had more built up areas with fixed roads, so the selection of GCPs flowed smoothly, however in areas two and three was harder because of the larger presence of vegetation, and especially dunes and beaches, being more complex to define reliable GCPs. This process brings uncertainties to the project. The errors of the GCPs in this study were in the range of 0,01 to 0,04 meters.

A reflection over the importance of the GCPs is taken into account in this thesis report. After all the methodology applied for DEM extraction, creating block models, running calculations, it is clear how the setting up of the GCPs is crucial for the whole project. Performing the practical part on the 1981 aerial photographs flowed much more smoothly than with the set of 1945, especially because for 1981 there was a camera report available. Even being possible to calculate the camera parameters for the 1945, this estimation brings many uncertainties for the study. This was particularly observed when dealing with the area three for the 1945 photos, which firstly was hard to even perform a triangulation in the block file, and after many attempts, it provided a poor-quality point cloud data in terms of point count and point density.

What also needs to be addressed considering GCPs is the location of the study area. For this research, selecting GCPs along the dunes, beaches, and dense vegetation areas, was a hard task to accomplish. Choosing these points in coastal zones puts the whole DEM extraction procedure in a high level of difficulty. The points may be in a small quantity, not very well distributed, what in the end affects the results. It is different when one needs to perform the same methodology in build-up areas, such as cities or villages.

5.2 DEMs

The DEMs created during this research reconstructed the surface from the years of 1945 and 1981 for the East-Vlieland island using historical aerial photographs. They were made in ERDAS Imagine and provided the 3D aspect for such a historical data. Two DEMs were extracted using the NCC algorithm, for the years of 1981 and 1945, and one DEM through the SGM method for the year of 1981. It was not possible to carry out a second DEM for the year of 1945, due to the poor point clouds data done with the SGM method.

The DEM-NCC of 1981 showed that the coast and the beaches correspond to the low elevation values in the area, while the dunes and the forest/vegetation configures the highest areas. The same disposition is noticed for the other two DEMs, 1981 DEM-SGM and 1945 DEM-NCC. Even expecting better results from the process made with the SGM method, according to literature (see Dall'Asta, 2016), the standard deviation of the 1981 DEM-NCC was lower than the one from the DEM-SGM of 1981, being 4,8 and 9,3. As already mentioned before, a smaller standard deviation means that the values are closer to the mean and can be more accurate (Alexiou and Ebrahimi, 2018). The standard deviation of the 1945 DEM-NCC is 3,3, however, the results are not very good, especially because the DEM has many holes and empty spaces, brought by the 1945 input point cloud. The void fill method and the IDW interpolation during the DEM construction, triangulated those holes and spaces deriving coarse areas along the DEM, influencing afterwards, the comparisons for the DoDs and the volume calculations for the year of 1945.

It is necessary to draw the attention to the reliability of the surface models from the LiDAR and AHN datasets. The years of 2014 and 2017 LiDAR, and the AHN from 2014, are the most reliable input data available in this research, while the LiDAR data from 1997 and 2004 were given with several noise, influencing then the further processing steps.

The DEMs made within this thesis represented the surface of East-Vlieland back in time. It is interesting to note that even though this activity provides many discussions about the reliability and quality of the deliverables, it is must be said that it is indeed possible to extract and perform 3D data, as well as view them in 3D, from historical aerial photographs (see figure 26). As the 3D data acquisition is always increasing, the need for new and different methods and techniques is also important, and the ability to use old data like historical aerial imagery is a positive addition to the topic.

5.3 DoDs

In order to compare the DEMs in this study, the DoDs were created by differencing the oldest data from the newer data. By this, one can understand, analyse and locate where the changes in volumes happened in the studied time-period. A total of 15 DoDs was generated, from the comparison between the 1981 DEM-NCC with LiDAR of 1997, 2004, 2014, 2017 and AHN of 2014; 1981 DEM-SGM with LiDAR of 1997, 2004, 2014, 2017 and AHN of 2014; 1945 DEM-NCC with LiDAR of 1997, 2004, 2014, 2017 and AHN of 2014.

The DoDs were presented in difference in cubic meters, which showed lower values in hot colours normally located along the coast, and/or spread in the vegetation/forest, this probably explained by the deforestation that took place during the decades, giving space for build-up areas. The higher values were commonly lying in the dunes portion, marked by the green colour, located just nearby of the beaches, crossing the whole study area, from west to east. The results clearly showed that the correlation made using the DEM-NCC of 1981 ended better, with contrasting changes in specific areas, like the city, the vegetation at the south part, and the dunes in the extreme east.

Applying the DoD quantitative technique to compare and quantify topographic and geomorphic changes proved to be an exceptionally approach for this research. The reasons are that, firstly, this is a relatively simple procedure, making use of simple mathematical operations. Secondly, it tends to highlight where the main changes are located. However, attention should always be kept because the method compares raster datasets as a whole, and it is important to distinguish noise/errors from the real geomorphological changes.

The classified maps of the DoDs for all studied years, brought an interesting perspective to analyse the outcomes. In that sense, one can highlight where the changes occurred along the study area. The increase of volume can be explained by sediment deposition, considering the beaches and the dunes, and also for the growth of the villages, and the expansion of the harbour at the southeast portion. Classified maps that used the LiDAR of 1997 and 2004 compared with the three DEMs provided not a good and authentic result. It is as if the island had been completely created over the studied years (from 1945 or 1981 to 1997 or 2004), which, of course, is not true. These effects can be entirely attributed to the input datasets of LiDAR in this case, pointing out the importance of being careful with the errors, accuracy and precision of the input data, such as photographs, GCPs and tie points, point clouds and DEMs.

5.4 Volumetric changes

The volumetric changes were given by the subtraction of the older DEMs from the newer DEMs, specifically differencing the extracted DEMs of 1981 and 1945 from the LiDAR and AHN rasters. Comparing the years of 1997 and 2004 with 1981 and 1945, the results showed an outstanding increasing of volume in the scale of billion. As already explained, the LiDAR data of 1997 and 2004 came with non-realistic elevation values, influencing badly these calculations.

Moreover, taking into account the years of 1981 (DEM-NCC) and 2014, 2017 (LiDAR) and 2014 (AHN), the volume decreased by 49.409.817 ± 3 m^3, 49.952.592 ± 3 m^3, 49.572.741 ± 3 m^3, respectively. Now, considering the 1981 DEM-SGM, the values are way too different from the ones shown above, being a decrease of 329.856.271 ± 3 m^3, 330.399.046 ± 3 m^3, 419.948.726 ± 3 m^3. Finally, the volumetric changes obtained for the comparison of the years 2014, 2017 (LiDAR), and 2014 (AHN) with 1945 (DEM-NCC) are also a decrease in volume of 13.435.719 ± 3 m^3, 13.413.568 ± 3 m^3, 17.870.111 ± 3 m^3, respectively.

The calculations showed that the changes in volume are different considering which image matching process was applied, NCC or SGM. However, in general, all the results are revealing that the landscape of East-Vlieland decreased in volume within the studied time-frame of 72 years. Most probably, the reason is highly related to human intervention in the area, where deforestation took place. But also, it can be explained by erosion process that occurred along the coast, where the action of the sea is actively outstanding. This is especially observed in the beach lying at the extreme east of the study area (east of area three), which is represented in the figures 33, 34, 35, and their corresponding DoDs classified maps, where the decrease of volume is easily noticeable.

5.5 Quality Assessment

The process of creating DEMs is subject to errors, as each step is dependent from the other. This means that, all datasets created during the processing part needs to be evaluated before being used further, in other words, they should have a minimum level of acceptance or usability. In this research, there were created several types of data, such as georeferenced aerial photographs, point clouds, DEMs, DoDs, classified DoDs and volume calculations. These datasets were already scrutinized along this thesis report, indicating good and bad results.

The GCPs in the exterior orientation had enough accuracy to perform the point clouds data and later the DEMs. The point clouds made provided good results in general, but some details can be pointed out. For this research the point cloud made with the NCC method from the year 1981 returned the best results, this is noticed because it had less outliers and a smaller standard deviation. The statistical values for the point cloud of 1945 made with the NCC algorithm were also notable, however

it is not considered a good point cloud due to very small value for point density, highlighted by the holes and empty spaces, influencing badly further process like the extraction of DEM.

The point cloud data for 1981 using the SGM method had the worse standard deviation value, meaning that the elevation values are not closer to the mean, reducing the accuracy of the data. In the other hand, this dataset comprised the best results for pixel count and point spacing, and consequently for point density, ensuring more detailed features for the data produced later. In addition, it must be pointed out that this point cloud had several outliers, usually appearing in the form of squares, and normally located on the edges of the stereopairs. This has affected the subsequent products, where it is possible to visualize the boundaries of each stereopair of the study area.

In the end, the point clouds made with the SGM method for the year of 1945 could not be used in this study due to the very bad result obtained, depicted in the appendix E. The elevation values appeared in the interval from -6731,4 to 4065,5 meters, which in no way represents the reality.

The performed DEMs were assessed through distinct methods, being the RMSE of GCPs (discussed above) and their participation in the orthorectification process, and also by visual inspections. It is observed that the DEMs resulted in orthophotos with good resolutions for the year of 1981, with the best one made with the NCC method, visually presenting less blurry aspects. For 1945, no orthophoto could be created, showing that the 1945 DEM-NCC in the end was not an acceptable for use, because its GCPs, and consequently elevation values, are not reliable.

The visual checks were the most used assessment of the DEMs during this research. There were created terrain profiles to see if the relief corresponds with what was achieved with the triangulation of GCPs, and also with the expected surface considering the stereo analyst viewer in ERDAS. The 1981 DEM-NCC cross section better represented the reality, not having peaks without any sense, showing that the low elevation areas are located in the beaches, while the higher areas corresponds to the dune's region and to the portion of the village.

Another derivative from the DEMs made in this thesis were the contour maps, being useful to visually assess the quality of the surfaces. In general, all three DEMs provided good results for the contour maps, not having too many isolines cutting each other. The best contour lines created, or the more detailed, was definitely made from the 1981 DEM-SGM, which shows more isolines than the other two products. This is consequence of point density of this dataset, being the best among all DEMs created during this research.

6. Conclusion

In this thesis, there were used two sets of aerial imagery to reconstruct DEMs and orthophotos of East-Vlieland. Even the lack of detail inherent to aerial photographs, especially in historical ones, the photographs used in this research resulted in representative DEMs from East-Vlieland. The extraction procedure of DEMs successfully reconstructed the 3D surface of the study area for the years of 1981 and 1945. The DEMs were used as input to calculate the volumetric changes occurred along 72 years, comparing with LiDAR and AHN datasets.

In this chapter, the main research question and sub questions are answered considering the results obtained in this thesis. The main research question is:

"How much was the volumetric change in cubic meters of the landscape and the coastal areas of East-Vlieland based on the comparison between the digital elevation models (DEMs) derived from historical aerial photographs and the coastal LiDAR datasets along the years of 1945, 1981, 1997, 2004, 2014 and 2017?"

The volumetric changes were calculated making use of the comparison between raster datasets representing DEMs of the study area. The calculations were done by subtracting the older DEMs from the newer DEMs, in other words, differencing the constructed DEMs of 1981 and 1945 from the LiDAR and AHN datasets. The comparison between 1997 and 2004 with the older DEMs, showed unreal volumetric changes for East-Vlieland, with the values being higher than 1 billion cubic meters. So, these unrealistic comparisons must not be taken into account to answer this question.

At the same time, the calculations comparing the years of 1981 and 1945 with the 2014 and 2017, LiDAR and AHN data, provided results more in accordance with the real situation. The volumes showed a decrease in cubic meters for the time frame of 72 years, mostly resulting from human activity and the interaction of the sea with the beaches and dunes. The values were 49.409.817 ± 3 m^3, 49.952.592 ± 3 m^3, 49.572.741 ± 3 m^3, comparing 1981 DEM-NCC/2014 LiDAR, 1981 DEM-NCC/2017 LiDAR, and 1981 DEM-NCC/2014 AHN, respectively. Correlating 1981 DEM-SGM/ 2014 LiDAR, 1981 DEM-SGM/ 2017 LiDAR, and 1981 DEM-SGM/ 2014 AHN, the values were 329.856.271 ± 3 m^3, 330.399.046 ± 3 m^3, 419.948.726 ± 3 m^3, respectively. Then, comparing 1945 DEM-NCC/2014 LiDAR, 1945 DEM-NCC/2017 LiDAR, and 1945 DEM-NCC/2014 AHN, the volumetric changes were 13.435.719 ± 3 m^3, 13.413.568 ± 3 m^3, 17.870.111 ± 3 m^3, respectively.

The sub questions are also answered in this concluding chapter. Sub questions:

"Where did the largest change occur in the coast of East-Vlieland considering the 2D and 3D products along the studied time periods?"

Considering the 2D and 3D products, the largest change occurred in the dunes' region located in the north part of the study area and in the south to southwest portion. Firstly, the dunes' represented the biggest change of increasing volume. The dunes run through west to east with a continuous, relatively thin, shape (see figure 46, for example). The areas in the south-southwest are mostly represented by vegetation, and they configure the largest changes in decreasing volume. The reason for this is mostly related to the suppression of the vegetation by human activity, the construction of new buildings and houses, enlarging the villages located at East-Vlieland. Another part that is of attention for large changes, is the beach on the extreme east portion of the area. The sediments there were mostly carried out due to the action of the ocean.

"What differences can be pointed out using the methods Normalized Cross Correlation (NCC) and Semi-Global Matching (SGM) for creating point clouds in the study area?"

Both methods returned with good results for image-based point clouds. They showed some differences in the statistical values of the point clouds, one being better in the standard deviation (NCC) for instance, and the other bringing better results for point count and point density (SGM). Performing point clouds using these calculations require a lot of effort, being an intensive and time-consuming process. The setting up of the block files for both methods are almost the same, however as the SGM does not work with aerial photographs from frame cameras, it was necessary to use the

imagery as they were from a digital camera. The uncertainty in this case (SGM method) is more related to the setting of pixel size in x and y directions. The uncertainty for the block file for frame cameras, or when using the NCC method, it is also related to the fiducial points, and as the 1981 imagery in this project came with a camera calibration report, the identification of those points was done without difficulties. The selection of GCPs can also bring errors to perform the two algorithms, because it is a mandatory step in the DEM extraction procedure.

Another difference that can be added is that the SGM method is more sensitive than the NCC regarding the quantity and distribution of GCPs. This was clearer when the SGM could not provide a good point cloud results for the 1945 imagery. Even though, some settings were changed, tweaked in the Tridicon manager, the results continued showing several errors. On the contrary, the NCC method could perform normally for 1945 photos, even the results not being very good, still it provided an outcome usable.

"Which method is most appropriate or accurate for creating point clouds in the study area, NCC or SGM?"

Considering all products made in this research, like the point clouds, the DEMs, the DoDs, the classification maps of the DoDs, the orthophotos, the 3D visualizations, terrain profiles, histograms, almost all of them showed better results, more reliable values, better visual checks, for the ones created using the NCC method, when comparing with the products made with SGM. It can be said that for historical aerial photographs, the NCC method worked better than the SGM in standard deviation and visually aspects. NCC had better statistical values than the SGM, and also the quality assessment of those products confirmed that the ones made with NCC point clouds, had better visual quality and accuracy. It is still interesting to think about this question, especially because at the begging of this research, it was expected that SGM will performs better, considering what is presented in the literature, see Hirschmueller (2005), and Haala and Rothermel (2012). With this is mind, it can be pointed out that the SGM method worked better for image matching process when considering point count and point density. So, in the end, with this point of view, the SGM reached the expectations and was the best method. It is clear that, if the point clouds of SGM did not have those huge outliers (in squares shape), the deliverables would be better than those of the NCC method, given the quantity of points in the 1981-SGM point cloud dataset.

6.1 Recommendations

The present research made use of historical aerial photographs to perform DEM extraction and calculate volumetric changes during a time-frame in the East-Vlieland, in the Netherlands. Hereby are some recommendations suggested by the author for further researches and approaches within the theme.

First, when possible, finding the camera calibration reports for historical photographs can help the interior and exterior parameters setting. Having them, there is no estimation in this step, reducing the chance of miscalculations for the sensor and photos characteristics. This will positively affect the process for image matching. It is also suggested to always collect as much as possible GCPs over the study area. During this research, Google Earth Pro was used as topographic reference, however one can search for other possibilities to be used to collect the GCPs, not only one source, especially when the study area is located in a coastal zone, where there are beaches, dunes and a lot of water, being hard to set up those points in this situation.

Another recommendation can be made towards the image matching algorithms. For this study it was used the NCC and the SGM method. Remembering, to perform the NCC it was used the eATE in ERDAS, and to use SGM there are two options in the software, XPro and Tridicon. For this research, the calculations were made using only the Tridicon option. Considering the time frame to perform this thesis, and the time spent running these processes, which can easily be escalated from days to weeks, it was not possible to try out the XPro. Especially for the 1981 dataset the results showed many outliers marking the boundaries of the stereropairs, so some questions remain: did this happen because of the Tridicon process? What will be the response using XPro?

According to ERDAS Imagine support (2019), both buttons use the SGM in the same way, without any differences, only that XPro accepts aerial photographs, while Tridicon accepts both aerial photographs and satellite images.

The topic of this study is of high interest within the remote sensing field. What should be interesting is trying to apply the same line of research in one large city (considering its expansion along decades), where even in old photographs, GCPs can be easily located, and then the image matching methods to create point clouds can be better compared.

7. References

Alexiou, E., Touradj, E. (2018). Point cloud quality assessment metric based on angular similarity. *International Conference on Multimedia and Expo (ICME)*, 6 p.

Balasubramanian, A. (2017). Digital Elevation Model (DEM) In GIS. Centre for Advanced Studies in Earth Science, University of Mysore, Mysore, 34 p.

Bickel, V.T., Manconi, A., Amann, F. (2018). Quantitative Assessment of Digital Image Correlation Methods to Detect and Monitor Surface Displacements of Large Slope Instabilities. *Remote Sensing*, 10(6), 865, 1-15.

Bird, E.C.F. (1985). Coastline changes: a global review. Wiley and Sons, Chichester, United Kingdom, 219 p.

Clavijo, A.P.R. (2013). Comparisons and problem identification on Local and Global Digital Elevation Models. Master Thesis, Politecnico Di Milano, Italy, 141 p.

Dall'Asta, E. (2016). Semi-Global techniques in Image Matching and Change Detection with applications to Civil and Environmental Engineering. Doctoral Thesis, Università degli Studi di Parma, Italy, 223 p.

Dall'Asta, E., Roncella, R. (2014). A Comparison of Semiglobal And Local Dense Matching Algorithms for Surface Reconstruction. *In:* The International Archives of the Photogrammetry, Remote Sensing and Spatial Information Sciences, 5, 187-194.

Dottori, F., Di Baldassarre, G., Todini, E. (2013). Detailed data is welcome, but with a pinch of salt: Accuracy, precision, and uncertainty in flood inundation modeling. *Water Resources Research*, 49, 6079-6085.

Drosos, V., Farmakis, D. (2006). Airborne laser scanning and DTM generation. *In:* Manolas, E. (Eds.), Naxos international conference on sustainable management and development of mountainous and island areas, 206–218.

ERDAS Imagine support (2019). eATE Concept and Theory. *Software Usage Instructions*. (Accessed in 02-02-2019). https://hexagongeospatial.fluidtopics.net/#/reader/~P7L4c0T_d3papuwS98oGQ/Tz3z1DCRQ1Na6JcVTnZ~bw

ERDAS Imagine support (2019). Tridicon Semi-Global Matching. Concept and Theory. *Software Usage Instructions*. (Accessed in 02-02-2019). https://hexagongeospatial.fluidtopics.net/reader/~P7L4c0T_d3papuwS98oGQ/Lz481bg6c~9_G1r4JccWeQ

Falkner, E., Morgan, D. (2002). Aerial Mapping – Methods and Applications. Florida, United States, CRC Press Company, 2nd Edition, 192 p.

Feagin, R. A., Sherman, D. J., Grant, W. E. (2005). Coastal Erosion, Global Sea-Level Rise, and the Loss of Sand Dune Plant Habitats. *Frontiers in Ecology and the Environment*, 3(7), 359-364.

Florinsky, I.V. (2016). Digital Elevation Models. *In:* Digital Terrain Analysis in Soil Science and Geology, 2nd Edition, Chapter 3, 77-108.

Gilliam, J.J. 1972. Aerial photography and related products| Aids in expediting the construction and development of urban land-use maps. Master Thesis, University of Montana, United States of America, 81 p.

Haala, N. (2011). Multiray Photogrammetry and Dense Image Matching. *Photogrammetric Week '11, Ed. D. Fritsch, Wichmann, Berlin/Offenbach*, 185-195.

Haala, N., Rothermel, M. (2012). Dense multi-stereo matching for high quality digital elevation models. *Journal of Photogrammetry, Remote Sensing and Geoinformation Science*, 4, 331–343.

Hillen, M.M., Jonkman, S.N., Kanning, W., Kok, M., Geldenhuys, M.A., Stive, M.J.F. (2010). Coastal defence cost estimates - Case study of the Netherlands, New Orleans and Vietnam. Report of measurements and observations, Communications on Hydraulic and Geotechnical Engineering, TU Delft, Department Hydraulic Engineering, 88 p.

Hirschmueller, H. (2005). Accurate and Efficient Stereo Processing by Semi-Global Matching and Mutual Information. *IEEE Conference on Computer Vision and Pattern Recognition*, 2, 807-814.

Hirschmueller, H. (2008). Stereo Processing by Semiglobal Matching and Mutual Information. *IEEE Transactions on Pattern Analysis and Machine Intelligence*, 30(2), 1-14.

Jaud, M., Rouveure, R., Faure, P., Moiroux-Arvis, L., Monod, M. (2014). Method for orthorectification of terrestrial radar maps. *ISPRS Journal of Photogrammetry and Remote Sensing*, 97, 185-194.

Kaliraj, S., Chandrasekar, N., Ramachandran, K.K. (2017). Mapping of coastal landforms and volumetric change analysis in the south west coast of Kanyakumari, South India using remote sensing and GIS techniques. *The Egyptian Journal of Remote Sensing and Space Sciences*, 20, 265-282.

Kim, B.O., Yun, K.H., Lee, C.K. (2014). The Use of Elevation Adjusted Ground Control Points for Aerial Triangulation in Coastal Areas. *KSCE Journal of Civil Engineering*, 18(6), 1825-1830.

Kim, H. (2015). 3D Classification of Power Line Scene Using Airborne Lidar Data. Doctoral Thesis, York University, Canada, 185 p.

Konecny, G. (1985). The International Society for Photogrammetry and Remote Sensing - 75 Years Old, or 75 Years Young. *Photogrammetric Engineering & Remote Sensing*, 51(7), 919-933.

Lal, R. (2001). Soil degradation by erosion. *Land degradation & development*, 12(6), 519-539.

Leatherman, S. P. (2003). Shoreline change mapping and management along the U.S. east coast. Journal of Coastal Research, SI38, 5-13.

Linder, W. (2016). Digital photogrammetry. A Practical Course. Springer-Verlag, Berlin, Heidelberg, 4th Edition, 214 p.

Liew, L.H., Wang, Y.C, Cheah, W.S. (2012). Evaluation of Control Points' Distribution on Distortions and Geometric Transformations for Aerial Images Rectification. *In:* International Symposium on Robotics and Intelligent Sensors 2012 (IRIS 2012), Procedia Engineering 41, 1002-1008.

Martínez-Carricondo, P., Agüera-Vega, F., Carvajal-Ramírez, F., Mesas-Carrascosa, F.J., García-Ferrer, A., Pérez-Porras, F.J. (2018). Assessment of UAV-photogrammetric mapping accuracy based on variation of ground control points. *International Journal of Applied Earth Observation and Geoinformation*, 72, 1-10.

McKeen, S. A., Wilczak, J., Grell, G., Djalalova, I., Peckham, S., Hsie, E., Gong, W., Bouchet, V., Menard, S., Moffet, R., McHenry, J., McQueen, J., Tang, Y., Carmichael, G. R., Pagowski, M., Chan, A., Dye, T., Frost, G., Lee, P., Mathur, R. (2005). Assessment of an ensemble of seven real time ozone forecasts over eastern North America during the summer of 2004. *Journal of Geophysical Research*, 110, 16 p.

Milan, D.J., Heritage, G.L., Large, A.R.G., Fuller, I.C. (2011). Filtering spatial error from DEMs: Implications for morphological change estimation. *Geomorphology*, 125, 160-171.

Muller, J. (2015). Comparing high quality digital elevation models to estimate ponding in urban systems. Master Thesis, Utrecht University, The Netherlands, 107 p.

Mutlu, M., Popescu, S. C., Zhao, K. (2008). Sensitivity analysis of fire behaviour modeling with LIDAR-derived surface fuel maps. *Forest Ecology and Management*, 256, 289–294.

Natural Resources Canada. (2016). Concepts of Aerial Photography. (Accessed in 02-10-2018). https://www.nrcan.gc.ca/earth-sciences/geomatics/satellite-imagery-air-photos/air-photos/about-aerial-photography/9687

Nebiker, S., Cavegn, S., Eugster, H., Laemmer, K., Markram, J., Wagner, R. (2012). Fusion of Airborne and Terrestrial Image-Based 3D Modelling in Road Infrastructure Management – Vision and First Experiments. *In:* International Archives of the Photogrammetry, Remote Sensing and Spatial Sciences, Vol. XXXIX-B4, XXII ISPRS Congress, Melbourne, Australia, 79-84.

Nguyen, T. (2015). Optimal Ground Control Points for Geometric Correction Using Genetic Algorithm with Global Accuracy. *European Journal of Remote Sensing*, 48, 101-120.

Pulighe, G, Fava, F. (2013). DEM extraction from archive aerial photos: accuracy assessment in areas of complex topography. *European Journal of Remote Sensing*, 46(1), 363-378.

Remondino, F., Spera, M.G., Nocerino, E., Menna, F., Nex, F., Gonizzi-Barsanti, S. (2013). Dense image matching: Comparisons and analyses. *In:* 2013 Digital Heritage International Congress (DigitalHeritage), Marseille, France, 47-54.

Rijkswaterstaat, 2018. Kustonderhoud. (Accessed on 31-08-2018). https://www.rijkswaterstaat.nl/water/waterbeheer/bescherming-tegen-het-water/maatregelen-om-overstromingen-te-voorkomen/kustonderhoud

Ruff, A.W. (1954). The use of aerial photographs for the graduate thesis. Economic Geology, 49(7), 779-782.

Salichtchev, K. A. (1973). Some reflections on the subject and method of Cartography after the Sixth International Cartographic Conference. Cartographica, Toronto: University of Toronto Press, 14, 111-116.

Savage, N. H., Agnew, P., Davis, L. S., Ordóñez, C., Thorpe, R., Johnson, C. E., O'Connor, F. M., Dalvi, M. (2013). Air quality modelling using the Met Office Unified Model (AQUM OS24- 26): model description and initial evaluation. *Geoscientific Model Development*, 6, 353-372.

Schenk, A. F. (1996). Automatic Generation of DEMs. *In:* Cary, T., Jensen, J. and Nyquist, M. (eds.) Digital Photogrammetry. An Addendum to the Manual of Photogrammetry. *American Society for Photogrammetry and Remote Sensing*, Bethesda, Maryland, 247-250.

Schenk, T. (2005). Introduction to Photogrammetry. Department of Civil and Environmental Engineering and Geodetic Science, The Ohio State University, Columbus, 95 p.

Sijmons, K. (2018). Lecture of Introduction to Photogrammetry. International Institute for Geo-Information Science and Earth Observation (ITC), 124 p.

Suri, S. (2010). Automatic Image to Image Registration for Multimodal Remote Sensing Images. Doctoral Thesis, Technische Universität München, Germany, 220 p.

Tran, T.A., Raghavan, V., Masumoto, S., Vinayaraj, P., Yonezawa, G. (2014). A geomorphology-based approach for digital elevation model fusion – case study in Danang city, Vietnam. *Earth Surface Dynamics*, 2, 403-417.

Ullah, S., Adler, P., Dees, M., Datta, P., Weinacker, H., Koch, B. (2017). Comparing image-based point clouds and airborne laser scanning data for estimating forest heights. *iForest -Biogeosciences and Forestry*, 10, 273-280.

U.S. Army Corps of Engineer. (1993). Engineering Manual EM 1110-1-1000 - Photogrammetric Mapping Report. Principles of Photogrammetry, Chapter 10, 19 p.

Van der Sande, Soudarissanane, S., Khoshelham, K. (2010). Assessment of Relative Accuracy of AHN-2 Laser Scanning Data Using Planar Features. *Sensors*, 10, 8198-8214.

Van Meijeren, H. (2017). Assessing the differences between Dutch elevation datasets AHN2 and AHN3. Master Thesis, Wageningen University, The Netherlands, 48 p.

Verhagen, H.J. (1990). Coastal Protection and Dune Management in The Netherlands. *Journal of Coastal Research*, 6(1), 169-179.

Walstra, J. (2006). Historical aerial photographs and digital photogrammetry for landslide assessment. Doctoral Thesis, Loughborough University, Loughborough, England, 228 p.

Water boards, 2019. AHN. (Accessed on 08-02-2019). http://www.ahn.nl/index.html

Werbrouck, I., Antrop, M., Van Eetvelde, V., Stal, C., De Maeyer, Ph., Bats, M., Bourgeois, J., Court-Picon, M., Crombé, Ph., De Reu, J., De Smedt, Ph., Finke, P.A., Van Meirvenne, M., Verniers, J., Zwertvaegher, A. (2011). Digital Elevation Model generation for historical landscape analysis based on LiDAR data, a case study in Flanders (Belgium). *Expert Systems with Applications*, 38, 8178-8185.

Williams, R.D. (2012). DEMs of difference. Geomorphological Techniques, British Society for Geomorphology, 2(3.2), 1-17.

Wolf, P. R. and Dewitt, B. A. (2000). Elements of Photogrammetry. With Applications in GIS. McGraw-Hill, Boston, 608 p.

Zhang, B., Miller, S., DeVenecia, K. (2006). Automatic Terrain Extraction Using Multiple Image Pair and Back Matching. *In:* American Society for Photogrammetry and Remote Sensing Annual Conference, Reno, Nevada, 1-11.

Zhang, J., Zhang, H., Zhang, Z. (2004). Exterior orientation for remote sensing image with high resolution by linear feature. *In:* Proceedings of The International Archives of the Photogrammetry, Remote Sensing and Spatial Information Sciences, Istanbul, Turkey, 35(B/3), 76–79.

Zhang, Y., Xian, C., Chen, H., Grieneisen, M.L., Liu, J., Zhang, M. (2016). Spatial interpolation of river channel topography using the shortest temporal distance. *Journal of Hydrology*, 542, 450–462.

Zhao, F., Huang, Q., Gao, W. (2006). Image Matching by Normalized Cross-Correlation. *In:* 2006 IEEE International Conference on Acoustics Speed and Signal Processing Proceedings, 729-732.

Appendix A: *Ground control points*

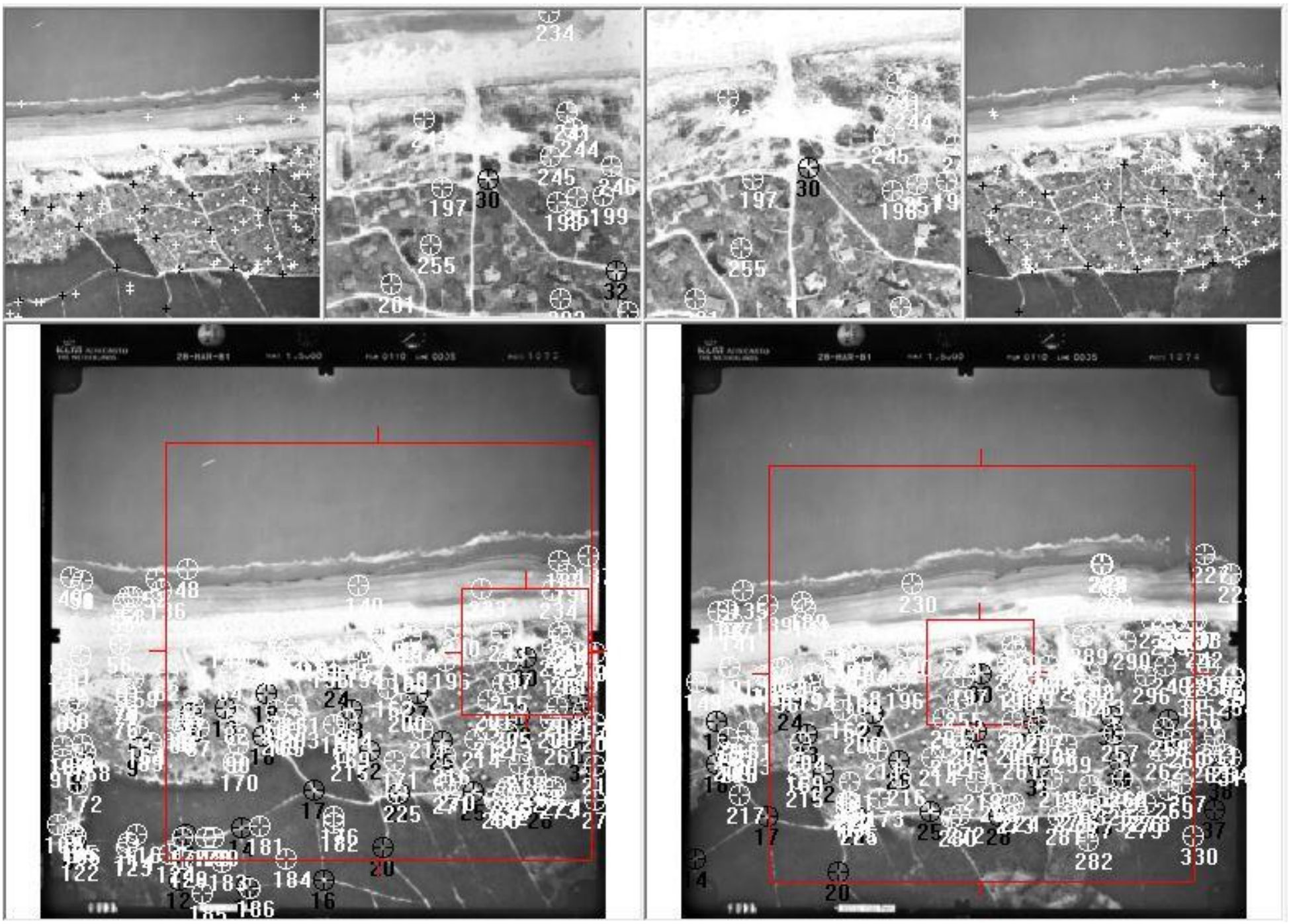

Figure A1: ERDAS Imagine viewer from part of East-Vlieland showing selected GCPs and tie points in one of the aerial photographs of 1981. GCPs are in black colour and tie points are in white colour.

Appendix B: ***Point cloud 1981 of the three areas – NCC algorithm***

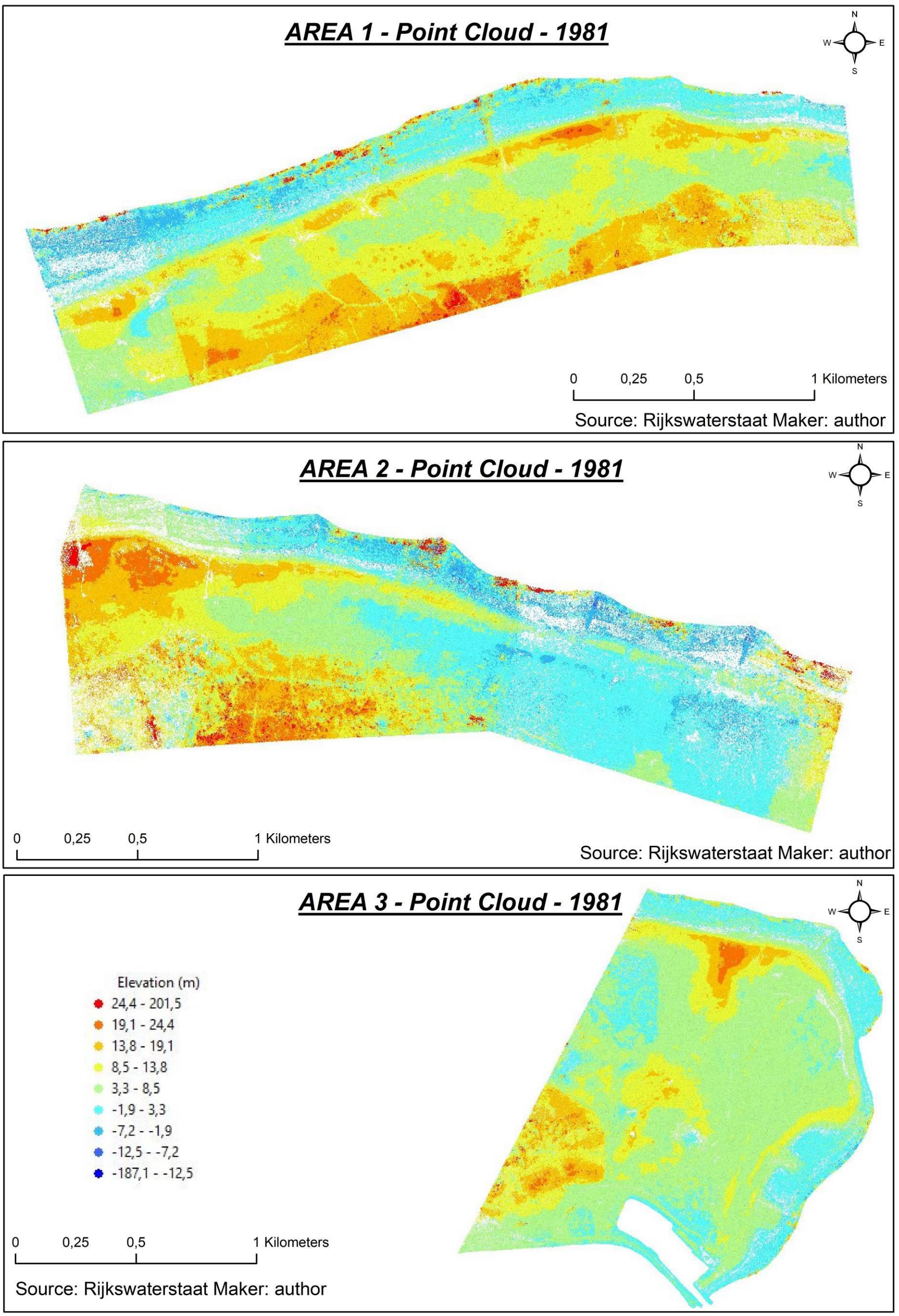

Figure B1: Point clouds from the year of 1981 generated by the NCC method.

Appendix C: ***Point cloud 1981 of the three areas – SGM algorithm***

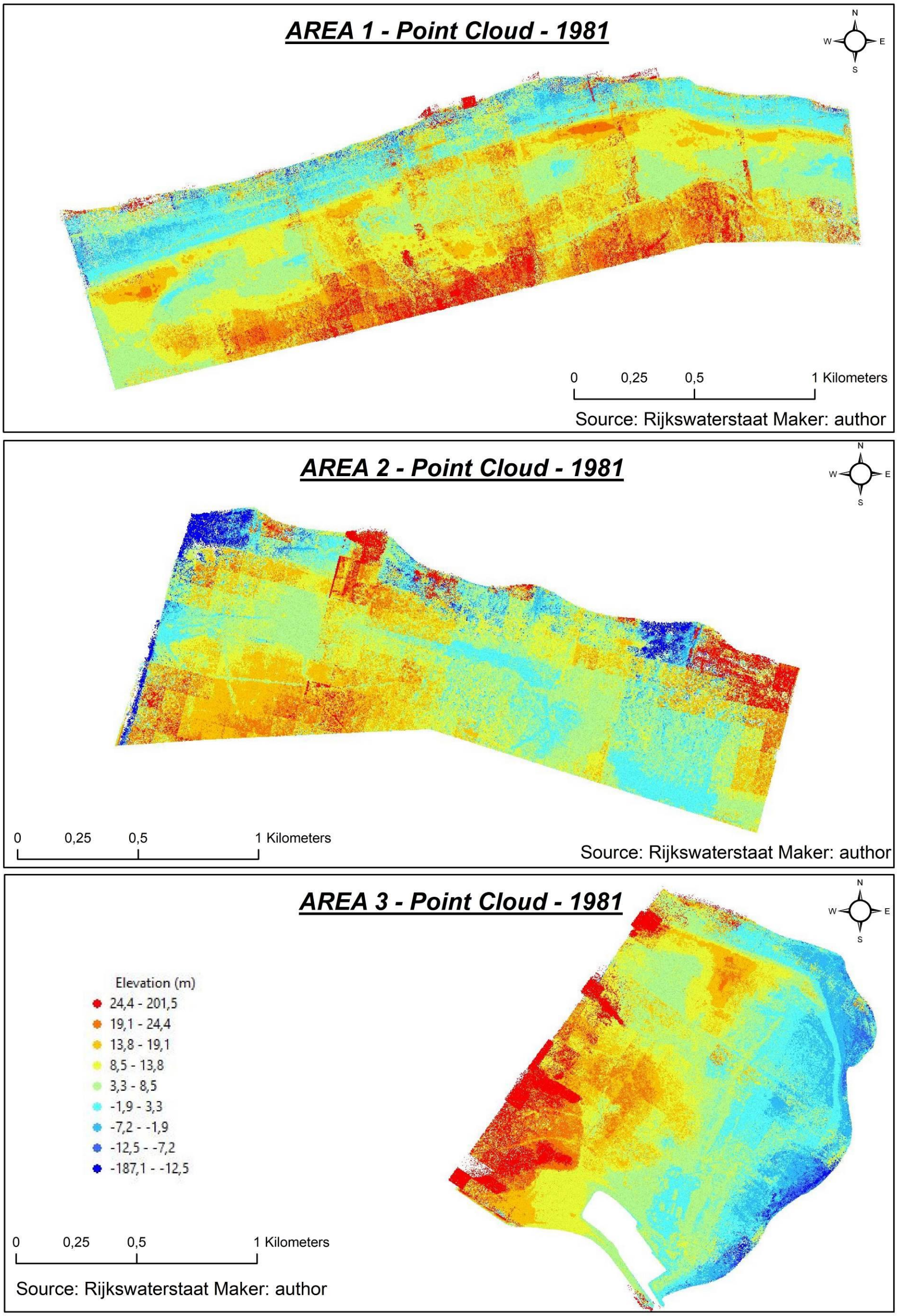

Figure C1: Image-based point clouds of 1981 made through the SGM algorithm.

Appendix D: ***Point cloud 1945 of the three areas – NCC algorithm***

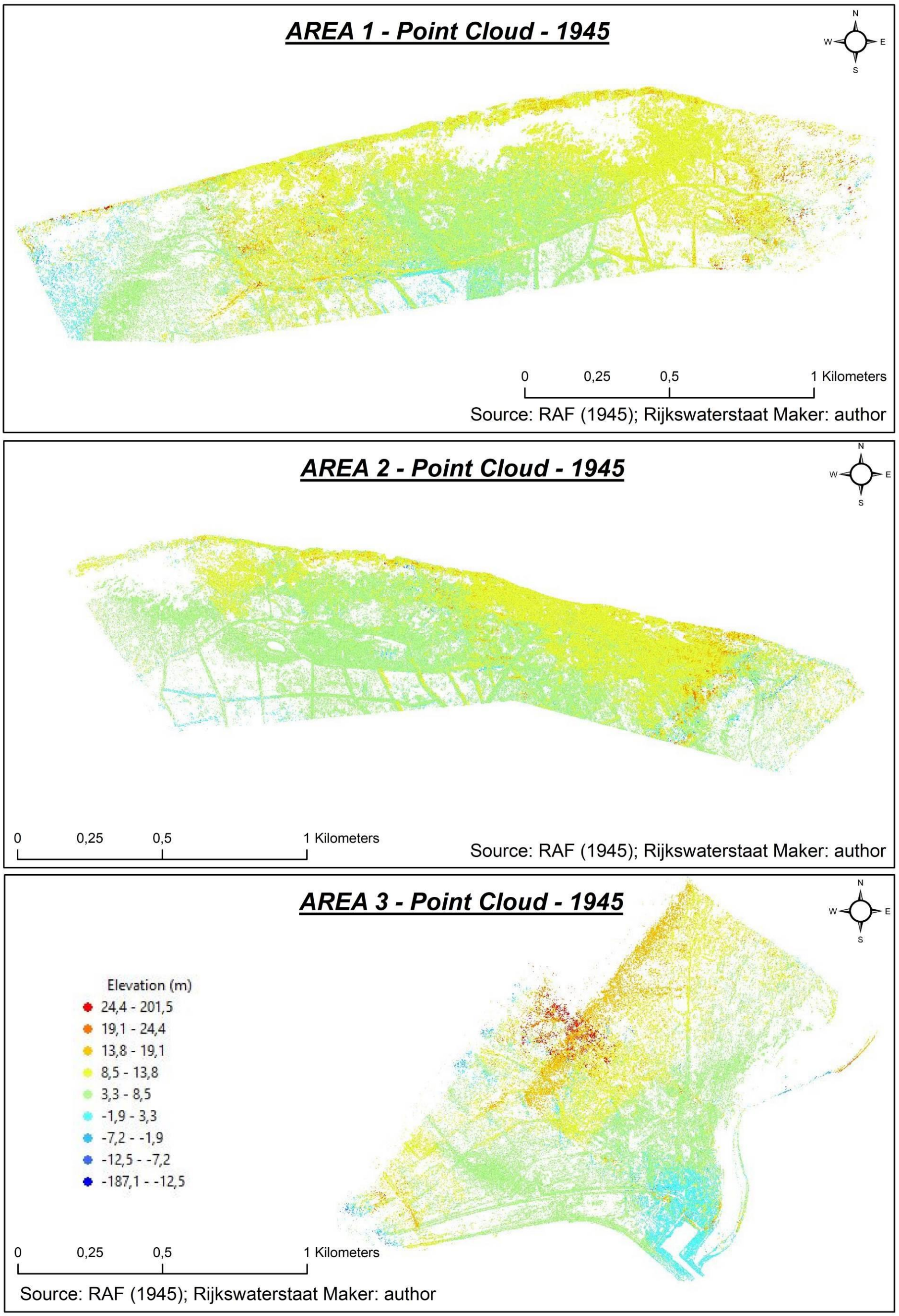

Figure D1: Imaged-based point clouds from the year of 1945 performed through the NCC algorithm.

Appendix E: ***E1 - Point cloud 1945 of area 1 and 2; E2 - 3D visualization of area 1; SGM algorithm***

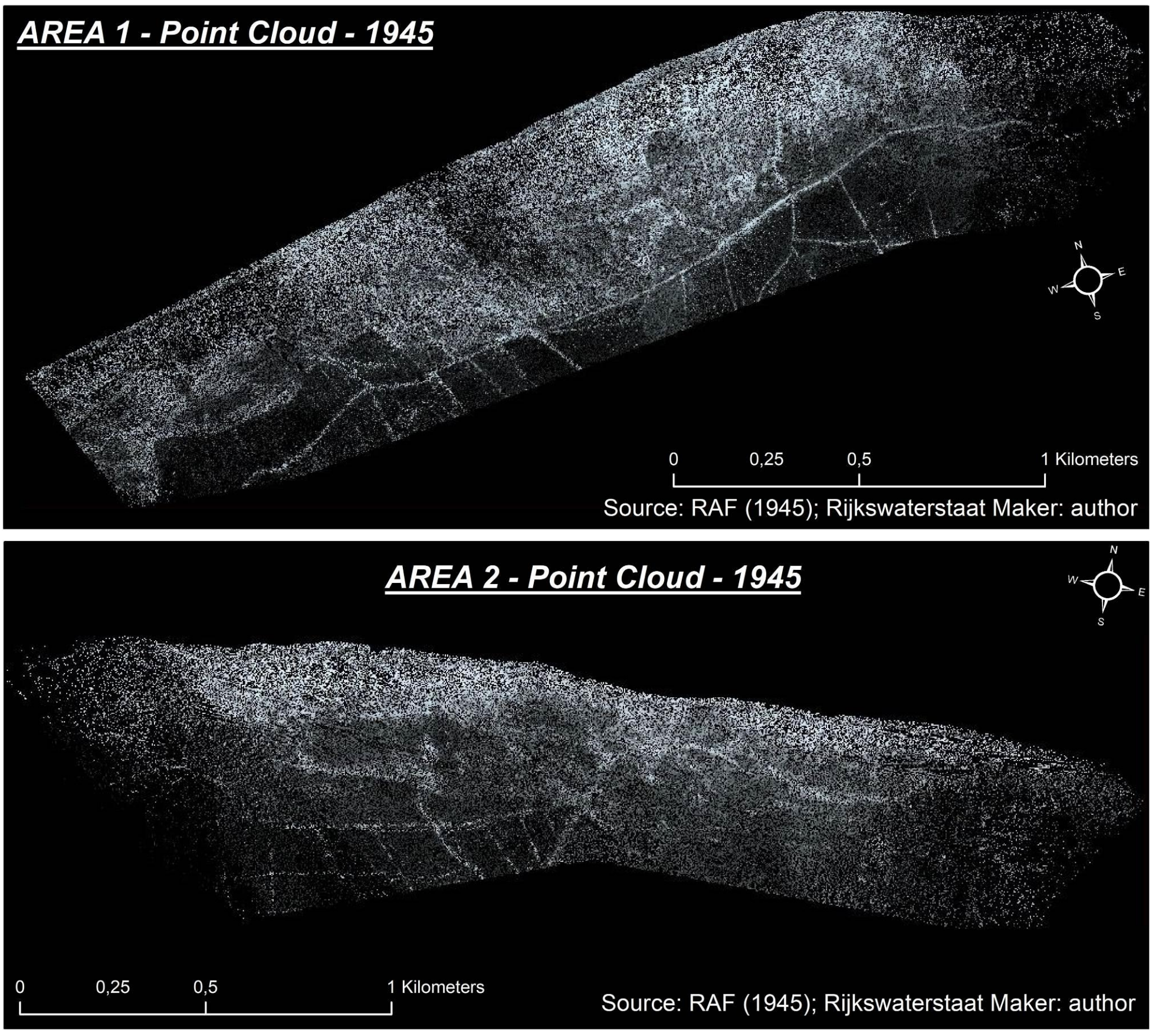

Figure E1: Areas 1 and 2 of the image-based point clouds of 1945 made through the SGM algorithm in the ERDAS Imagine viewer.

A

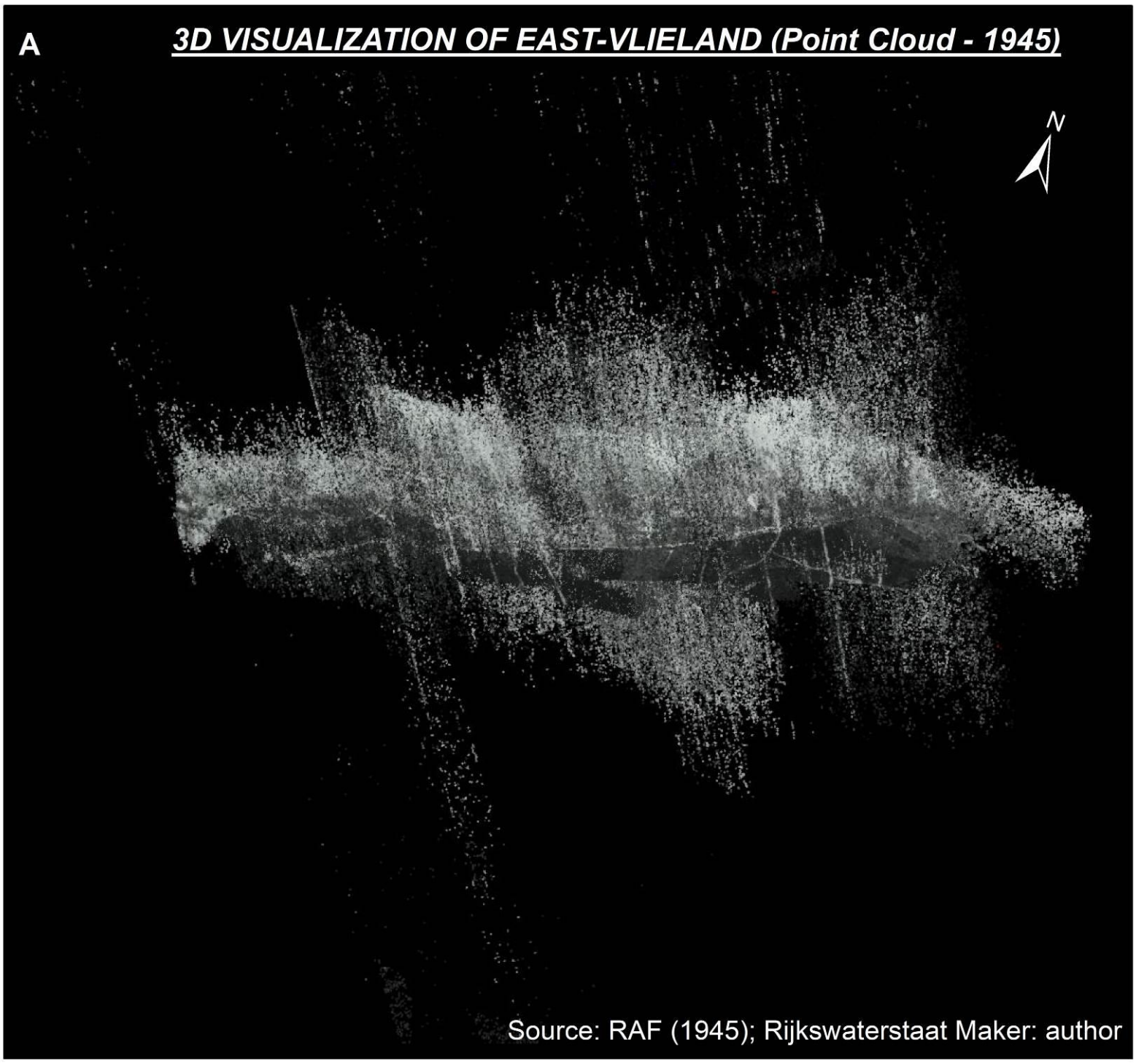

B

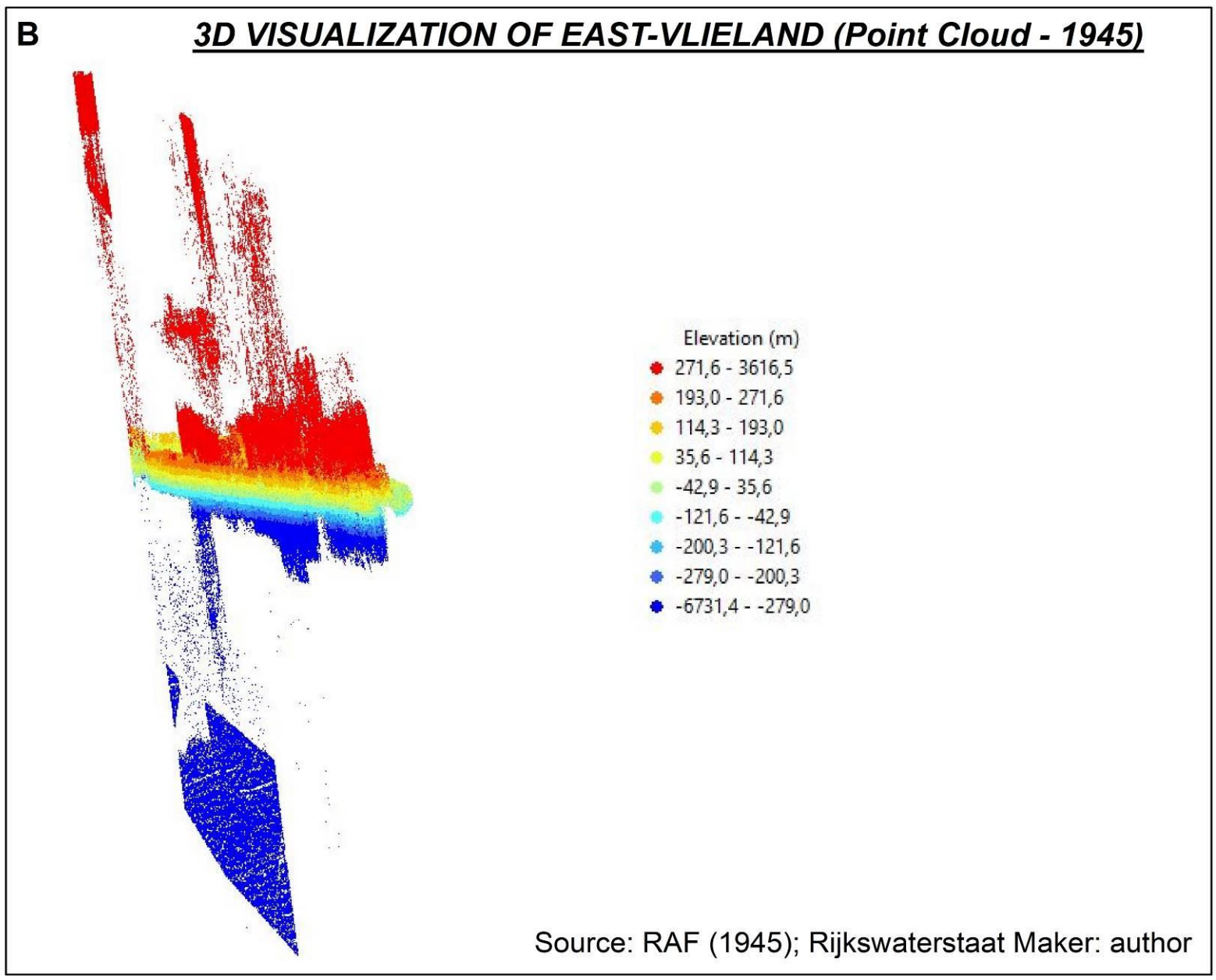

Figure E2: A) 3D visualization of point cloud data of 1945 area 1 made with SGM method. View in Erdas Imagine. B) 3D visualization in ArcScene.of 1945 area 1 point cloud dataset, created with the SGM algorithm. View to NNW.

Appendix F: ***F1- Orthophoto 1981 DEM-NCC; F2 - Orthophoto 1981 DEM-SGM***

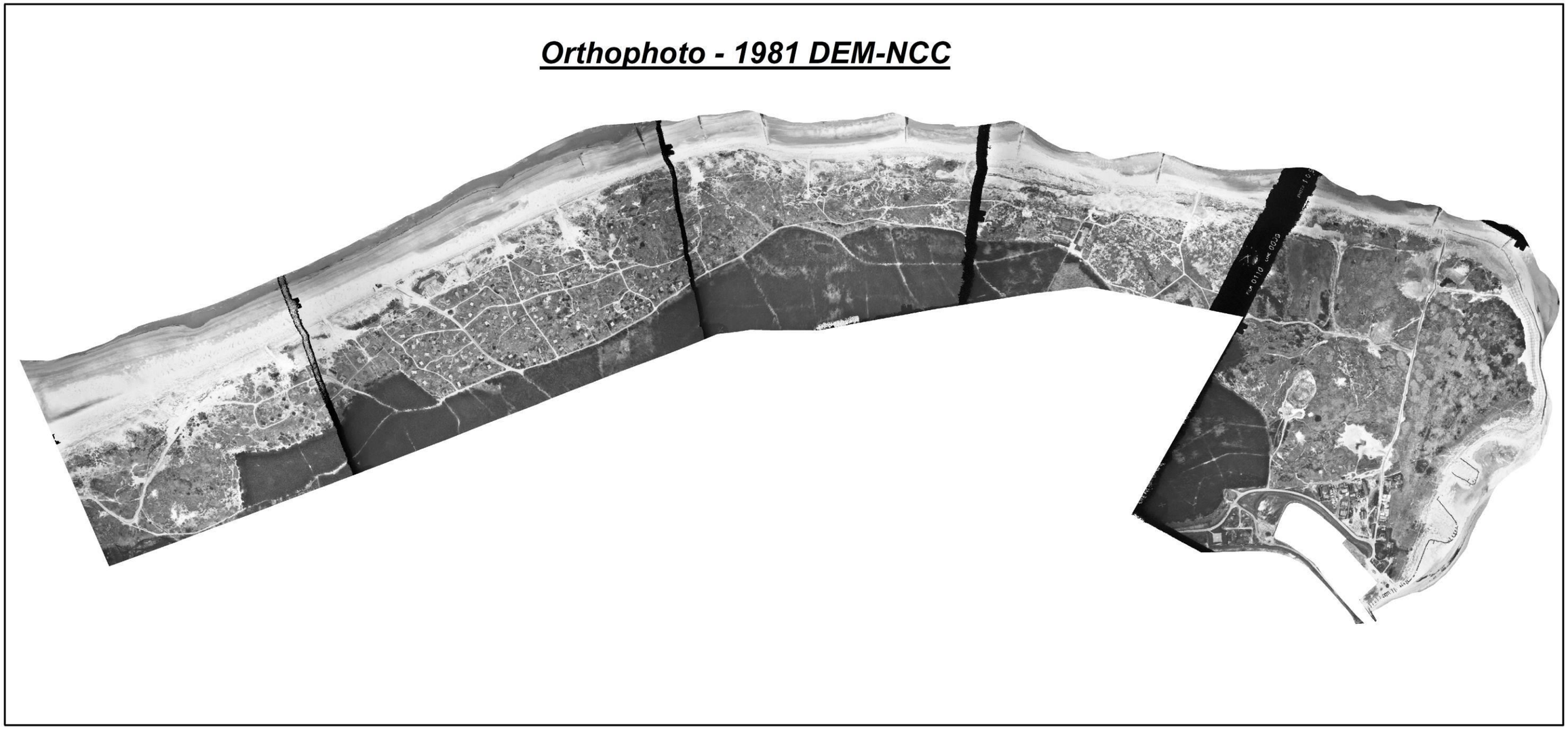

Figure F1: Orthophoto of the 1981 imagery combined with the 1981 DEM-NCC.

Orthophoto - 1981 DEM-SGM

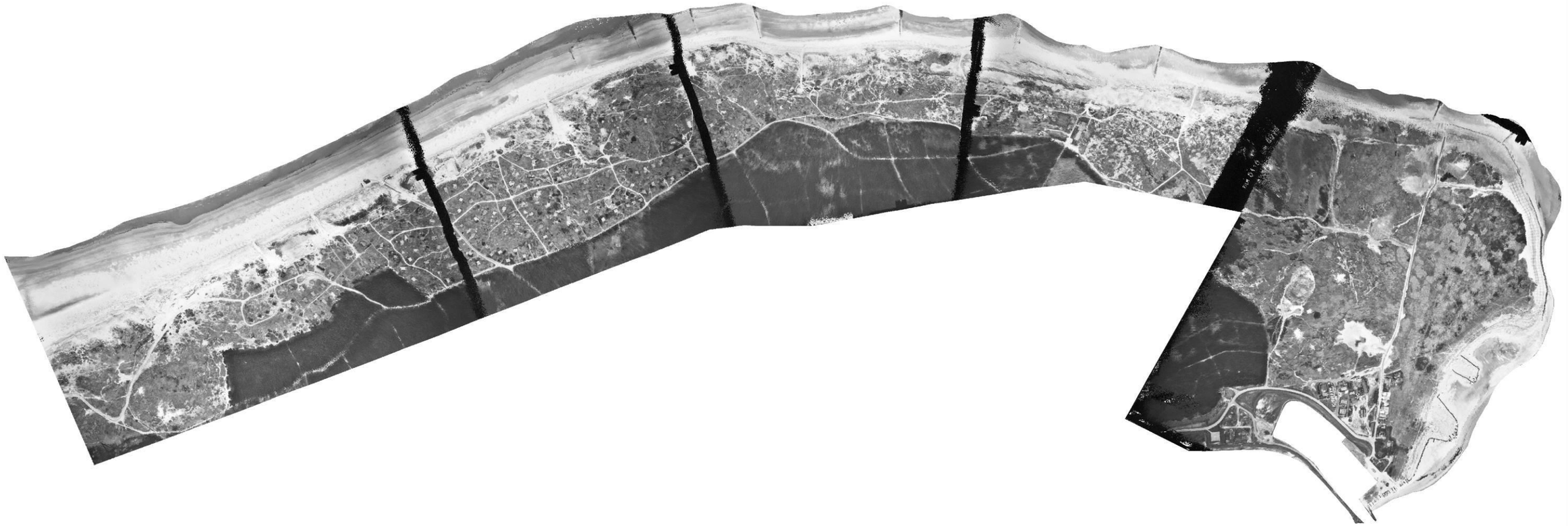

Figure F2: Orthophoto of the 1981 aerial photographs, made with the 1981 DEM-SGM.

Appendix G: ***General workflow and concept of this thesis***

GIMA Geographical Information Management and Applications

Utrecht University

Historical Aerial Imagery for DEM Extraction to Quantify Volumetric Changes between the Years of 1945 and 2017, in the East-Vlieland Coast, the Netherlands

MSc Jose Antonio Cirillo de Assis[1], Drs. Maarten Zeylmans Van Emmichoven[1]

Study Area - East-Vlieland

Methodology

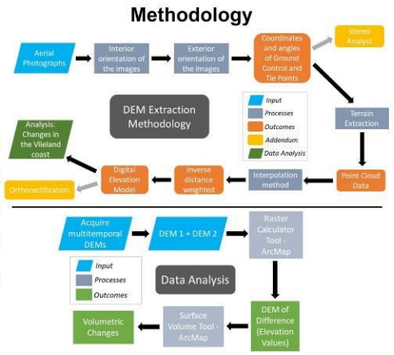

Two Overlapping Aerial Photographs

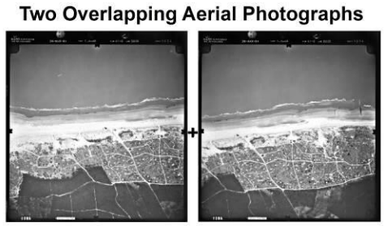

Stereopair

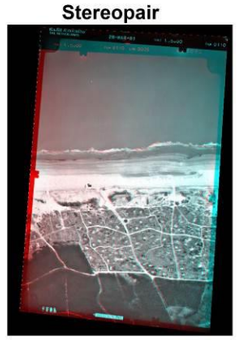

DEM of East-Vlieland of 1981

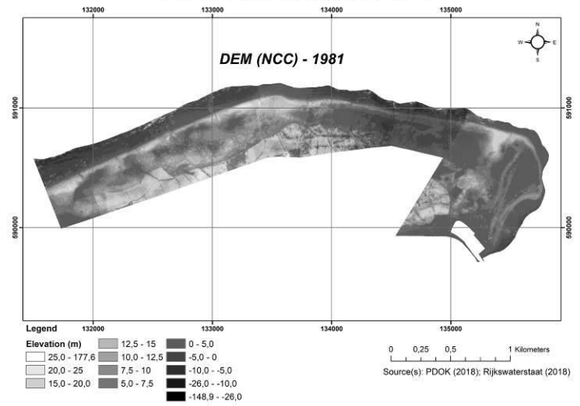

3D VISUALIZATION OF EAST-VLIELAND (DEM - NCC - 1981)

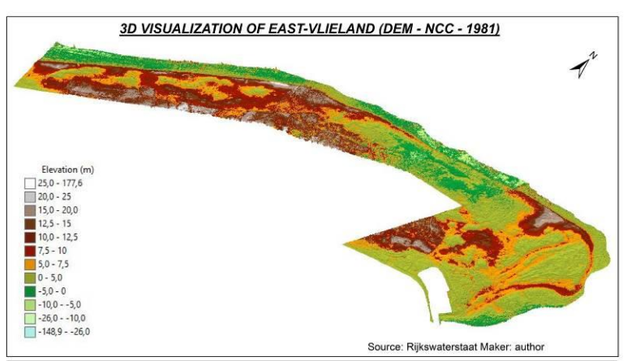

3D VISUALIZATION OF EAST-VLIELAND (Point Cloud - 1981)

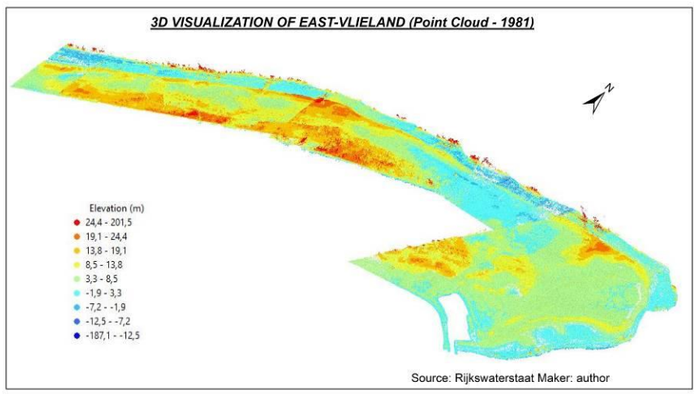

ZOOM IN AREA 3

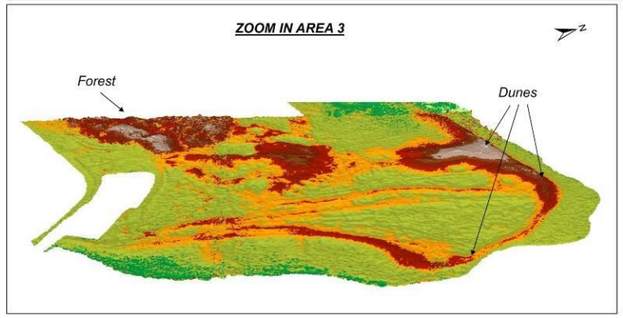

Classified DEMs of Difference

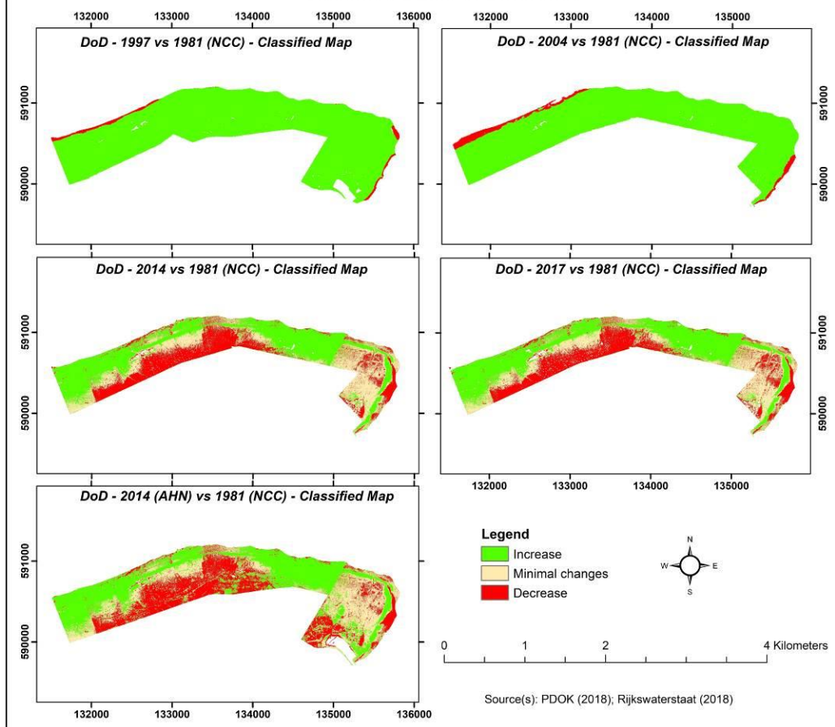

Volumetric Changes

	DEM-NCC		DEM-SGM
Datasets	1981	1945	1981
LiDAR 1997	1.843.617.569 ± 3	1.070.566.124 ± 3	1.473.241.585 ± 3
LiDAR 2004	1.504.561.580 ± 3	1.008.221.788 ± 3	1.224.115.125 ± 3
LiDAR 2014	-49.409.817 ± 3	-13.435.719 ± 3	-329.856.271 ± 3
LiDAR 2017	-49.952.592 ± 3	-13.413.568 ± 3	-330.399.046 ± 3
AHN 2014	-49.572.741 ± 3	-17.870.111 ± 3	-419.948.726 ± 3

Orthophoto - 1981 DEM-NCC

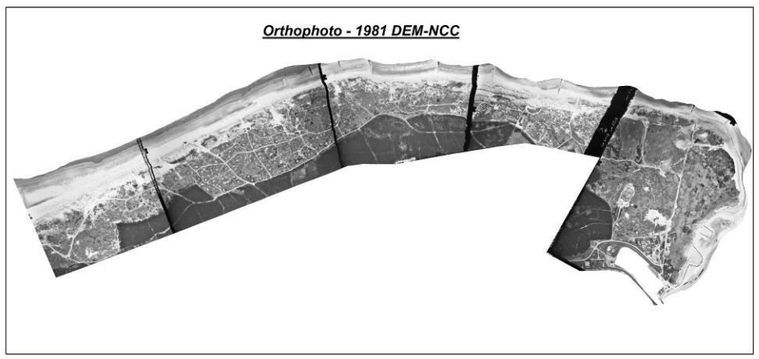

1 Utrecht University, Princetonlaan 8a, 3584 CB Utrecht, The Netherlands